ATOMIC SCALE MODELING OF SILICATE INTERFACE PROPERTIES FOR HIGH-*K* GATE DIELECTRIC APPLICATIONS

A DISSERTATION

SUBMITTED TO THE DEPARTMENT OF ELECTRICAL ENGINEERING

AND THE COMMITTEE ON GRADUATE STUDIES

OF STANFORD UNIVERSITY

IN PARTIAL FULFILLMENT OF THE REQUIREMENTS

FOR THE DEGREE OF

DOCTOR OF PHILOSOPHY

Atsushi Kawamoto

August 2001

I certify that I have read this dissertation and that, in my opinion, it is fully adequate in scope and quality as a dissertation for the degree of Doctor of Philosophy.

Robert W. Dutton (Principal Advisor)

I certify that I have read this dissertation and that, in my opinion, it is fully adequate in scope and quality as a dissertation for the degree of Doctor of Philosophy.

Peter B. Griffin

I certify that I have read this dissertation and that, in my opinion, it is fully adequate in scope and quality as a dissertation for the degree of Doctor of Philosophy.

Kyeongjae Cho

Approved for the University Committee on Graduate Studies:

Abstract

Aggressive scaling has led to silicon dioxide (SiO_2) gate dielectrics as thin as 15 $\mathring{A}$ in state-of-the-art CMOS technologies. As a consequence, static leakage power due to direct tunneling through the gate oxide has been increasing at an exponential rate. As technology roadmaps call for sub-10 $\mathring{A}$ gate oxides within the next five years, a variety of alternative high-*k* materials are being investigated as possible replacements for SiO_2. The higher dielectric constants in these materials allow the use of physically thicker films, potentially reducing the tunneling current while maintaining the gate capacitance needed for scaled device operation.

Atomic scale modeling methods based on first principles density functional theory are applied to a promising class of alternative dielectrics known as silicates (e.g. $ZrSi_xO_y$). Since the quality of the Si interface will ultimately determine the feasibility of an alternative dielectric, this work has focused on the interface properties of silicates in the context of MOS scaling limits.

Model interface calculations have been performed to show that oxide-like bonding of zirconium is energetically favored over silicide-like bonding at the Si interface; extended suboxide states within the interfacial transition region significantly limit the scalability of

the silicate system from the point of view of equivalent oxide thickness. First principles calculations have also been performed to quantify the expected lowering of the conduction band offset with increasing Zr concentration. The use of charge transfer dipoles at the interface has been proposed as a means of overcoming the inherent asymmetry of silicate band offsets. Because limitations are shown to arise at a Si/SiO_2-like interface, calculations suggest that possible solutions to overcoming them can be built on extensive knowledge of the Si/SiO_2 system.

Acknowledgments

I would like to thank the many people whose support and encouragement throughout my time at Stanford have made this research possible. First, I would like to thank my advisor, Professor Bob Dutton, who I first met virtually through email from the Stanford Japan Center in Kyoto. He has always encouraged me to think independently and to define my own research agenda, allowing me to develop the skills to do research. I thank him for enthusiastically supporting my adventure into the world of atomic scale modeling and for sharing his wisdom, insight and humor with me throughout the years. His passion for the profession has been an inspiration.

I would like to thank Dr. Peter Griffin for mentoring me on a nearly daily basis, patiently steering me in the right direction even as I changed research topics several times in my early years as a graduate student. His diverse expertise and critical review of my research have been immensely valuable.

I am indebted to Professor KJ Cho for teaching me nearly everything I know about atomic scale simulations. I thank him for treating me not only as a member of his own group, but also as a friend and colleague. I am proud to be among the first generation of students who had the opportunity to work with him at Stanford.

I would like to thank Professor Krishna Saraswat for serving on my oral defense committee and for teaching me many of the graduate level courses in semiconductor device and process physics.

I owe a special thanks to Professor Jim Plummer for teaching EE 111 my junior year, which even after eights years and 103 courses, remains my favorite class at Stanford. I hope that he will continue to inspire new generations of students to pursue further study in the field through his passionate teaching style.

I would like to acknowledge the National Science Foundation for providing financial support for this project through the Graduate Research Fellowship and DesCArtES (Distributed Center for Advanced Electronics Simulations) programs. The fellowship was especially valuable in providing the freedom to explore and discover my intellectual interests in graduate school.

I would like to thank the collaborators who have made this research more meaningful and enjoyable. John Jameson has been an incredible colleague to work with. I am glad to have shared the many ups and downs of our research at Stanford together. Dr. Shinji Onga of Toshiba has been a strong ally of my research and an invaluable resource for insight into real-world industrial challenges. The high-*k* research groups at Texas Instruments and IBM have been valuable mentors. I am especially indebted to Dr. Shaoping Tang of Texas Instruments for helping to shape the early direction of this research.

I am fortunate to have had the opportunity to interact with many of the students in the Dutton and Plummer groups. The many conversations and get-togethers at times provided valuable insight into research and at others welcome relief from it.

I would like to thank the knowledgeable staff in our group for their support throughout the years: Dr. Dan Yergeau, Fely Barrera, Maria Perea, Miho Nishi and Dr. Zhiping Yu. I am especially grateful to Dr. Dan Yergeau for sharing his software expertise on numerous occasions. Many of the exotic software programs I needed for my research would never have compiled, let alone performed, without his expertise.

I am indebted to my friends who have stood by me throughout the years, even as the frustrations of research sometimes kept me from fulfilling my obligations to them: Adrian, Elena, Gallant, Gu, Laura, Steve and Thien. I thank them all for their unwavering friendship.

I would like to thank my parents, Shinichi and Masako, my brother, Kensaku, and my grandparents, Fusataro, Sachi and Yoshino, for their love, support and many sacrifices which have made not only this research, but also my education in America, possible.

Finally, I would like to express my gratitude to my best friend and fiance Denise who has patiently supported me in so many ways throughout graduate school. I thank her for enriching my life with her endless energy, constant humor and love.

Table of Contents

List of Tables

List of Figures

List of Terms

DFT	density functional theory
DFPT	density functional perturbation theory
E_g	bandgap energy
EOT	equivalent oxide thickness
GW	quasiparticle approach to evaluating the exchange-correlation potential through the one-particle Green's function (G) and the screened Coulomb interaction (W)
Hf	hafnium
Hf_x	model Si/Hf silicate interface containing abrupt transition region with Hf incorporation *x* layers above the Si interface, where *x* assumes values of 1 and 3
Hf_{xs}	model Si/Hf silicate interface containing extended suboxide region with Hf incorporation *x* layers above the Si interface
$HfSi_xO_y$	Hf silicate; can also be expressed as $(HfO_2)_x(SiO_2)_{1-x}$
I_{gate}	gate leakage current
I_{off}	subthreshold leakage current
k	relative dielectric constant
LDA	local density approximation
MD	molecular dynamics
Si/SiO_2	silicon/silicon dioxide
Si^{x+}	partial oxidation state of Si with *x* oxygen neighbors ($x < 4$); also referred to as suboxide state
TB	tight binding
t_{ox}	gate oxide thickness
Zr	zirconium

Zr_x	model Si/Zr silicate interface containing abrupt transition region with Zr incorporation *x* layers above the Si interface, where *x* assumes values of 1 and 3
Zr_{xs}	model Si/Zr silicate interface containing extended suboxide region with Zr incorporation *x* layers above the Si interface
$ZrSi_xO_y$	Zr silicate; can also be expressed as $(ZrO_2)_x(SiO_2)_{1-x}$
$Zr_1Si_3O_8$	model bulk Zr silicate crystal with 8.3 atomic percent Zr
$Zr_2Si_2O_8$	model bulk Zr silicate crystal with 16.7 atomic percent Zr

Chapter 1

Introduction

1.1 Motivation

Moore's law scaling of planar metal-oxide-semiconductor (MOS) technology has maintained its dizzying pace in recent years. High performance microprocessors have surpassed the 1GHz barrier, and ever-increasing levels of integration are making possible system-on-chip solutions for a variety of novel applications. Throughout the history of integrated circuits, shrinking the dimensions of the transistor has required that many difficult challenges be overcome. Not surprisingly, the current push towards sub-0.1um technology generations requires numerous innovations aimed at overcoming substantial challenges. Increasingly, the requirements outlined by the International Technology Roadmap for Semiconductors (ITRS) indicate that no known solutions exist for a variety of critical technologies [1]. In particular, it is clear that today's gate dielectric material, silicon dioxide (SiO_2), will soon reach the predicted limits of scaling, thus presenting a fundamental challenge to continued scaling [2].

In recent years, substantial research effort has been focused on developing alternative gate dielectric materials to replace SiO_2. The daunting challenge of replacing a material which benefits from nearly 30 years of research and development has prompted interest in

novel computational approaches. In particular, atomic scale simulations can computationally screen candidate dielectrics by predicting their properties based on the microscopic interactions between atoms and electrons in the system.

1.2 Scope and Organization

This thesis investigates a promising class of alternative dielectrics known as silicates through the use of first principles density functional theory calculations. The research focuses primarily on the interface properties of the silicate system.

The thesis is organized as follows:

Chapter 2 reviews recent trends in gate oxide scaling to show that further scaling of SiO_2 is limited by static power dissipation and other fundamental considerations. As an alternative to continuing to scale SiO_2, the use of alternative high-*k* gate dielectrics is discussed. Several of the most important material properties for such high-*k* dielectrics are also reviewed. Known properties of zirconium and hafnium silicates, which are the focus of this research, are also described.

Chapter 3 provides a review of atomic scale modeling theory. The characteristics of the three main approaches, classical interatomic potentials, tight binding, and first principles density functional theory (DFT), are discussed along with examples of specific applications. Based on the requirements for modeling high-*k* dielectrics, DFT is identified as the most promising method for the properties of interest.

Chapter 4 describes model interface calculations aimed at investigating possible scaling limitations imposed by structural properties at the Si/silicate interface. Various properties are studied to clarify the nature of bonding at the Si interface. Detailed consideration of the interface structure and energetics leads to the conclusion that suboxide bonding within the interfacial transition region presents a significant challenge to scaling the silicate system.

Chapter 5 describes model interface calculations aimed at investigating possible scaling limitations imposed by electronic properties at the Si/silicate interface. Specifically, the scaling trends of silicate band offsets at the Si interface are studied. Based on analysis of the electronic structure of silicates, the degradation of the potential barrier is shown to primarily affect the conduction band offset, leading to asymmetric barrier heights as the transition metal concentration is increased. By explicitly altering the surface termination, charge transfer dipoles at Si the interface are investigated as a possible means of restoring symmetry in the band offsets.

Chapter 6 describes the contributions made by this research and suggests recommendations for future work.

Chapter 2

Gate Oxide Scaling

This chapter reviews recent trends in gate oxide scaling to motivate the imminent need for alternative high-*k* gate dielectric materials. Known properties of the silicate material system, which are the focus of this research, are also reviewed.

Section 2.1 provides a brief review of metal-oxide-semiconductor field-effect transistor (MOSFET) scaling. The operation of the MOSFET is shown to depend critically on several important properties of the gate capacitor dielectric material, SiO_2.

Section 2.2 reviews recent trends in gate oxide scaling to show that aggressive scaling of SiO_2 has led to substantial static power dissipation arising from direct carrier tunneling through the oxide layer. Recent experimental and theoretical work on the fundamental scaling limit of SiO_2 are also discussed.

Section 2.3 describes the use of high-*k* gate dielectrics which are being pursued as an alternative to continuing to scale SiO_2. Several of the most important properties of such materials are also described.

Section 2.4 describes the motivation for and the known properties of zirconium (Zr) and hafnium (Hf) silicate materials.

2.1 MOSFET scaling

Recall that a MOSFET ideally acts as a three-terminal switch, either connecting or isolating the drain (D) and source (S) terminals based on the voltage applied to the controlling gate (G) terminal, as illustrated in Figure 2.1(a). In practice, this switching action is achieved through the use of a gate capacitor, as illustrated in Figure 2.1(b). Depending on the polarity of the voltage applied to the gate terminal, either positive or negative charge is induced in the channel region along the bottom plate of the gate capacitor. The channel charge either connects or isolates the drain and source nodes depending on the type of carrier contained in those regions.

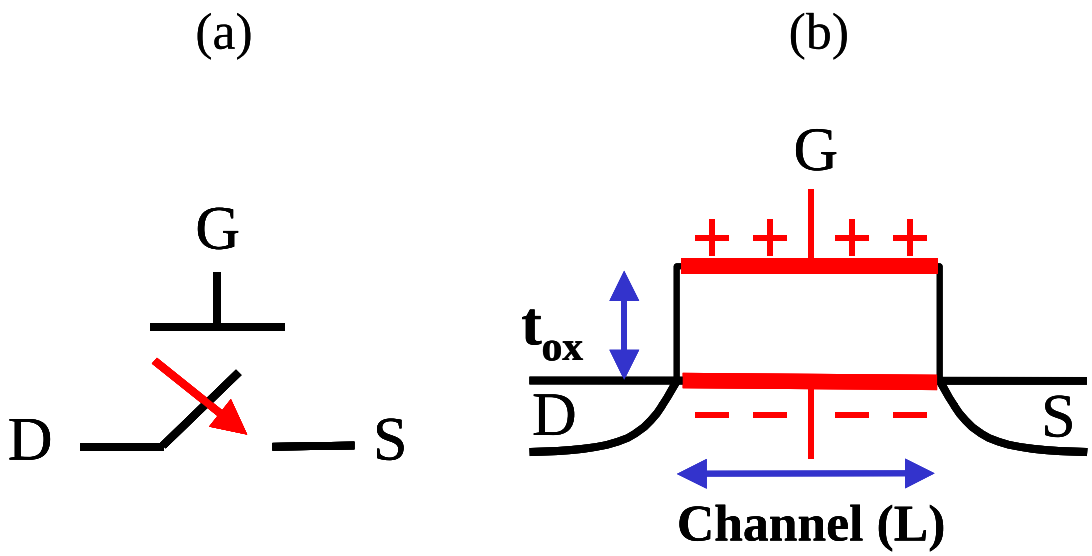

Figure 2.1 (a) The MOSFET ideally acts as a 3-terminal switch. (b) Practical realization of the MOSFET requires a gate capacitor.

The operation of the MOSFET depends critically on several properties of the gate dielectric material, SiO_2. The wide insulating bandgap (E_g) of SiO_2 electrically isolates charges in the gate and channel regions, so that the controlling gate terminal does not interfere with the flow of current in the channel region, as illustrated in Figure 2.2(a).

Also, the interface between SiO_2 and the underlying Si substrate is electrically of very high quality, allowing electric field lines originating at the gate electrode to penetrate into the channel region to accumulate or invert the surface charge. Prior to the development of the Si/SiO_2 system, attempts to realize a field-effect transistor (FET) were hampered by the abundance of electrically active defects at the dielectric/semiconductor interface.

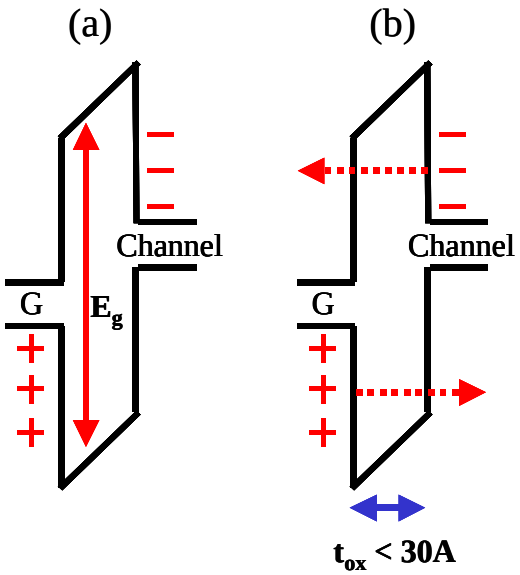

Figure 2.2 (a) Simplified band diagram of the MOS system. (b) Direct tunneling of carriers through the insulator potential barrier can occur for thin dielectric layers.

The amount of charge (Q) induced in the channel region is given by the product of the gate oxide capacitance per unit area (C_{ox}) and the voltage drop across the gate capacitor (V),

$$Q = C_{ox}V. \tag{2.1}$$

Since C_{ox} can be modeled as a parallel-plate capacitor, its value is given by

$$C_{ox} = \frac{k_{ox}\varepsilon_o}{t_{ox}}, \tag{2.2}$$

where k_{ox} is the relative dielectric constant, ε_0 is the permittivity of free space, and t_{ox} is the physical thickness of the dielectric material. Based on these relations, the drain-source current for a long-channel MOSFET operating in the saturation region can be expressed as

$$I_{ds} = \frac{1}{2}\mu C_{ox}\frac{W}{L}(V_{gs} - V_t)^2, \tag{2.3}$$

where μ is the channel mobility, W and L are the width and length of the channel region, respectively, V_{gs} is the gate-source potential, and V_t is the threshold voltage. Equations 2.2 and 2.3 reveal that reducing the lateral (L) and vertical (t_{ox}) dimensions of the device increases the current flow between the drain and source. Intuitively, this is because reducing t_{ox} increases C_{ox} and hence the amount of channel charge, and reducing L decreases the distance the channel charge must travel to conduct a current. Reducing the gate oxide thickness (t_{ox}) along with the channel length (L) also helps to maintain the gate electrode's control over short channel effects. Increased gate capacitance allows the gate potential to modulate more channel charge and is especially important as the supply voltage scales down. Much of the progress in Si microelectronics has been driven by the ability to continually shrink these and other critical dimensions of the MOSFET to increase performance and decrease die area, a process referred to as scaling [3].

2.2 Recent gate oxide scaling trends

The gate oxide has been aggressively scaled in recent generations. Figure 2.3 shows extrapolated gate oxide scaling targets based on published data from recent Intel technologies [4]. The technology node refers to the smallest poly-Si gate length which can be defined by photolithography and roughly corresponds to the minimum channel length for a given process technology. A more complete list of projected transistor parameters is given in Table 2.1. The predictions are based on extrapolations of published state-of-the-art 180nm technologies assuming channel length, supply voltage, and gate oxide thickness scaling factors of 0.7, 0.8, and 0.8, respectively [5-7]. These projections, representative of the current targets for high-performance logic technology, aggressively outpace those

compiled in the 2000 update of the International Technology Roadmap for Semiconductors (ITRS), as shown in Table 2.2 [1].

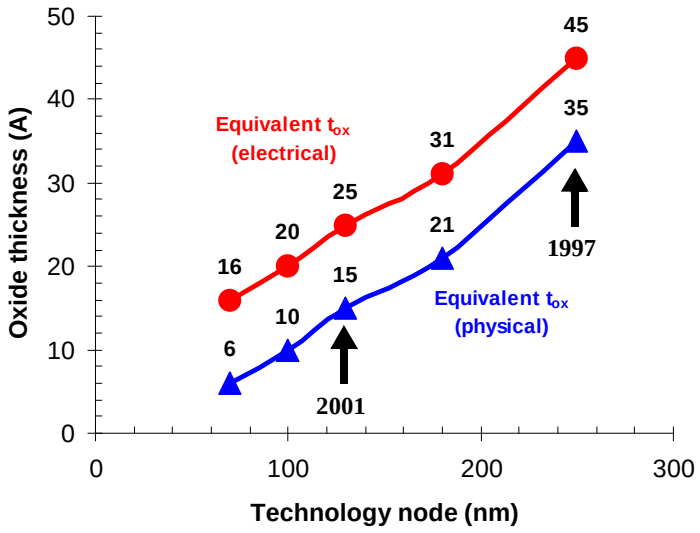

Figure 2.3 Extrapolated gate oxide scaling trend for recent CMOS technologies.

Table 2.1 Projected transistor parameters for future technology generations.

Generation (nm)	**180**	**130**	**100**	**70**	**Scaling factor**
L_{gate} (nm)	100	70	50	35	0.7x
Vdd (V)	1.5	1.2	1.0	0.8	0.8x
T_{ox}, electrical (A)	31	25	20	16	0.8x
T_{ox}, physical (A)	21	15	10	6	0.8x
I_{off} at 25°C (nA/um)	20	40	80	160	2x

Table 2.2 Selected excerpts from the 2000 update of the International Technology Roadmap for Semiconductors.

Year **Technology Node**	**1999** **180nm**	**2001** **130nm**	**2004** **90nm**	**2008** **60nm**	**2011** **40nm**	**2014** **30nm**
L_{gate} (nm)	120	90	70	45	32	22
T_{ox}, physical (A)	19-25	15-19	12-15	8-12	6-8	5-6
Gate leakage at 100°C (nA/um)	7	10	16	40	80	160
				Solutions unknown		

The two data sets in Figure 2.3 refer to the equivalent electrical and physical thickness of the gate oxide. The equivalent oxide thickness (EOT) refers to how thin a pure SiO_2 layer would need to be in order to meet the gate capacitance requirements of a given technology. In a modern MOSFET device, the gate oxide behaves electrically as if it were 8-10 $\mathring{A}$ thicker than its physical thickness, because depletion in the poly-Si gate and quantization in the inversion layer each extend the centroids of charge modulated by the gate voltage by 4-5 $\mathring{A}$ [8].

From Figure 2.3, it is clear that the physical thickness of the gate oxide is rapidly approaching atomic dimensions. The 250nm technology, which entered volume production in 1997, used an SiO_2 layer with approximately 40 $\mathring{A}$ physical t_{ox}, corresponding to approximately 20 monolayers of SiO_2. In contrast, the 100nm and 70nm technologies, scheduled for production in the next 5 to 10 years, will require gate capacitance values achievable only with SiO_2 layers as thin as 10 $\mathring{A}$ and 7 $\mathring{A}$, respectively, to guarantee proper device operation. A 10 $\mathring{A}$ film consists of only three to four monolayers of SiO_2.

2.2.1 Gate leakage and static power dissipation

A significant consequence of aggressively scaling the gate oxide is the resulting direct tunneling of carriers through the potential barrier presented by the insulator layer. As

illustrated in Figure 2.2(b), when the thickness of the potential barrier becomes less than approximately $30\,\mathring{A}$, substantial tunneling currents can flow through the gate oxide, leading to large static power dissipation. In addition, the gate and channel regions are no longer isolated from each other when tunneling occurs. Recent studies have shown that gate leakage can significantly impact circuit performance as a consequence, especially for analog and dynamic logic circuits [9].

Figure 2.4 shows extrapolated trends in power dissipation for high-performance CMOS logic based on published data from recent Intel technologies [4,10]. Both active and static power components are shown. Traditionally, the main source of power dissipation in CMOS circuits has been active switching, which depends on the rate at which node capacitances are charged and discharged,

$$P_{active} = NCV^2 f. \tag{2.4}$$

N is the number of switching transistors, C is the total switched capacitance, V is the supply voltage, and f is the frequency of operation. The observed increase in active power with each generation reflects the trend towards higher levels of integration and higher frequency of operation, which more than offsets the reduction in device capacitance and supply voltage. Much more alarming is the rapid increase in static (i.e. standby) power dissipation beyond the 180nm technology node. Static power is primarily due to subthreshold (I_{off}) and gate (I_{gate}) leakage currents. The extrapolation of the I_{gate} component is based on quantum mechanical modeling of gate tunneling currents through ultra-thin SiO_2 layers by Lo *et al* [8,11]. As shown in Figure 2.4, standby power has been increasing much more rapidly than active power in recent generations, and if current trends continue, standby power will actually surpass active power beyond the 70nm generation. Clearly, the exponential increase in the gate leakage, which arises from direct tunneling of carriers through the gate oxide, presents a serious limit to future CMOS scaling.

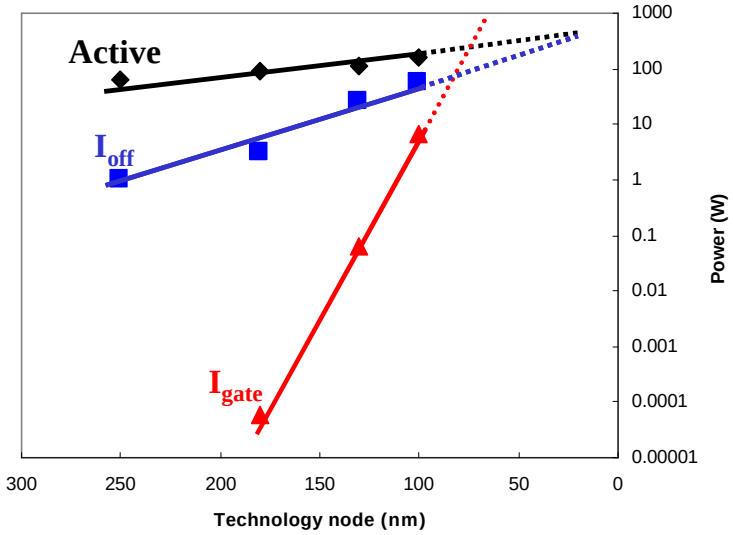

Figure 2.4 Extrapolated trend of active and leakage power dissipation for state-of-the-art CMOS technologies.

2.2.2 Scaling limit of SiO_2

In addition to limitations arising from static power dissipation, there has recently been great interest in determining if a more fundamental limit to scaling SiO_2 exists. One of the most convincing experiments which demonstrated that such a fundamental limit indeed exists is the work of Muller *et al* from Bell Labs [12,13]. Using a scanning transmission electron microscope (STEM) probe with $2\,\mathring{A}$ resolution, they studied the chemical composition and electronic structure of oxide layers as thin as 7-12 $\mathring{A}$ through detailed electron-energy-loss spectroscopy (EELS) measurements. By moving the probe site-by-site through the ultra-thin SiO_2 layers, they mapped the local unoccupied density of electronic states, which provides insight into the local energy gap of the material, as a function of the probe position. In their work, the local energy gap was given by the separation between the highest occupied and lowest unoccupied states. They found that three to four monolayers of SiO_2 were needed to ensure that at least one monolayer maintained a fully bulk-like bonding environment, giving rise to the wide, insulating

bandgap of SiO_2. Since the first and last monolayers form interfaces with Si and poly-Si respectively, they have bonding arrangements intermediate to those of bulk Si and bulk SiO_2 and hence have energy gaps smaller than that of bulk SiO_2. Based on these insights, Muller *et al* concluded that the fundamental scaling limit of SiO_2 is likely to be in the range of 7 to 12 $\mathring{A}$. Another important insight from their study was that for a 10 $\mathring{A}$ oxide, a 1 $\mathring{A}$ increase in the root-mean-square (RMS) interface roughness can lead to a factor of 10 increase in the gate leakage current, showing that the growth of such thin layers must be precisely controlled on atomic scales.

There has been remarkable agreement between experiment and theory regarding the scaling limit of SiO_2. Theoretical studies by Tang *et al* employing a Si/SiO_2 interface model based on the β-cristobalite form of SiO_2 showed that the band offset at the interface degraded substantially when the SiO_2 layer was scaled to less than three monolayers [14]. The large reduction in the band offset was attributed to a reduction in the SiO_2 bandgap and also suggested 7 $\mathring{A}$ as the scaling limit of SiO_2. A more recent study by Kaneta *et al* using a Si/SiO_2 interface model based on β-quartz SiO_2 directly computed the local energy gap as a function of position through the interface [15]. While the transition from bulk Si to bulk SiO_2 in their model was structurally abrupt, it was found that the full bandgap of SiO_2 was not obtained until the second monolayer of SiO_2 was reached. Again, these calculations suggest that approximately 7 $\mathring{A}$ of SiO_2 is the minimum required for substantial band offsets to develop at the interface, indicating the formation of a large bandgap.

Thus, both experiment and theory suggest that the bulk properties of SiO_2, including the wide, insulating bandgap needed to isolate the gate and channel regions, cannot be obtained for films less than 7 $\mathring{A}$ thick. Since technology roadmaps predict the need for sub-6 $\mathring{A}$ gate oxides in future generations, it is unlikely, both from static power dissipation and fundamental materials science points of view, that SiO_2 will scale beyond the 70nm generation.

2.3 High-*k* gate dielectrics

As an alternative to continuing to scale SiO_2, recent effort has focused on the development of alternative high-*k* gate dielectrics. Recall that the traditional approach to scaling the gate dielectric has been to reduce t_{ox} to increase C_{ox},

$$C_{ox} = \frac{k_{ox}\varepsilon_o}{t_{ox}}. \tag{2.5}$$

But now that gate leakage currents due to direct tunneling have reached unacceptably high levels, the more recent high-*k* approach is to increase the physical thickness of the film ($t_{high\text{-}k}$) to reduce the tunneling currents, yet at the same time obtain higher values of gate capacitance by using a dielectric material with a higher dielectric constant ($k_{high\text{-}k}$) relative to SiO_2,

$$C_{high-k} = \frac{k_{high-k}\varepsilon_o}{t_{high-k}}. \tag{2.6}$$

Over the past several years, a wide variety of high-*k* dielectrics have been investigated as possible replacements for SiO_2. Compared to just two or three years ago, a much shorter list of candidates is still being pursued today, due to the stringent requirements placed on the MOS dielectric material. In considering candidate gate dielectrics, it should be recalled that the dominance of the Si MOSFET over competing technologies has largely been attributed to the high quality of thermally grown SiO_2 and the resulting Si/SiO_2 interface. Other substrate materials provide higher intrinsic carrier mobilities or concentrations, yet none can match the electrical performance of the Si/SiO_2 interface. Not surprisingly then, the most stringent requirements arise from the need to develop an alternative dielectric material whose Si interface properties match the high quality of the Si/SiO_2 interface.

In the following sections, some of the important materials properties required of high-*k* dielectrics are reviewed. Such considerations lead to the conclusion that only a few basic classes of materials are capable of meeting the requirements for a replacement dielectric material. Several excellent review papers discuss these and other material considerations

for high-*k* dielectric applications in further detail [16-18]. A particularly important consideration is that the chosen high-*k* dielectric be scalable to future technology generations. Because of the immense costs associated with developing a replacement material for SiO_2, which benefits from nearly 30 years of research, the industry requires a material which will not only meet the requirements for the upcoming 100nm or 70nm technologies, but can also be scaled to end-of-the-roadmap technology nodes.

2.3.1 Target dielectric constant

To first order, a high-*k* film can be physically thicker than a pure SiO_2 layer by the ratio of its dielectric constant to that of SiO_2, and still provide the same gate capacitance, since

$$C_{ox} = \frac{k_{ox}\varepsilon_o}{t_{ox}} = C_{high-k} = \frac{k_{high-k}\varepsilon_o}{t_{high-k}} \tag{2.7}$$

and

$$t_{high-k} = \left(\frac{k_{high-k}}{k_{ox}}\right) t_{ox}, \tag{2.8}$$

thus potentially reducing direct tunneling currents substantially. Equation 2.8 is often expressed in terms of the equivalent oxide thickness (EOT) described in Section 2.2. In the context of high-*k* dielectrics, EOT is defined as the thickness of a pure SiO_2 layer which provides the same gate capacitance as a high-*k* layer,

$$EOT = t_{ox} = \left(\frac{k_{ox}}{k_{high-k}}\right) t_{high-k}. \tag{2.9}$$

Recall from Figure 2.3 that the gate capacitance targets for the upcoming 100nm and 70nm technologies require dielectrics with physical EOT values of $10\,\mathring{A}$ and $6\,\mathring{A}$, respectively. At first glance, it would seem that an arbitrarily high *k*-value would allow a substantially thick dielectric film to meet very small EOT targets. In practice, the extreme gate thickness-length aspect ratio that would result from a very high *k*-value and hence a very thick insulator leads to fringing field effects which undermine the gate electrode's

ability to maintain control of the channel. Device simulations have explored the impact of large *k*-values on threshold voltage roll-off and subthreshold swing to determine the upper range of desirable dielectric constants, which generally is believed to be on the order of 30 to 50 [19]. The lower range of acceptable dielectric constants depends on the EOT requirements of a given technology generation. It is generally believed that pure or nitrided SiO_2 with dielectric constants close to 4 will provide physical EOTs down to about 16 $\mathring{A}$; near-term alternatives such as Si_3N_4 or oxynitride stacks with nitrided SiO_2 interfaces with *k*-values near 7 will provide physical EOTs down to about 11 $\mathring{A}$; and pure metal oxides or pseudo-binary alloys of metal oxides with dielectric constants in the range of 15 to 25, providing a factor of four to six improvement over SiO_2, will provide physical EOTs down to about 6 $\mathring{A}$ [20].

It should be noted that some of the near-term materials such as Si_3N_4 and the metal oxide Al_2O_3 are attractive from the point of view of integration, since substantial experience and equipment infrastructure for processing both materials exist. Due to the relatively low gains in the dielectric constant relative to SiO_2, however, these materials are likely to be intermediate solutions at best. It is also worth mentioning that the ferroelectric class of materials which has been pursued for 1Gb and beyond dynamic random access memory (DRAM) storage capacitors provide *k*-values in the range of 100 to 1000, far in excess of the requirements for a gate dielectric [16]. In addition, ferroelectric materials generally require a complex composite structure to promote stability and adhesion to adjoining layers, so that using them as transistor gate dielectrics is not feasible. Hence, substantial new investments in materials research and technology development are needed, above and beyond the existing efforts in the DRAM community, to realize alternative gate dielectrics for logic technologies.

Many high-*k* materials consist of oxides and alloys of d-electron transition metals. Representative transition metal oxides include: column 3B materials such Y_2O_3 and La_2O_3; column 4B materials such as ZrO_2 and HfO_2; and column 5B materials such as Ta_2O_5. It is well-known that the static (i.e. low frequency) dielectric constants of such

metal oxides have significant electronic and ionic contributions at the frequencies of interest [21]. The electronic contribution arises from the polarization of electrons in response to an applied electric field, whereas the ionic contribution depends on the displacement of the ions themselves in response to an electric field. To first order, the additional shells of electrons in a heavy transition metal compared to a lighter atom allow for greater electronic polarization for a given electric field strength. It has also been observed that the d-electron metal transfers nearly all of its valence electrons to the oxygen atom, resulting in increased ionicity and hence polarization. In addition, the bonding between many d-electron transition metals and oxygen exhibit a softening of the phonon mode. In other words, the natural vibration frequency associated with the metal-oxygen bond is lowered. This allows the relatively low frequency excitation common in microelectronics applications to couple into the vibrational mode, leading to large displacements of the metal atom. The ability to model both the electronic and ionic components of the dielectric response is thus important for investigation of high-*k* materials. Different approaches to computing the dielectric constant are compared in Section 3.3.1.2.

In addition to pure transition metal oxides, there is also considerable interest in pseudo-binary alloys for high-*k* applications. Representative examples include the silicate system, such as $ZrSi_xO_y$, which can be thought of as an alloy between the pure metal oxide ZrO_2 and SiO_2, $(ZrO_2)_x(SiO_2)_{1-x}$; and the aluminate system, such as $LaAl_xO_y$, which is an alloy between La_2O_3 and Al_2O_3, $(La_2O_3)_x(Al_2O_3)_{1-x}$. The motivation for the use of these alloys over pure metal oxides arises from their interface properties with Si, as described in Section 2.4.

2.3.2 Bandgap and band offsets

Since an important function of the gate dielectric is to isolate the gate terminal from the current-carrying channel region, it needs to be a good insulator. SiO_2 provides a wide bandgap on the order of 9eV, substantially larger than the 1eV bandgap of Si. A closely

related property is the height of the potential barrier presented to tunneling electrons from the conduction band and to tunneling holes from the valence band. At the Si/SiO_2 interface, these band offset energies are relatively symmetric, so that barriers on the order of 4eV are presented to both electrons and holes. Any degradation of the bandgap results in lower band offset energies which compromise the potential tunneling reduction obtained by using a material with a higher dielectric constant and hence a physically thicker film.

It has been observed that most high-*k* materials have smaller bandgaps relative to SiO_2. Figure 2.5 illustrates the approximately inverse relation between bandgap and static dielectric constant obeyed by a number of representative high-*k* dielectrics. This behavior is expected qualitatively since stronger polarizability implies weaker bonding, and weaker bonding implies a smaller separation between bonding and antibonding energies [22]. The implied tradeoff between dielectric constant and bandgap severely limits the applicability of candidate materials at the upper range of target dielectric constants. For example, early

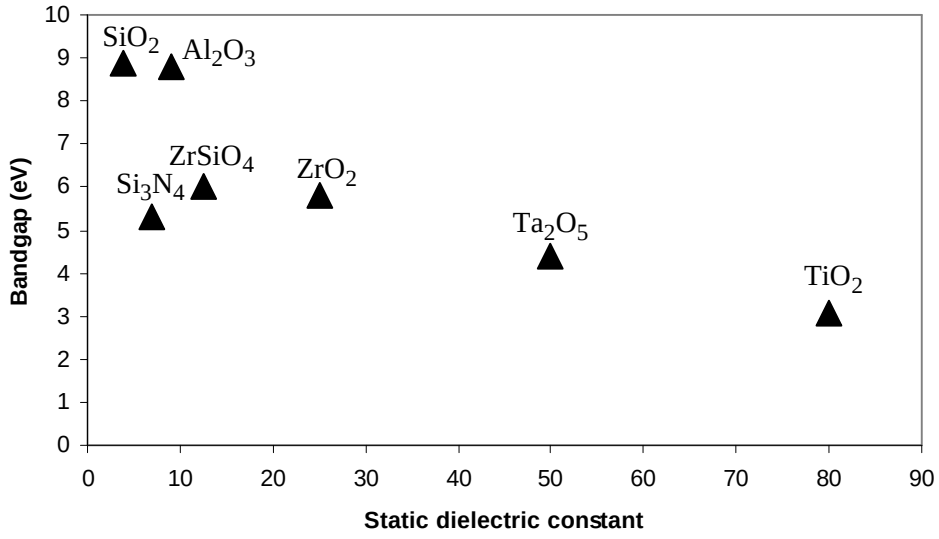

Figure 2.5 Plot of bandgap vs static dielectric constant for representative high-*k* gate dielectric materials.

high-*k* efforts focused on Ta_2O_5 and TiO_2, since they provided large dielectric constants and substantial processing experience with the materials existed from DRAM applications [23-26]. However, their bandgaps are substantially smaller than that of SiO_2, with estimated values of 4.5eV and 3.5eV for Ta_2O_5 and TiO_2, respectively [17]. Interestingly, Al_2O_3 presents an exception to this general trend and provides approximately twice the *k*-value of SiO_2 while maintaining a large bandgap. Limitations arising from the apparent tradeoff between the dielectric constant and the bandgap for the silicate system are investigated in Chapter 5.

2.3.3 Si interface properties

The feasibility of any high-*k* dielectric ultimately depends on the quality of its interface with Si. Two particularly important interface considerations are thermal stability and defect formation. Many of the early metal oxides such as Ta_2O_5 and TiO_2 which were pursued because of their previous use in DRAM processes have been found to be thermally unstable in direct contact with Si [24,26,27]. For both materials, reactions have been observed in which thick interfacial layers form between the metal oxide and the Si substrate. Specifically, Alers *et al* observed the formation of a 2.0nm thick interfacial region after Chemical Vapor Deposition (CVD) of Ta_2O_5 on HF-last-Si at 400°C [24]. Similar observations of interfacial reaction have been made for TiO_2 films deposited directly on HF-last-Si [26]. Since the channel transport properties were determined by nominally Si/SiO_2-like interfaces for both materials, reasonable channel mobilities were obtained. The Si/SiO_2 interface is known to have a very low density of interface states arising from unsaturated surface bonds and other electrically active imperfections. Interface states lead to degradation of on-current, since carrier mobility is limited by scattering at the interface due to the strong vertical electric fields present in the channel. In the case of the TiO_2 device, deliberate efforts to suppress the growth of the interfacial layer led to substantial charging and degradation of peak channel mobility from 150cm^2/V-sec to 60cm^2/V-sec.

For both Ta_2O_5 and TiO_2, the formation of an interfacial oxide layer appears inevitable and necessary to maintain good transport properties at the Si interface. In fact, interfacial reaction is expected for these materials based on analysis of equilibrium phase diagrams [17]. While it is difficult to directly determine the chemical composition of such thin layers, it is generally believed that an SiO_2-like layer with a relatively low dielectric constant forms, as illustrated by Figure 2.6. The formation of an interfacial low-*k* layer between the Si substrate and the high-*k* film is highly undesirable, since then the gate dielectric appears electrically as a series capacitance whose effective capacitance is less than that of the high-*k* layer alone,

$$\frac{1}{C_{eq}} = \frac{1}{C_1} + \frac{1}{C_2}. \tag{2.10}$$

Assuming that the interfacial layer has the dielectric properties of SiO_2, Equation 2.10 can be re-written in terms of the following relation for the EOT of the dielectric stack,.

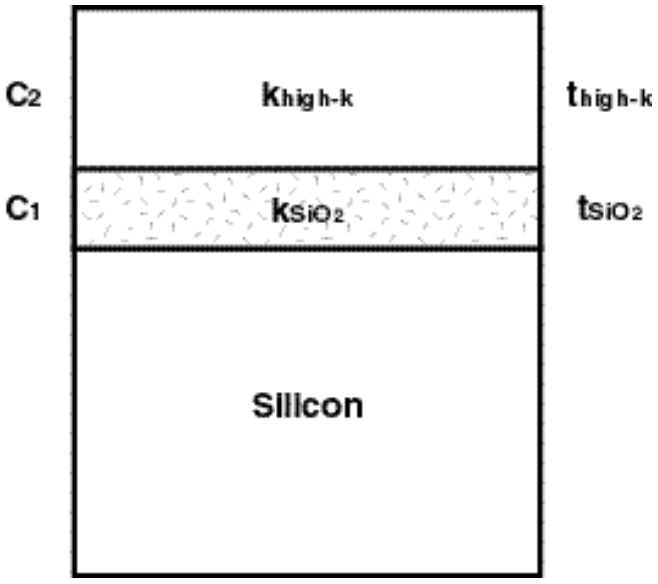

Figure 2.6 Diagram illustrating a high-*k* gate dielectric stack with a low-*k* interfacial layer.

$$t_{eq} = t_{SiO_2} + \left(\frac{k_{SiO_2}}{k_{high-k}}\right) t_{high-k} \quad (2.11)$$

For a given EOT (t_{eq}) target, any non-zero t_{SiO2} reduces the thickness of the high-*k* film which can be used, thus increasing the tunneling transmission through the stack. Furthermore, the minimum EOT can never be less than t_{SiO2}, so that the interfacial oxide layer limits the maximum achievable capacitance of the gate stack.

2.4 Zirconium and hafnium silicates

Zirconium (Zr) and hafnium (Hf) silicates are promising high-*k* dielectrics developed largely to overcome the interface stability issues suffered by many high-*k* binary metal oxides [28-30]. Ternary phase diagrams of the Zr-Si-O system reveal that the binary metal oxide ZrO_2 as well as the compound silicate $ZrSiO_4$ should be thermodynamically stable in direct contact with Si. Since Zr and Hf are isoelectronic elements, it is expected that HfO_2 and $HfSiO_4$ should also be stable on Si.

In practice, interface reactions, much like those described in the previous section for other metal oxides, have been observed for nearly all ZrO_2 and HfO_2 films deposited directly on Si [26,31,32]. High resolution transmission electron microscope (HRTEM) measurements by Campbell *et al* revealed that interfacial layers of 0.9nm and 1.2nm thickness were formed when depositing ZrO_2 and HfO_2 directly on Si, respectively [26]. Medium energy ion spectroscopy (MEIS) and x-ray photoelectron spectroscopy (XPS) analysis showed that the interfacial layer was SiO_2-like, not a silicate. In contrast, Lee *et al* found that ZrO_2 and HfO_2 films deposited directly on Si using a magnetron sputtering technique gave rise to a silicate interfacial layer [31]. Copel *et al* also found that ZrO_2 deposition by atomic layer chemical vapor deposition (ALCVD) on HF-last-Si led to discontinuous nucleation with islands of ZrO_2 interspersed along the Si interface [32]. Atomic force microscopy also revealed a large RMS roughness of 5.7 $\mathring{A}$ along the interface.

The variability in the interfacial layer following ZrO_2 and HfO_2 deposition leads to the conclusion that the growth of such layers is difficult to control. Instead, recent efforts toward integrating ZrO_2 and HfO_2 films have focused on first growing a high quality, well controlled, ultra-thin SiO_2 layer prior to ZrO_2 deposition. Perkins *et al* deposited ALCVD ZrO_2 films on chemically grown oxides and obtained EOT < $14\,\mathring{A}$ [33]. Having an underlying SiO_2 layer also leads to the desirable electrical properties of a Si/SiO_2 interface which helps to maintain high channel carrier mobilities. Of course, the minimum EOT is still limited by the extent of the interfacial SiO_2 layer as described previously.

Another potential problem with ZrO_2 and HfO_2 is that they have been observed to crystallize at relatively low temperatures. Polycrystalline films may exhibit high leakage paths along grain boundaries which act as trapping centers. Thus, in general, amorphous dielectrics which resist recrystallization up to relatively high temperature are desirable for gate dielectric applications.

To overcome the challenges of pure ZrO_2 and HfO_2 films, Wilk and Wallace proposed the use of Zr and Hf silicates as promising high-*k* gate dielectrics [17,28-30]. By alloying two different oxides, such as ZrO_2 and SiO_2 in the case of Zr silicate, $(ZrO_2)_x(SiO_2)_{1-x}$, they believed that it may be possible to retain the desirable properties of both oxides while eliminating the undesirable properties of each. By explicitly incorporating SiO_2 during deposition of ZrO_2 precursors, the driving force for reaction between the dielectric and the Si substrate is reduced, so that the interface is more likely to behave like the desirable Si/SiO_2 interface. This allows better control of the Si interface properties. It is generally believed that silicate deposition results in a single, uniform high-*k* layer in direct contact with Si. Combining a poly-crystalline film like ZrO_2 with an amorphous one like SiO_2 also leads to an amorphous silicate phase.

At the same time, by incorporating some amount of ZrO_2 into the SiO_2 film, the enhanced polarizability of Zr-O bonds relative to Si-O bonds leads on average to a higher dielectric constant for material. While many different silicate systems are possible, column IVB elements such as Zr and Hf are expected to substitute well for Si atoms, thus

reducing the possibility of forming dangling (i.e. unsaturated) bonds at the Si interface. The notion of doping SiO_2 with Zr or Hf also leads to a natural scaling scenario for the silicate system. By progressively increasing the Zr or Hf concentration, the *k*-value can be steadily increased, up to a limit, to meet the gate capacitance requirements for future technology generations.

The increased control over interface properties comes at the expense of a lower dielectric constant relative to pure ZrO_2 or HfO_2. Depending on the metal concentration, the dielectric constant is believed to scale between 4, corresponding to pure SiO_2, and approximately 15 to 20 for stoichiometric $ZrSiO_4$ or $HfSiO_4$, since pure ZrO_2 and HfO_2 are thought to have dielectric constants close to 25 and 35, respectively [30]. Si-rich compositions are preferred to maintain thermal stability with the Si substrate. Preliminary theoretical work by Jun *et al* suggests that both $ZrSiO_4$ and $HfSiO_4$ have dielectric constants near 12, toward the lower end of the above range [34]. As described in Section 2.4.3, it is not yet clear exactly how the dielectric constant scales between these extremes.

The lower dielectric constant of the silicates relative to the pure metal oxides does not necessarily imply a smaller gate capacitance. To illustrate this point, Figure 2.7 shows two possible gate stack structures. Figure 2.7(a) depicts a pure metal oxide (e.g. ZrO_2 with k = 25) which requires a 5 $\mathring{A}$ interfacial SiO_2 layer with k = 4. Figure 2.7(b) shows a silicate layer (e.g. Zr silicate with k = 16) which forms a single, uniform high-*k* layer in direct contact with Si. Using Equations 2.9 and 2.11, it is straightforward to show that both gate stack structures achieve the same equivalent gate capacitance, corresponding to EOT values of 10 $\mathring{A}$. Surprisingly, the lower-*k* silicate layer can be physically thicker than the higher-*k* ZrO_2 layer, so that less tunneling is expected for the silicate stack. This is due to the fact that the silicate is believed to form a single, uniform high-*k* layer, thus avoiding the formation of a low-*k* interfacial region.

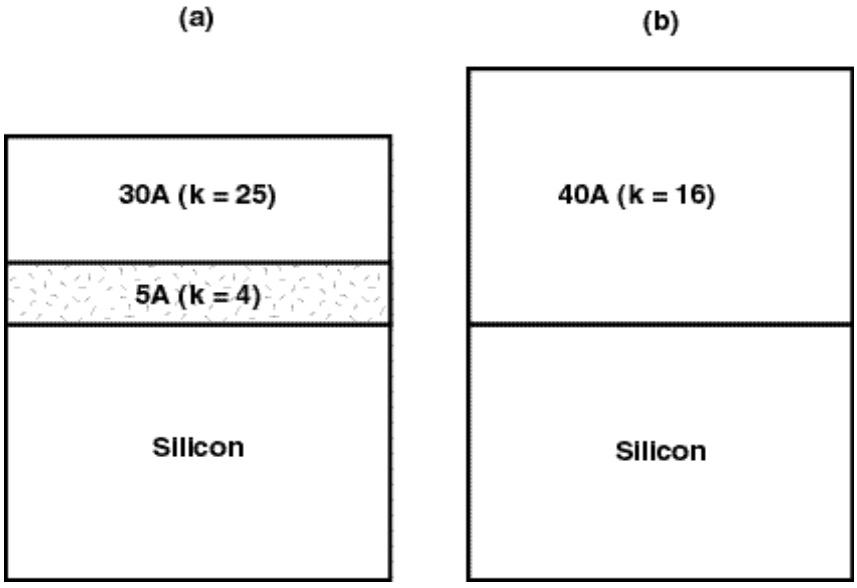

Figure 2.7 (a) A gate dielectric stack formed of a high-*k* layer and a low-*k* interfacial layer. (b) A stack formed of a single, uniform layer with intermediate *k*-value. Both stacks provide 10A EOT.

2.4.1 Atomic structure

Zircon ($ZrSiO_4$) is the only experimentally known crystalline silicate and hence has served as an important reference model upon which early understanding of silicate structure has been based [35]. The tetragonal unit cell consists of parallel chains of edge-sharing four-fold coordinated SiO_4 and ZrO_4 units. A cross-section of the atomic structure is shown in Figure 2.8. The dashed lines indicate second nearest neighbor bonds between Zr atoms of a given chain and O atoms from a parallel chain. Similar bonds exist with additional chains in and out of the plane, so that Zr atoms are eight-fold coordinated by O atoms.

An important experimental observation is that the local atomic structure, namely the Zr coordination, depends on the concentration of Zr in the silicate film. Based on extended x-ray absorption fine structure spectroscopy (EXAFS) measurements of Zr silicate films, Lucovsky *et al* have found that the average Zr coordination increases from 4.5 ± 1 for samples with ~3.3 atomic percent Zr to 7.2 ± 1 for samples with ~8.3 atomic percent Zr

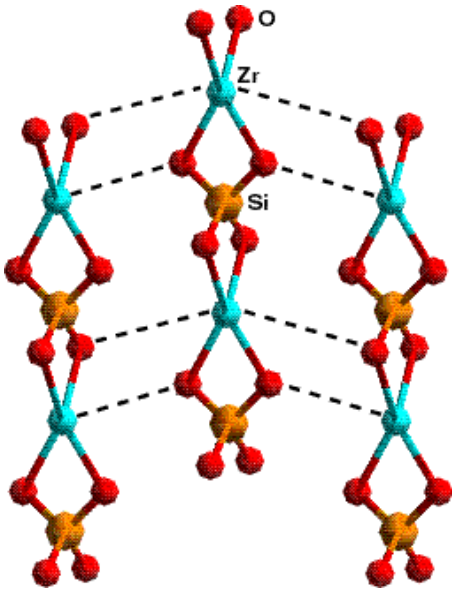

Figure 2.8 Ball-and-stick model of a plane of $ZrSiO_4$. The dashed lines indicate bonds between neighboring ZrO_4 units.

[36]. Since the initial introduction of silicates into an advanced CMOS process will likely employ a relatively low Zr or Hf concentration, assuming tetrahedrally bonded Zr units is a reasonable starting point for modeling. The silicate then consists of corner-sharing SiO_4 and ZrO_4 tetrahedra, whose structure may be modeled by selectively doping various crystalline forms of SiO_2 with Zr or Hf. However, at higher concentrations, eight-fold coordinated Zr bonding units characteristic of $ZrSiO_4$ should be explicitly modeled. Unfortunately, it is difficult to form a well-defined interface between $ZrSiO_4$ and Si that allows controlled study of the interface structure. Therefore, all interface models considered in Chapters 4 and 5 assume tetrahedral bonding around the Zr or Hf atom. While it cannot be directly employed in interface calculations, the bulk properties of $ZrSiO_4$ are investigated and compared to those of silicate models with tetrahedrally coordinated Zr atoms in Chapter 5.

2.4.2 Interface structure

Wilk and Wallace have performed extensive XPS measurements on Zr and Hf silicate films deposited directly on Si to investigate the chemical composition of such films [30]. As expected from the atomic structure of $ZrSiO_4$ just discussed, the XPS measurements indicated the presence of Zr-O, Hf-O, and Si-O bonding in the films. They observed no evidence for the formation of Zr-Si or Hf-Si bonding, which would have indicated phase separation of the silicate into silicide and oxide phases. These measurements, in addition to healthy capacitance-voltage (C-V) curves obtained from MOS capacitor structures utilizing the silicate films, suggest that even at the interface, which is expected to be Si-rich, silicide phases containing Zr-Si or Hf-Si bonds do not form. While fortunate from the point of view of device electrical properties, the physical mechanism preventing the formation of silicide-like bonds at the Si interface is largely unknown. Model interface calculations performed to clarify these and other issues related to the structure of the Si/ silicate interface will be described in Chapter 4.

2.4.3 Electronic structure

In the case of pseudo-binary alloys, it is not yet clear how the dielectric constant will scale as the alloy composition is changed. For example, Figure 2.9 shows three possible ways the dielectric constant may scale for the Zr silicate system. One possibility is linear mixing from pure SiO_2 (k = 4) to stoichiometric $ZrSiO_4$ (k = 12-15). Commonly referred to as Vegard's law, such linear mixing is observed for a variety of physical properties in many alloy materials. Many alloys also exhibit sub-linear mixing behavior and experimental work has led some researchers to believe that the silicate system actually follows this trend [37]. Others have found evidence for super-linear scaling between the endmembers. In particular, Lucovsky and Rayner have shown that the three datapoints shown in Figure 2.9, which were extracted from published experimental work, can be fit by the upper curve [36]. The curve is based on a microscopic model of the silicate in which the dielectric behavior changes along with the average metal coordination as the

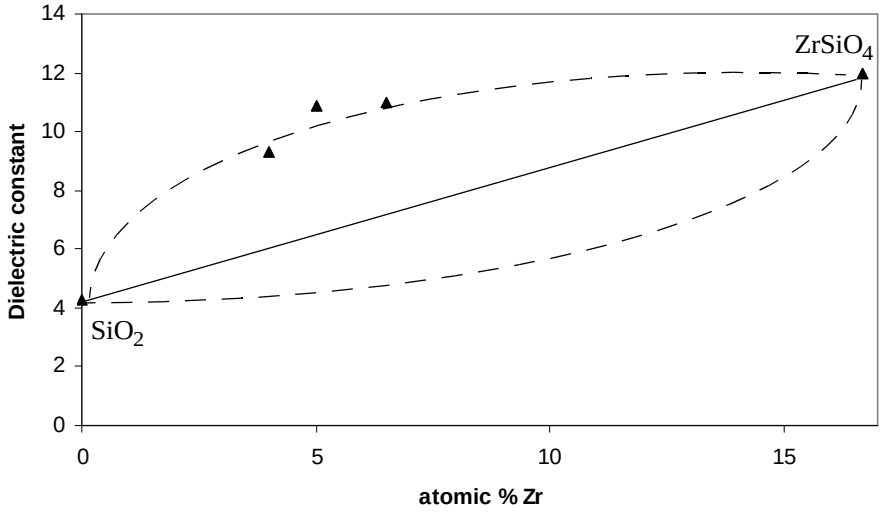

Figure 2.9 Possible scaling of Zr silicate dielectric constant. The symbols indicate measured values [36].

metal concentration is increased, as described in Section 2.4.1. Lucovsky's model is still controversial, especially since a number of fitting parameters were used to define the scaling trend. However, if the super-linear behavior turns out to be correct, it would imply that the dielectric constant of SiO_2 can be increased substantially by adding relatively small concentrations of Zr or Hf. Clarifying the scaling behavior is therefore an important task. Theoretical approaches to predicting the dielectric response are described in Section 3.3.1.2, along with some preliminary results for the Zr silicate system.

2.5 Summary

This chapter has reviewed recent trends in gate oxide scaling. The aggressive scaling requirements for upcoming technologies suggest that SiO_2 cannot be scaled beyond the 70nm generation. The desirable properties of alternative high-*k* dielectric materials have also been described. An important consideration is that the chosen dielectric material be scalable to future technology nodes. Of the various requirements, it is likely that achieving

a high quality interface with the underlying Si substrate will be the most stringent. This requirement has motivated the development of the silicate system, which is believed to form a high quality Si/SiO_2-like interface while eliminating the need for an explicit interfacial oxide layer, which limits the achievable EOT values of gate stacks employing pure metal oxides.

Chapter 3

Atomic Scale Modeling Theory

This chapter provides a review of atomic scale modeling theory. Based on the requirements for modeling high-*k* gate dielectrics, first principles density functional theory (DFT) is identified as the most promising method. The discussion closely follows the material we presented in Reference 38.

Section 3.1 reviews conventional approaches to modeling integrated circuit fabrication. The need to model and understand properties of novel materials motivates the use of atomic scale modeling methods, which can predict material properties based on microscopic interactions between atoms and electrons.

Section 3.2 reviews the main approaches to atomic scale modeling, including both classical and quantum mechanical methods. Examples of specific applications of each approach are described.

Section 3.3 considers the requirements for modeling high-*k* dielectrics and identifies DFT as the most promising approach. Important limitations of the DFT approach are also described, along with possible remedies for overcoming such limitations. Technical details of the atomic scale calculations presented in Chapters 4 and 5 are also provided.

3.1 Modeling for integrated circuits

Over the years, a hierarchy of models has been developed to support integrated circuit (IC) design and fabrication, as depicted in Figure 3.1. Since there is a tradeoff between the accuracy and computational cost of a given model, modeling generally requires a hierarchical approach. Across levels of the hierarchy, various abstractions are used to mask details of the underlying levels. For example, system designers typically specify the high-level functionality of a design at the register transfer level (RTL), which deals only with the logical implementation and hides the details of the underlying transistor implementation. This allows the high-level behavior of entire systems consisting of potentially hundreds of millions of transistors to be simulated and verified. Even within a given level, a hierarchy exists so that the cost and accuracy of models can be balanced to meet the requirements of a specific simulation. For example, process simulations for dopant diffusion employ increasingly complex models with additional parameters to account for higher-order effects which are quickly gaining first-order importance in scaled

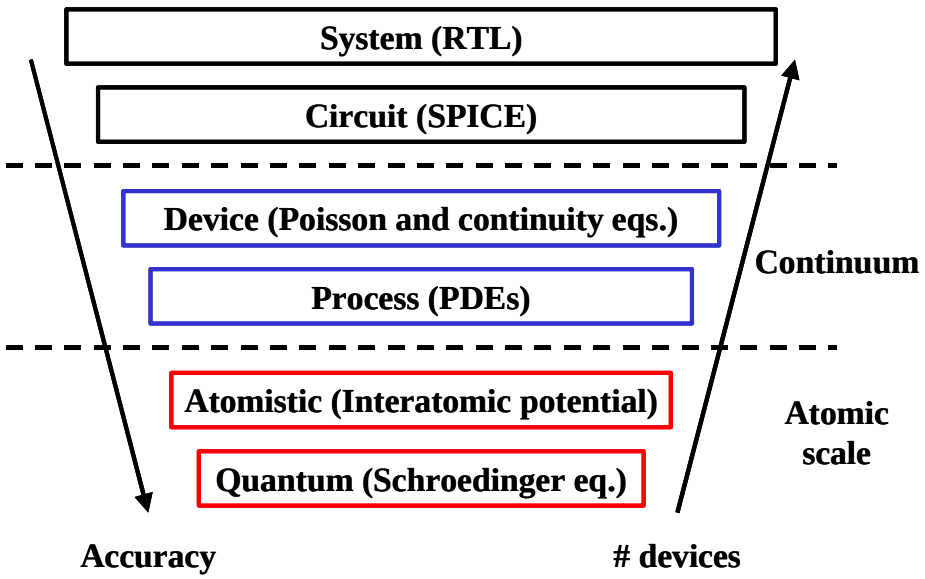

Figure 3.1 Hierarchy of models for IC design and fabrication

devices. A variety of model choices exist at the system, circuit, device, and process levels to tailor the accuracy of a model to the specific needs of a design.

The development of Si/SiO_2 technology has relied heavily upon conventional device and process simulators such as PISCES and SUPREM. These tools rely on a continuum description of materials and typically solve partial differential equations (PDE) governing such physical mechanisms as diffusion and oxidation to evaluate a device design or a fabrication process. These constitutive relations often have an empirical basis, so that material properties must be supplied as inputs to the simulation program, either from known experimental values or by treating them as explicit fitting parameters. The success of this approach for Si/SiO_2 can largely be attributed to the extensive data and insight gained from many decades of experimental work on the system. Extending this approach to the development of alternative gate dielectrics may be challenging, however, since the time and cost of populating an extensive knowledge database for each candidate material system are prohibitive.

In contrast, atomic scale modeling, which includes atomistic and quantum simulations, can actually predict material properties based on the microscopic interactions between atoms, in the case of atomistic simulation, or between electrons, in the case of quantum simulation. Atomic scale modeling is then a promising way to fill the knowledge voids of various high-*k* dielectrics by computationally screening potential materials and predicting their microscopic behavior. The predictive accuracy of atomic scale modeling comes at a substantial computational expense, so that only select features of an individual transistor can be modeled. The physical dimensions of modern CMOS devices are still too large to be modeled entirely at the atomic scale. However, some of the most critical dimensions of the device are rapidly approaching atomic dimensions, so that atomic scale modeling of those regions are becoming both necessary and feasible. A particularly good example is the ever-shrinking gate oxide described in Chapter 2. The gate oxide, which is only about $15\,\mathring{A}$ thick in today's 130nm technology, represents the smallest physical dimension of a scaled MOSFET.

3.2 Hierarchy of atomic scale models

Conventional device and process simulations rely on a PDE-based continuum approach which describes only the average, macroscopic properties of materials. In contrast, for atomic scale modeling, an explicit interaction rule between all atoms or between all electrons in the simulated system must be established. The vast array of atomic scale simulation methods can be classified into three major classes of modeling approaches: empirical interatomic potentials, tight binding, and density functional theory. Table 3.1 compares the main distinctions between these approaches. In turn, these approaches can be broadly classified into two main categories depending on how they model physical phenomena in the simulated system: classical and quantum mechanical.

Table 3.1 Classification of atomic scale computational models.

	Empirical interatomic potential	**Tight binding (TB)**	**Density functional theory (DFT)**
Classical or quantum model?	classical	quantum	quantum
Fitted parameters?	yes	yes	no
Electronic structure? (bands, gap states)	no	yes	yes
Basis set in expansion of wave function	n/a	minimal; atomic orbitals	complete; plane waves
Iterate to self-consistency?	n/a	no	yes
Computational cost relative to interatomic potential	1	10^2-10^3	10^5

3.2.1 Classical models

Classical atomic scale models do not explicitly take into account the role of electrons in determining material properties. Instead, physical mechanisms are described solely in

terms of the interactions between atoms in a classical ball-and-spring manner. The interaction energy is expressed by an interatomic potential energy function whose form is often derived empirically and thus makes use of fitted parameters. Because they are computationally efficient, interatomic potentials have been widely used in applications which require the collective behavior of large numbers of atoms to be simulated.

Classical potentials are often associated with molecular dynamics (MD). In an MD simulation, the dynamical trajectories of atoms governed by the forces predicted by interatomic potentials are followed as a function of time. State-of-the-art MD calculations on parallel machines have studied the dynamical properties of systems containing millions of atoms for applications as diverse as nanoelectronics and protein folding [39,40]. Interestingly, atomic scale modeling of biological or chemical systems is typically limited to classical MD approaches due to the relatively large physical dimensions of cellular phenomena, and widely used simulation packages for such applications are available [41]. Recently, MD simulations have also found increasing application in process modeling, notably in source-drain and channel engineering. Representative examples include the modeling of point defect diffusion and ion implantation damage [42,43].

The Si/SiO_2 system has been extensively modeled by interatomic potential approaches. Starting with the work of Stillinger and Weber, literally dozens of empirical potentials have been proposed for Si, including the well-known form due to Tersoff [44-46]. These potentials describe the covalent bonds of Si by fitting analytical formulations of the interaction energy to an extensive database of known Si properties. A number of potentials have also been developed to describe the SiO_2 system, based on the early work of Tsuneyuki [47,48]. It is well-known that SiO_2 has both covalent and ionic bonding character, and the Ewald sum is typically used to ensure rapid convergence of the interaction energy between charged ions in an infinite periodic solid [49]. Until recently, these potentials were only able to model bulk or surface phenomena in Si and SiO_2 separately, thus preventing direct study of the interface between Si and SiO_2. A recent potential developed by Watanabe extends the Stillinger-Weber formulation to enable

modeling of systems containing both Si and SiO_2 and has been used to study the large-scale structure of the Si/SiO_2 interface, including the effects of steps and terraces along the interface [50-52].

Classical interatomic potentials have two important shortcomings that may limit their use for alternative dielectric studies. First, because they are classical models which only take into account the interactions between atoms, they cannot describe properties arising from the electronic structure of a material, such as the bandgap and the dielectric constant. These are precisely the properties which need to be investigated for high-*k* dielectric applications. In addition, the extensive parameter fitting required to formulate an empirical potential is costly and time-consuming, and each model is generally only reliable for properties included in the fitting database. There is no straightforward way to extend an empirical potential formulation and parameter set extracted for Si or SiO_2 to alternative gate dielectric materials.

Much of the early effort in this research focused on the implementation of interatomic potential models for the Si/SiO_2 system within a molecular dynamics simulation package developed at Stanford [53]. However, due to the limitations just described, it was not possible to extend the Si/SiO_2 model formulations to the material systems of interest, such as the silicates. However, since that time, much more data on the silicate material has become available from both experimental and theoretical work, so that it may now be possible to parametrize a potential for the silicate system based on known material properties. Such a potential would be useful for predicting the large-scale structure of silicates which are beyond the computational limits of more rigorous methods. For example, it may be possible to investigate the structure of silicates in the amorphous phase or to consider phase separation phenomena through finite temperature MD simulations.

3.2.2 Quantum mechanical models

An important shortcoming of classical models is that they cannot describe the electronic structure of materials which arises from electron interactions. In contrast,

quantum mechanical models explicitly treat electron interactions by solving the Schroedinger equation, the governing equation of quantum mechanics. Quantum mechanics is the fundamental description of matter at the atomic scale and predicts macroscopic material properties almost exclusively in terms of the interactions of electrons. By starting with a fundamental description of materials, quantum mechanical approaches attempt to avoid the need to introduce empirical formulations and extensive fitting parameters.

Within this framework, the electronic structure of a material is represented by a wave function Ψ. To determine Ψ, one must solve the *N*-electron Schroedinger equation,

$$\left[\frac{-\bar{h}^2}{2m}\nabla^2 + V_{II} + V_{Ie} + V_{ee}\right]\Psi(\vec{r}_1, \ldots, \vec{r}_N) = \varepsilon\Psi(\vec{r}_1, \ldots, \vec{r}_N). \quad (3.1)$$

The first term on the left represents kinetic energy and V_{II}, V_{Ie}, *and* V_{ee} denote the potential energy arising from ion-ion, ion-electron, and electron-electron interactions, respectively. Most computational techniques expand Ψ in a pre-defined set of basis functions. Solving for Ψ is then analogous to determining the degree to which each basis function contributes to the overall wave function. The accuracy and cost of the calculation increase as the set of basis functions is made more complete.

When evaluating the Schroedinger equation, one generally invokes the Born-Oppenheimer approximation, which allows ionic and electronic degrees of freedom to be treated separately. Electrons are assumed to rearrange within the fixed potential field presented by stationary ions, which is reasonable since electron dynamics occur on substantially shorter time scales than those of the ionic cores.

3.2.2.1 Density functional theory

Density functional theory (DFT) refers to a specific technique used to rigorously solve the Schroedinger equation. This approach is often referred to as “first principles.” Direct solutions of the *N*-electron Schroedinger equation for a system more complicated than a couple of hydrogen atoms quickly become intractable due to the large number of free variables. The coupled electron-electron interactions also prevent a direct separation of

variables approach. DFT, which provides the foundation for the majority of modern first principles methods, provides a rigorous way to decouple the electron-electron interactions. By reformulating the problem in terms of the *ground-state* electron density, Hohenberg, Kohn, and Sham showed that one can replace Equation 3.1 with an exactly equivalent set of independent, one-electron Schroedinger equations (referred to as the Kohn-Sham equations) [54,55],

$$\left[\frac{-\hbar^2}{2m}\nabla^2 + V'_{II} + V'_{Ie} + V'_{ee}\right]\psi_i(\vec{r}) = \varepsilon\psi_i(\vec{r})\,;\ \mathrm{i} = 1, \ldots, \mathrm{N}. \tag{3.2}$$

The index *i* refers to different eigenstates of the solution. There are now *N* such equations for each electron in the system, and the primed potential energy terms depend on the ground state charge density,

$$n(\vec{r}) = \sum_i \left|\psi_i(\vec{r})\right|^2. \tag{3.3}$$

Iterative solutions become necessary, since the eigensolution ψ_i needs to be self-consistent with the V' potentials which depend on ψ_i through $n(\vec{r})$.

Using a formal proof based on the variational principle, Hohenberg and Kohn showed that the potential energy terms, and hence the Hamiltonian and correct many-body ground state, are a unique functional of the ground state charge density $n(\vec{r})$, giving rise to the name density functional theory [54]. It is important to recognize that the formalism only states that the potential is a functional of the ground state electron density and does not explicitly specify the form of the functional dependence. In particular, the dependence of the exchange-correlation energy of the electron-electron interaction on the ground state density are not known exactly. However, Kohn and Sham showed that if $n(\vec{r})$ varies slowly, the exchange-correlation energy can be expressed as a function of the local charge density and the exchange-correlation energy of a uniform electron gas of the same density [55]. This approximation is referred to as the local density approximation (LDA). Ceperley and Alder have numerically tabulated the exchange-correlation energy of a uniform electron gas through quantum Monte Carlo calculations, and a parametrization of

these values by Perdew and Zunger is commonly used in calculations which invoke the LDA [56,57].

Pseudopotentials are used to reduce the cost of evaluating the ion-electron interaction. The motivation behind pseudopotentials arises from the observation that electrons in a periodic solid feel a very strong potential near the ionic cores and a much weaker potential elsewhere. The wavefunction must remain orthogonal to the occupied states bound to the core of the atom, requiring that the wavefunction oscillate rapidly near the core. These oscillations are very expensive to model accurately and extend the size of the basis set considerably. Interestingly, the kinetic energy of the valence wavefunction due to the rapid oscillations nearly cancels the strong potential of the ionic cores, so that the net potential in the core region is rather weak. Based on these observations, a pseudopotential approaches zero energy at the outer edge of the core region, thus eliminating wavefunction oscillation in the core. Various conditions are placed to ensure that the resulting pseudo-wavefunction reproduces the all-electron wavefunction outside of the core region. One important condition is that of norm conservation, which requires that the total valence charge outside of the core region for the pseudo and all-electron wavefunctions agree exactly. A number of schemes have been proposed for constructing such pseudopotentials from first principles [58-60]. Finally, a plane wave basis is generally used to expand the valence wave function.

Early implementations iteratively diagonalized the set of *N* Equations 3.2 until self-consistency was achieved, a procedure which scaled as $O(N^3)$, making it prohibitively expensive to study more than a few tens of atoms. More recent approaches overcome the limitations of direct diagonalization by recasting the problem into an iterative search for the lowest energy configuration. Modern implementations include the Car-Parrinello simulated annealing scheme and the more efficient methods based on conjugate gradient energy minimization [61]. These methods typically scale as $O(N^2)$, since they are dominated by the cost of computing the Fast Fourier Transform, which scales as Nlog(N), and by wave function orthonormalization, which scales as $O(N^3)$.

Of the three approaches to computing the total energy of a system, DFT provides the highest level of predictive accuracy. It is generally observed that DFT predicts basic ground state structural properties such as lattice constant and bulk modulus to within a few percent of the experimental values, with no parameter fitting [62]. The major drawback of the DFT approach is its intense computational cost, which severely limits the size of the system that can be simulated. A survey of the literature indicates that practical DFT simulations involving metal oxides are currently limited to a few hundred atoms. The interested reader is referred to several excellent reviews of the density functional theory approach for further details [61,63].

3.2.2.2 Tight binding

The tight binding (TB) approach significantly reduces the cost of solving the single-electron Schroedinger equations (Equation 3.2) by making several key approximations. First, a minimal basis set of valence atomic orbitals ϕ_i is used to expand the wave function for each of the *N* electrons in the system, so that typically 10-20 times fewer basis functions are used in TB compared to DFT. Second, self-consistency in the eigensolution is neglected so that iterative solutions are no longer required. Lastly, all interactions are parameterized. The conventional approach diagonalizes the set of *N* parameterized Equations 3.2. Pioneering work by Harrison has led to a set of universal TB parameters for every element on the periodic table, assuming orthogonality between neighboring atomic orbitals [64,65]. There have been extensions to Harrison's work which use a more general non-orthogonal basis and achieve better accuracy for specific systems, at the cost of additional empirical parameters which need to be fit to experimental results [66]. TB generally scales as $O(N^3)$.

The accuracy with which the total energy can be predicted in a TB simulation depends strongly on the formulation being used and the system being modeled. Some TB schemes achieve an accuracy comparable to that of DFT for a specific material, but do so at the cost of employing extensive parameter fitting. For example, Kwon *et al*'s model for Si provides a particularly good description of point defect creation energies and has been

used to investigate interstitial-vacancy recombination in transient enhanced diffusion (TED) studies [67,68]. However, because it uses more than 20 fitting parameters specific to the Si system, there is no straightforward way to extend the model to describe other materials. Others, such as Harrison's universal TB formulation and its extensions can be applied to any material system, since only a few fundamental parameters are used to model the entire periodic table. However, since it achieves its universality by avoiding extensive empirical fitting for specific systems, the universal TB method gives predictions which are generally only qualitatively accurate. Therefore, there is an important tradeoff between extensibility and accuracy in TB models. Furthermore, due to the many approximations made in basic TB theory, its predictions are generally not as accurate as those of DFT. The benefit, however, is that TB is roughly 10^2 to 10^3 times less expensive than DFT.

3.3 First principles DFT as the method-of-choice

Almost every physically observable quantity is related to the total energy of a system or to differences in the total energy. The utility of atomic scale calculations lies in their ability to calculate the total energy of a system based on the microscopic arrangement of atoms and electrons within the material. For the high-*k* dielectric application, the total energy approach enables the determination of such quantities as vibrational frequencies, defect creation energies, impurity binding energies, and activation barriers. If quantum mechanical models are used, properties related to the electronic structure, such as band structures, dielectric constants, and defect energy levels, can also be computed.

It has already been argued that quantum mechanical approaches are necessary in order to investigate properties related to the electronic structure of the gate dielectric material. In particular, first principles DFT methods are well suited for the high-*k* dielectric problem, especially in the early stages of research when relatively little experimental data is available. First principles calculations can provide insight into the microscopic behavior

of novel materials without requiring empirical fitting to known properties. Moreover, first principles calculations can play an increasingly important role as the number of novel materials required for Si microelectronics continues to increase rapidly, as illustrated in Figure 3.2. While substantial limitations still exist, first principles calculations can potentially reduce the experimental burden of developing so many novel materials by computationally prototyping candidate materials for a variety of applications. In contrast, tight binding approaches may be less desirable in the very early stages, since they generally require extensive fitting of the parameter set in order to accurately model material properties. As the database of material properties is populated through experiments or first principles calculations, tight binding may become a more attractive approach due to its reduced computational burden.

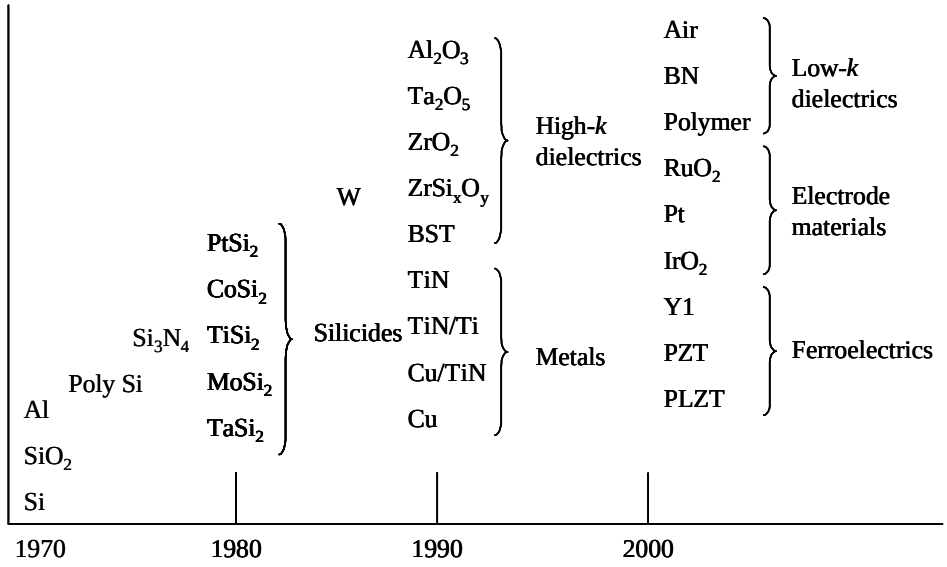

Figure 3.2 Timeline of novel materials for Si microelectronics [69].

3.3.1 Limitations of density functional theory

Although the DFT approach has the highest level of predictive accuracy, it has several important limitations. The most significant drawback is its intense computational cost, which limits both the length and time scales of phenomena which can be modeled.

Routine DFT simulations are typically limited to systems containing tens to hundreds of atoms. For the high-*k* application, it is important to note that materials consisting of transition metals and first-row nonmetals (e.g. nitrogen, oxygen) generally have sharply peaked valence states. These wavefunction peaks require a large number of basis functions to describe accurately, thus further limiting the size of the system that can be simulated. In addition, as explained in more detail in Section 3.3.3, molecular dynamics simulations are often too expensive to carry out at the DFT level, so that ions effectively have no kinetic energy, leading to a zero temperature system. This prevents direct study of some important high temperature phenomena for high-*k* materials, such as phase stability of pseudo-binary alloys.

Furthermore, the dominance of Si over other materials can ultimately be attributed to the near-perfect interface between Si and SiO_2. Any alternative high-*k* dielectric material that hopes to replace SiO_2 must achieve a similarly high degree of perfection in its interface with Si. As a consequence, many of the important interface considerations require explicit modeling of the Si/dielectric interface. Many more atoms need to be included in an interface model compared to a bulk structure. Consequently, realistic modeling of high-*k* dielectric interfaces becomes extremely expensive, pushing the limits of state-of-the-art first principles methods.

3.3.1.1 Underestimation of excited state energies

One notable exception to the accuracy of DFT is prediction of excited state energies, which are typically underestimated. Experience has shown that the main source of error is underestimation of the energy gap between the highest occupied valence band state and the lowest unoccupied conduction band state by as much as 50% [70]. Fundamentally, this discrepancy arises from the fact that DFT predicts the *ground state* of a material system. Since the energy of the ground state depends only on the energies of the occupied valence band states, the theory is not intended to predict the energies of the unoccupied conduction band states. Remarkably, for a wide range of materials, the separation between unoccupied conduction band states is well predicted by DFT, so that only the energy gap

value is in error [70]. In practice, most studies assume that the eigenvalues predicted by DFT are representative of the electronic band structure, including the conduction bands.

The underestimation of the band gap is an important limitation, since many of the properties of interest for the high-*k* application, such as band offsets at Si/dielectric interfaces, require accurate knowledge of the bandgap. Because such considerations are even more critical for optoelectronic applications, much of the theoretical progress in overcoming the limitations of DFT have been made by researchers working with III-V and II-VI material systems. The so-called quasiparticle (GW) approach to the electron self-energy is the best known correction to this problem [70-74]. Theory has shown that much of the error in excited state energies can be attributed to the LDA used to evaluate the exchange-correlation energy. In the GW approximation, the exchange-correlation potential is calculated by evaluating the self-energy operator by the one-particle Green's function (G) and the screened Coulomb interaction (W) [70,71]. This approach has been shown to accurately predict the bandgap and extended band structure of a variety of III-V and II-VI semiconductors, including band offsets at their interfaces [72,73]. The GW approach has recently been applied successfully to transition metal oxides as well [74].

Because the primary error is in the energy gap, rather than in the separation between unoccupied conduction states, a popular empirical correction is to apply the so-called scissors operator to DFT-LDA band structures [70,75]. In this approach, the conduction bands are rigidly shifted by the amount needed to match experimental measurements of the bandgap. If measurements are not available, the average quasiparticle shift obtained from more accurate GW calculations can be used. The GW approach is considerably more expensive than DFT-LDA and software packages for performing GW calculations are much less widely available. Nonetheless, GW studies of high-*k* band structures may be of significant value to the high-k community.

3.3.1.2 Prediction of static dielectric constant

The ability to predict the static (i.e. low frequency) dielectric constant is also important for the high-*k* application. As described in Section 2.3.1, the static dielectric

constants of most high-*k* materials have significant electronic and ionic contributions at the frequencies of interest. Recall that the electronic contribution arises from the motion of electrons in response to the applied electric field, whereas the ionic contribution depends on the motion of the ions themselves. For any high-*k* material, it is important to investigate the behavior of the dielectric constant, especially as film stress or defect conditions are changed. For the pseudo-binary alloys, it is particularly important to understand the dielectric behavior of the film as a function of its composition, since the alloying concentration is a key degree of freedom which needs to be tailored to achieve optimal material properties.

A number of first principles approaches have been developed to compute the dielectric response of a material system, including: direct evaluation of the dielectric function $\varepsilon(\omega)$ based on the band-to-band optical absorption spectrum [75-77]; calculation of the dielectric tensor by density functional perturbation theory (DFPT), which considers the response to an external perturbation (e.g. electric field) variationally in a self-consistent manner [78,79]; and calculation of the dielectric tensor based on the modern theory of polarization [80,81]. Calculation of the band-to-band optical absorption is straightforward and has been used to study the dielectric response of a variety of materials, including III-V systems, SiO_2, and Si_3N_4 [75-77]. The calculated static dielectric constants for materials such as Si and GaAs whose dielectric response consists primarily of electronic contributions are in good agreement with experiment. However, because this method does not take into account the ionic response, it significantly underestimates the dielectric constants of polar insulating oxides such as SiO_2.

In contrast, the variational DFPT method considers both the electronic and ionic response and has been demonstrated to accurately predict the static dielectric constants of a wide range of materials including SiO_2 [78,79]. Because this approach requires additional routines above and beyond standard DFT-LDA simulations, software packages for performing DFPT calculations are not widely available. More recently, direct calculation of the dielectric tensor using quantities directly obtainable from a standard

DFT-LDA simulation, such as total energy, stress, and forces, has been developed based on the so-called Berry-phase approach to polarization [80,81]. The underlying theory applies to any polar material and has been demonstrated to provide accurate static dielectric constants for materials such as GaN and InN, though work on insulating oxides such as SiO_2 have not yet been published.

Jun *et al* have recently applied the DFPT approach to the study of static dielectric constant scaling for the Zr silicate system [82,83]. As described in Section 2.4.3, possible departure of the dielectric constant from a linear mixing trend between pure SiO_2 and stoichiometric $ZrSiO_4$ is still intensely debated. Figure 3.3 shows the preliminary results of their calculations. The calculated dielectric constants for the endmembers SiO_2 and $ZrSiO_4$ are in good agreement with measured results. The predicted value for 11 atomic percent Zr seems to suggest super-linear behavior as argued by Lucovsky and Rayner [36]. Additional calculations at intermediate Zr concentrations are needed to further clarify the scaling behavior.

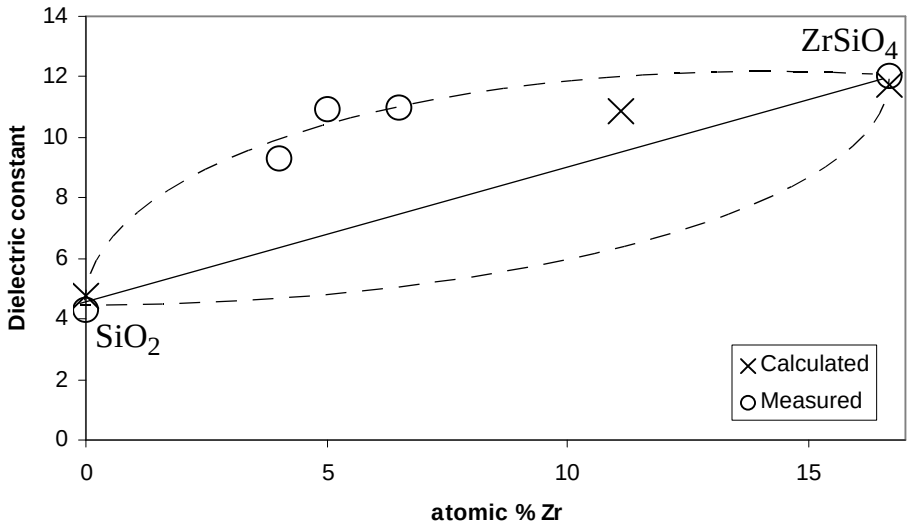

Figure 3.3 Predicted Zr silicate dielectric constant scaling vs composition.

3.3.2 Software programs and implementations

A number of widely used software packages are available for performing first principles DFT simulations for periodic systems [84-89]. These programs implement many of the computational algorithms and techniques described in Reference 61. They all use a plane wave basis set to expand the wave function and differ primarily in the type of pseudopotential used to describe the ion-electron interactions. Traditional DFT calculations have employed the norm-conserving pseudopotentials described in Section 3.2.2.1. Ensuring norm conservation significantly increases the number of basis functions needed to describe transition metals and first row nonmetals. By abandoning the norm conservation constraint, more recent approaches to constructing pseudopotentials have significantly reduced the number of basis functions needed to describe the wavefunction [90,91]. These pseudopotentials are often referred to as ultrasoft, in contrast to the more traditional hard pseudopotentials. Widely used software packages are also available for performing first principles simulations of molecular clusters using more localized basis sets [92].

All calculations presented in Chapters 4 and 5 use the Vienna Ab-initio Simulation Package (VASP) program [87-89]. VASP is widely used to perform first principles DFT calculations and has been applied to study diverse materials, including ZrO_2 polymorphs [93]. VASP utilizes several novel techniques which speed up convergence with respect to both electronic and ionic degrees of freedom [88,89]. It is one of the few widely available DFT packages to employ ultrasoft pseudopotentials, and this was a key reason the VASP package was chosen for this research, since transition metal oxides needed to be modeled. VASP provides well-tested ultrasoft pseudopotentials for most of the elements of interest on the periodic table. The exchange-correlation energy is described by the local density approximation (LDA) functional of Ceperley and Alder as parametrized by Perdew and Zunger [57].

3.3.3 Simulation procedure

It has already been mentioned that when solving the Schroedinger equation, one generally invokes the Born-Oppenheimer approximation. This allows the ionic and electronic degrees of freedom to be treated separately. Consequently, ionic positions are required as inputs to the electronic minimization step, as illustrated in Figure 3.4. During this procedure, the ionic positions are kept fixed and the wavefunction is iteratively optimized until self-consistency is achieved in the Schroedinger equation, leading to the ground state (i.e. lowest energy state) corresponding to the given ionic configuration.

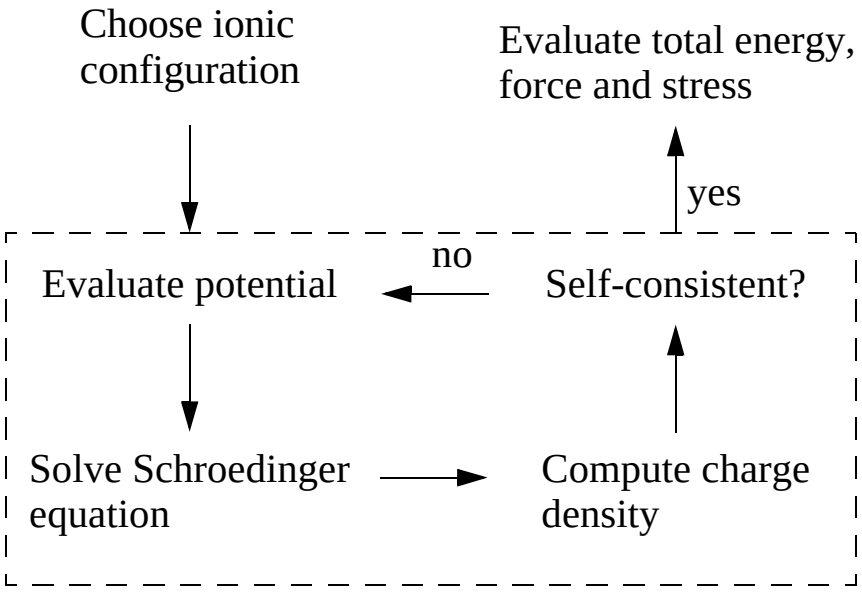

Figure 3.4 Flowchart for electronic minimization.

After each electronic minimization step, the total energy of the system can be further reduced by moving the ions based on the computed forces acting on them. Conjugate gradient algorithms can be employed to determine the optimal direction in which to move the ions. Each time the ions are moved, the electronic wavefunction must be reoptimized to find the ground state configuration, as illustrated in Figure 3.5. The sequence of ionic moves and electronic minimizations is commonly referred to as geometry optimization and can be continued until a specified convergence of the total energy is reached. The

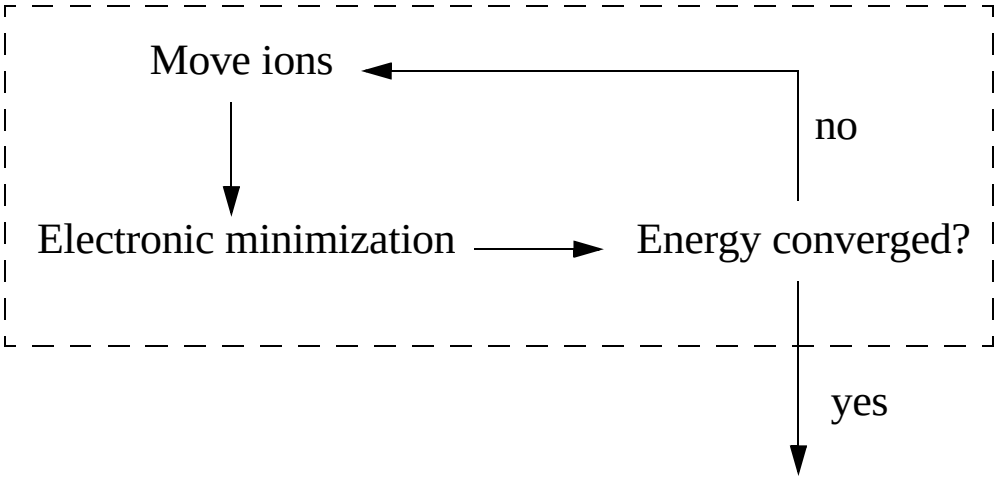

Figure 3.5 Flowchart for geometry optimization.

convergence criterion with respect to ionic motion can generally be more relaxed than that due to electronic motion.

Such a geometry optimization is commonly done at the DFT level to find the ground state configuration of a material system. An important limitation is that the resulting configuration only corresponds to the true ground state if the initial configuration placed the system in the basin of a global potential minimum, as illustrated in Figure 3.6. If instead the initial configuration corresponded to the basin of a local potential minimum, the ions would need to be given enough kinetic energy to overcome the local potential energy barriers. This requires a considerably more expensive dynamical simulation, much like the molecular dynamics (MD) simulations commonly performed with classical interatomic potentials.

In all calculations presented in Chapters 4 and 5, a plane wave basis cutoff energy of approximately 400eV (29 Rydberg) is used. Since the plane wave expansion is global in nature, the cutoff energy must be at least as high as that required by the element with the slowest convergence, in this case oxygen. Total energies are converged to at least 0.0001eV with respect to electronic relaxation and to at least 0.01eV with respect to ionic relaxation. In all cases where ionic relaxation is permitted, the residual forces acting upon

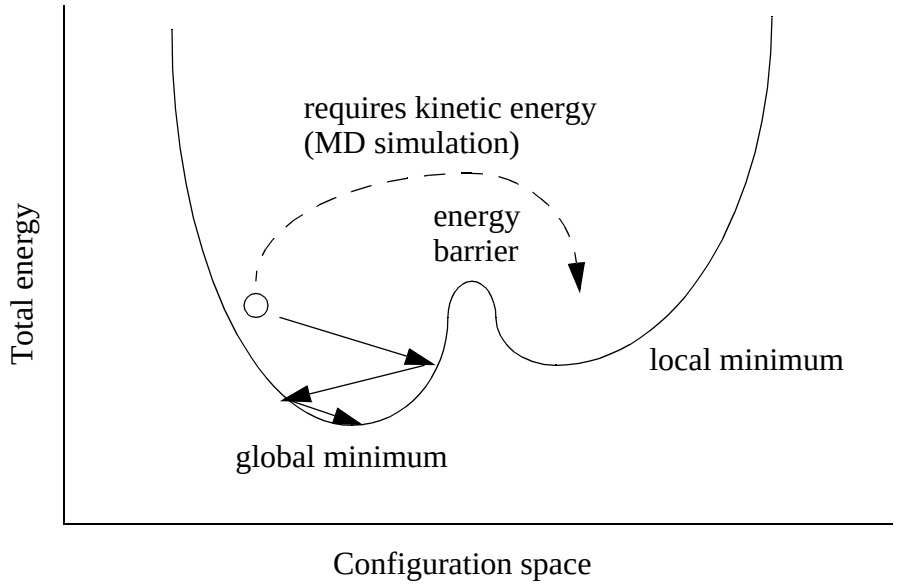

Figure 3.6 Illustration of potential energy surface for geometry relaxation.

the ions are less than 0.1eV/A. A Monkhorst-Pack k-point sampling mesh of 2x2x2 for bulk calculations and 2x2x1 for interface calculations was used for all calculations.

3.4 Summary

The introduction of many novel materials for alternative high-*k* gate dielectrics presents a fundamental new challenge to modeling. Based on the material properties of interest for the high-*k* application, models employing a quantum mechanical description are needed. The classical nature of the interactions and the dependence on extensive parameter fitting will likely limit the usefulness of empirical interatomic potentials. Tight binding approaches may become attractive once the material properties of interest become better understood through experimental or first principles means.

Because of its accuracy and extensibility, density functional theory (DFT) is currently the most promising approach for the high-*k* application. DFT still suffers from substantial

limitations, however, and it is likely that other approaches such as the GW approximation will need to used along with DFT to overcome the challenges of high-*k* dielectric research.

Chapter 4

Scaling Limits Imposed by Interface Structural Properties

This chapter investigates potential scaling limits imposed by structural properties at the Si/silicate interface. Specifically, scalability is discussed in terms of the equivalent oxide thickness (EOT) of the silicate gate stack. Detailed consideration of the interface structure leads to the conclusion that suboxide bonding within the interfacial transition region presents significant challenges to scaling the silicate system. The discussion closely follows the material we presented in Reference 94.

Section 4.1 identifies important properties of the interface which need to be investigated to clarify the Si/silicate gate stack structure.

Section 4.2 considers possible bulk silicate structures which may be used to form model interfaces with Si. The much longer equilibrium length of Zr-O and Hf-O bonds relative to Si-O bonds suggest that volume strains may play an important role in silicate materials.

Section 4.3 presents model Si/silicate interface calculations aimed at understanding the detailed structure and energetics of bonding at the interface. Interfaces containing both structurally abrupt and extended transition regions are considered.

Section 4.4 considers the scaling limitations imposed by the presence of suboxide bonding within the interfacial transition region. The added energy cost of forming Zr-Si or Hf-Si bonds within the transition region suggests that even silicates will form stacked gate structures with a low-*k* interfacial layer.

Section 4.5 compares structural properties of Zr and Hf silicates. Some discrepancies between the expected behavior of Zr and Hf silicates are attributed to limitations of the pseudopotential used to describe Hf.

4.1 Si/silicate gate stack structure

As described in Section 2.4.2, silicates are conventionally believed to form a single, uniform high-*k* layer in direct contact with the Si substrate, leading to the gate stack structure illustrated in Figure 4.1(a). There it was argued that a Zr silicate layer can be physically thicker than a pure ZrO_2 layer and still achieve the same EOT value, despite its lower *k*-value, because the silicate avoids the formation of a low-*k* interfacial oxide layer.

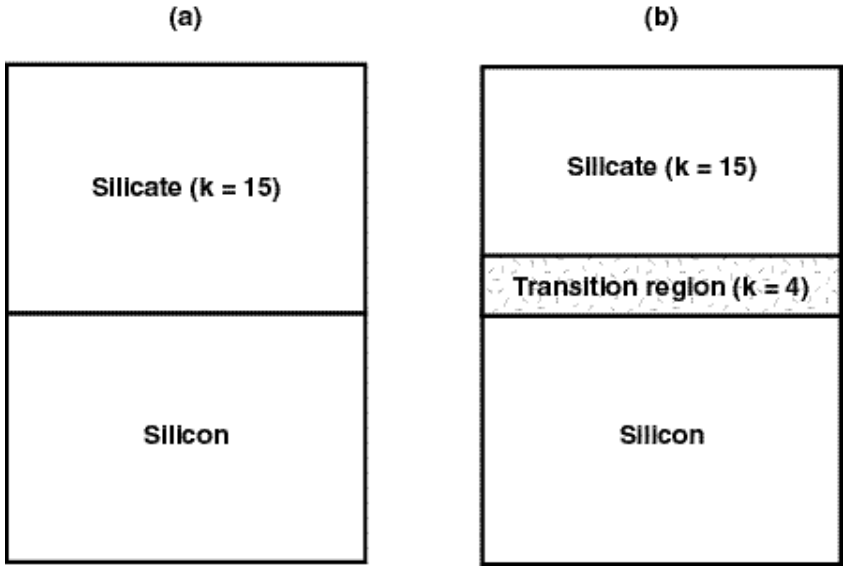

Figure 4.1 (a) Conventional view of Si/silicate interface. (b) Si/silicate interface with interfacial transition region.

There are several important considerations regarding this conventional view which should be addressed. First, if there is no interfacial SiO_2-like layer between the silicate film and the Si substrate, what is the nature of bonding at the Si interface? Since the silicate system contains Zr, Si, and O atoms, it is important to understand whether Si-Si, Si-O, or Si-Zr bonding is energetically favored at the Si interface. The bonding at the Si interface can significantly impact transport properties in the underlying channel region. In particular, Si-Zr bonding would imply the formation of a silicide-like phase at the interface, which is expected to degrade device performance. Interestingly, experimental work on the silicate system described in Section 2.4.2 suggests that silicide phases are not observed, either in the bulk or at the Si interface. In order to explain these observations, it is necessary to understand why Si-Zr bonding is not favorable at the Si interface.

In addition, since Zr atoms are substantially larger than the Si atoms they replace, it is important to clarify possible volume strain effects associated with Zr incorporation in the silicate film. The energetics of Zr incorporation close to the Si interface are also important. If it turns out that Zr incorporation close to the Si interface is not favorable, the silicate gate stack structure would appear as in Figure 4.1(b), in which a low-*k* transition region exists at the Si interface. The extent of this transition region would limit the maximum achievable capacitance of the gate stack, just as in the case of pure metal oxides which require an interfacial SiO_2 layer.

4.2 Bulk silicate structures

In order to study Si/silicate interfaces at the atomic scale, models of bulk silicate structures are first needed. Many experimental high-*k* dielectric films, including the silicates, are structurally amorphous. The main exceptions are some binary metal oxides, such as ZrO_2, which have been observed to form polycrystalline films. Unfortunately, the large computational cost of fully modeling long-range disorder prevents the direct study of amorphous materials at the DFT level. Instead, it is standard practice to use periodic

crystals which contain local bonding units characteristic of the amorphous material's structure. To the extent that the material's physical properties arise from the interactions within the local bonding units, this approach yields meaningful results. In particular, DFT modeling of SiO_2 has almost always been done using periodic crystalline models, even though SiO_2 is experimentally amorphous. Experience has shown that such an approach yields accurate results, largely because the important physics of SiO_2 is contained within the local SiO_4 tetrahedral bonding units. The extended continuous random network of SiO_4 units is accommodated through flexible, low energy cost O bonds at the corners of the tetrahedral units. It remains to be seen if crystalline models can be successfully applied to general amorphous high-*k* dielectrics. In the case of silicates, the use of crystalline models seems reasonable since silicates can be viewed as an incremental modification of SiO_2. Below, possible models of Zr and Hf silicates based on SiO_2 crystals for use in model interface calculations are developed.

Numerous first principles studies have investigated in detail the various crystalline polymorphs of SiO_2 [95-97]. Two particularly useful structures for possible silicate models are β-quartz and β-cristobalite [98,99]. The Si/β-quartz structure has been shown to possess the lowest interface energy, so that it represents the most realistic model Si/SiO_2 interface formed with a crystalline form of SiO_2 [15,100]. The Si/β-quartz SiO_2 interface model is used in this chapter to investigate the detailed energetics of Zr and Hf incorporation near the interface. β-cristobalite is a high symmetry form of SiO_2 which has been used in many of the early studies of SiO_2. A distinguishing feature of the Si/β-cristobalite interface structure is that the termination of the Si surface atom can easily be altered in a controlled manner [101,102]. The Si/β-cristobalite SiO_2 interface model is used in Chapter 5 to investigate the band offsets at Si/silicate interfaces.

β-quartz contains 3 formula units of SiO_2, so that 3 Si and 6 O atoms make up the unit cell. The experimental lattice constant and Si-O bond length from Wyckoff are reported in Table 4.1, along with results from a previous theoretical study. A full geometry optimization yielded structural parameters in good agreement with known values, as

Table 4.1 Structural properties of β-quartz SiO_2.

	a (A)	**c (A)**	**Si-O (A)**	**Si-O-Si (degrees)**
Experiment [98]	5.01	5.47	1.62	147
Previous theory [96]	5.05	5.55	1.63	147
Present theory	5.02	5.51	1.62	147

shown in Table 4.1. The resulting structure is shown in Figure 4.2. By replacing a single Si atom in β-quartz, a model silicate with approximately 11 atomic percent Zr or Hf concentration could be formed. The Zr and Hf initially formed Zr-O and Hf-O bonds of length 1.62 $\mathring{A}$, corresponding to the Si-O bond length in β-quartz. Longer equilibrium bond lengths are expected since Zr and Hf are larger atoms than Si. For example, Zr forms bonds of length 2.13 $\mathring{A}$ and 2.27 $\mathring{A}$ to its first- and second-nearest neighbor O atoms in the stoichiometric silicate $ZrSiO_4$ [35]. Similarly, the Zr-O bond lengths are between 2.04 $\mathring{A}$ to 2.26 $\mathring{A}$ in monoclinic ZrO_2, the lowest energy polymorph of ZrO_2 [103]. Hence,

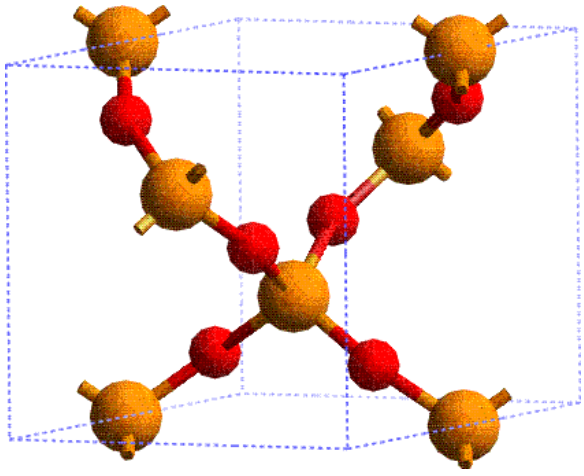

Figure 4.2 Crystal structure of β-quartz SiO_2 after full geometry relaxation.

substantial pressures were initially generated within the model Zr and Hf silicates, as reported in Table 4.2.

Table 4.2 Stress, volume expansion, and energy gain of relaxed Zr and Hf silicate models based on β-quartz SiO_2.

	stress of unrelaxed cell (kB)	**unrelaxed volume (A^3)**	**relaxed volume (A^3)**	**% volume expansion**	**energy gain from geometry relaxation (eV)**
Zr silicate	755	120	151	26	14.2
Hf silicate	538	120	147	23	9.7

The large stress due to Zr and Hf incorporation led to a high energy structure whose stability could be improved by allowing the unit cell to relax toward the total energy minimum. An unconstrained geometry relaxation procedure simultaneously optimized both atomic positions and lattice vectors to obtain the ground state configuration. The resulting bond lengths and bond angles are shown in Table 4.3 and compared to those of β-quartz SiO_2. The Zr-O and Hf-O bond lengths of 1.96 $\mathring{A}$ and 1.91 $\mathring{A}$ were 21% and 18% longer than the Si-O bond length in SiO_2, respectively. Figure 4.3 shows the lowering of total energy and unit cell pressure as the geometry relaxation proceeded. Substantial

Table 4.3 Structural properties of relaxed Zr and Hf silicate models based on β-quartz SiO_2.

	a (A)	**c (A)**	**α (degrees)**	**γ (degrees)**	**Si-O, Zr-O (A)**	**Si-O-Si, Zr-O-Si (degrees)**
β-quartz SiO_2	5.02	5.51	90	120	1.62	147
Zr silicate	5.53	6.01	90	125	1.60 - 1.61, 1.96	162, 153
Hf silicate	5.47	5.47	90	124	1.60, 1.91	160, 153

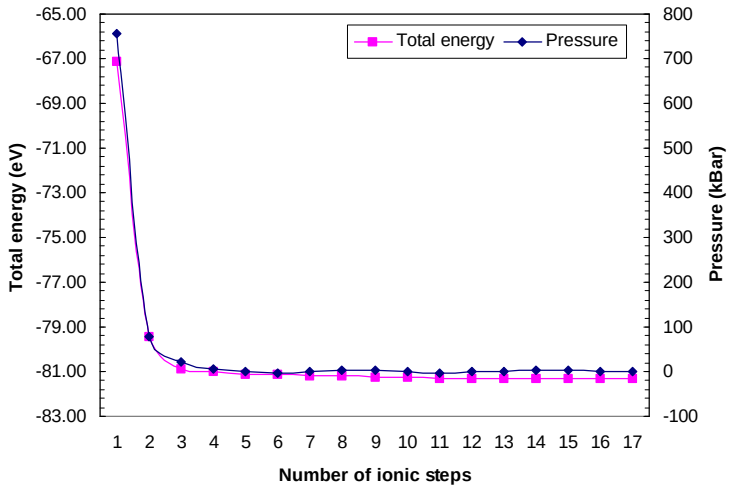

Figure 4.3 Plot of total energy and unit cell pressure vs number of ionic steps for relaxation of Zr-doped β-quartz SiO_2 crystal.

energy was gained from the relaxation procedure, so that a more stable structure was indeed obtained. Since the boundary conditions on the unit cell were free, the cell expanded to relax the internal strain, as shown in Table 4.2. Such free volume expansions are restricted in an actual silicate film, so that localized stress is likely to develop near regions of Zr or Hf incorporation.

4.3 Model Si/silicate interface structure

In order to understand the nature of bonding at the Si interface, model Si/silicate interface structures were constructed by attaching the silicate models developed in the previous section to crystalline Si. The assumption was made that for low metal concentrations, the local bonding structure of silicate films resembles that of tetrahedrally-bonded SiO_2. An Si/SiO_2 interface model was therefore used as the reference structure into which Zr and Hf atoms were selectively introduced.

4.3.1 Si/SiO_2 interface

The general prescription for forming a model interface between two crystalline materials is to attach the slabs in such a way that atoms are aligned in a well-defined manner while minimizing the lattice mismatch strain. The three main polymorphs of SiO_2 - quartz, cristobalite, and tridymite - have all been used in previous studies to form model Si/SiO_2 interfaces [15,100,101,104]. In each case, Si atoms on both sides of the interface are aligned by rotating the SiO_2 crystal appropriately. There is inevitably some lattice mismatch, and it is standard practice to adjust the SiO_2 lattice constants to align with the Si unit cell. The mismatch strain is accommodated on the SiO_2 side of the interface since SiO_2 is a thin film attached to a thick, rigid Si substrate. The polymorphs differ in the amount and type of mismatch strain introduced at the interface. The lattice constant of tridymite is larger than that of Si, while those of quartz and cristobalite are smaller.

In the case of the Si/SiO_2 interface, several experimental observations further guide the construction of the model structure. First, the density of interface traps which introduce electronic states into the Si bandgap is very small, on the order of one in 10^4 interface atoms [104,105]. This is remarkable considering that a large bond density mismatch exists at the interface. Specifically, bulk Si contains Si atoms tetrahedrally bonded to other Si atoms, whereas bulk SiO_2 contains Si atoms tetrahedrally bonded to O atoms. To avoid introducing dangling (i.e. unsaturated) bonds which would lead to electrically active traps at the interface, a structural transition region with bonding intermediate to that of bulk Si and bulk SiO_2 is required. It is well-known that the transition region contains suboxides, or sub-stoichiometric Si atoms, which have not been fully oxidized [106]. Consideration of the effects of suboxide species on the resulting interface structure is deferred to Section 4.3.6. More recently, it has become apparent that the formation of an oxygen bridge or silicon dimers at the interface also helps to eliminate interface states due to unsaturated bonds [100,104,105]. An oxygen bridge was chosen for the present interface structures.

The Si/β-quartz SiO_2 interface was chosen as the starting configuration for the silicate studies. It is believed to provide the most realistic model of the Si/SiO_2 interface, as several recent studies have shown that the β-quartz structure leads to the lowest interface energy [15,100]. The lateral dimensions corresponded to the Si lattice constant (5.43 $\mathring{A}$), while the vertical dimension contained seven Si layers (~8 $\mathring{A}$) and four monolayers of oxide (~8.5 $\mathring{A}$). In order to lattice-match to Si(001), the a-axis and c-axis of β-quartz SiO_2 were aligned to the a-axis of Si. The a-axis was elongated by 8% while the c-axis was compressed by 1.5% to match the Si lattice constant. The resulting unrelaxed structure had Si-O bond lengths of 1.71 $\mathring{A}$, about 6% longer than the equilibrium value of 1.62 $\mathring{A}$. The stress due to lattice mismatch resulted in an equivalent external pressure of -94kB. Energy could be gained and the stress could be partially relieved by relaxing the atomic structure. All atoms were relaxed except for the bottom three layers of Si, which were kept fixed. The lattice vectors of the unit cell were also held fixed. The boundary conditions were intended to model a thin film atop a thick substrate. The relaxed structure had Si-O bond lengths of 1.61-1.64 $\mathring{A}$, close to the expected equilibrium bond length in SiO_2. Approximately 7eV was gained from the relaxation procedure. Figure 4.4(a) shows the resulting structure which serves as the reference for an interface without Zr or Hf incorporation. Note the presence of a structural transition region containing an oxygen bridge which accommodates the transition from bulk Si to bulk SiO_2. The transition is structurally abrupt and takes place within one monolayer of the Si interface.

4.3.2 Zr and Hf incorporation

Model Si/silicate interfaces were then created by selectively substituting a single Zr or Hf atom for Si atoms at varying distances from the interface. To facilitate the analysis, the "interface" was identified as the last layer of Si atoms which retained bulk bonding properties. The atomic positions were again relaxed using the same boundary conditions as above. Substantial relaxations occurred, since Zr and Hf formed much longer bonds with neighboring atoms compared to Si. The models contained silicate films with

approximately 6 atomic percent Zr. The resulting structures for Zr incorporation one and three layers above the interface are shown in Figures 4.4(b) and 4.4(c) and are referred to as the Zr_1 and Zr_3 models, respectively. The corresponding structures for Hf were quite similar and are therefore not shown. Models with Zr and Hf incorporation two and four layers above the interface were not studied, since placing them at the boundary positions would artificially restrict atomic relaxation to the vertical dimension. The symmetry constraint is illustrated in Figure 4.5, where two lateral units cells of the Zr_2 and Zr_3 models are compared.

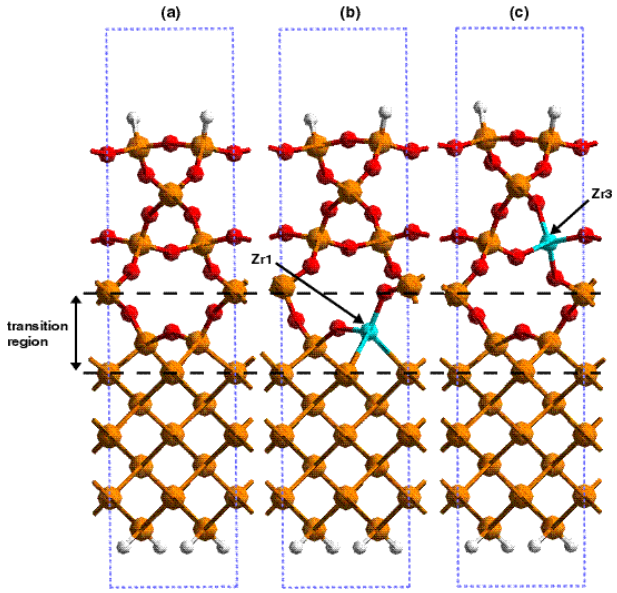

Figure 4.4 (a) Reference Si/SiO_2 interface model formed by attaching β-quartz SiO_2 to Si(001). Large atoms are Si, small atoms are O. The extremities are saturated with H. (b) and (c) Relaxed structures for model Si/silicate interface with Zr incorporation one layer (Zr_1 model) and three layers (Zr_3 model) above the interface.

4.3.3 Interface energetics

Since the type and number of atoms in each Si/silicate interface model are the same, their total energies can be directly compared. This approach can provide insight into the relative stability of several distinct bonding arrangements that can occur at Si/silicate

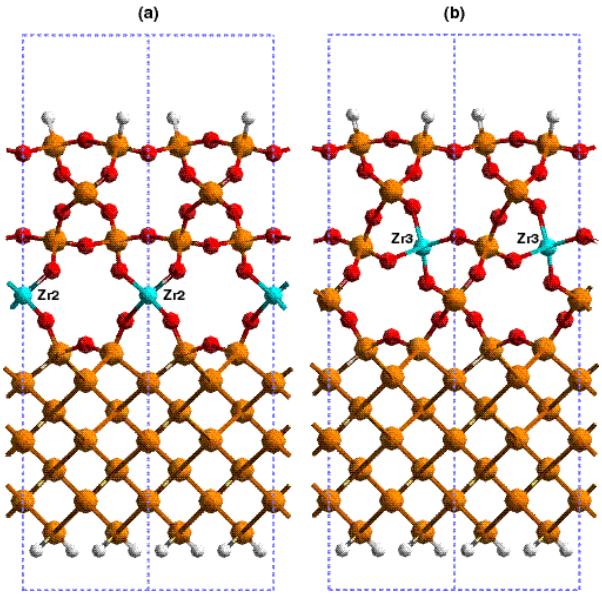

Figure 4.5 Two lateral unit cells of model Si/silicate interface with Zr incorporation (a) two layers (Zr_2 model) and (b) three layers (Zr_3 model) above the interface. The Zr_2 model contains Zr atoms at the boundaries of the unit cell which restrict atomic relaxation.

interfaces. In the Zr_3 and Hf_3 models, Zr and Hf are in bulk oxide-like environments, tetrahedrally bonded to four O atoms, leaving the interface with Si/SiO_2-like bonding. In the Zr_1 and Hf_1 models, Zr and Hf occupy positions at the interface forming two silicide-like bonds to Si and two bonds to O. The total energy of the Zr_3 model is observed to be 0.7eV less than that of the Zr_1 model. The total energy of the Hf_3 model is 1.3eV less than that of the Hf_1 model. The substantial energy differences suggest that SiO_2-like bonding is energetically favored over silicide-like bonding at the Si interface. The calculated energy differences help to explain the lack of silicide bonding observed at experimental Si/silicate interfaces as described in Section 2.4.2.

This energy difference is attributed to the added cost of forming silicide-like bonds at the interface. Simple bond counting shows that the Zr_1 model contains two Zr-Si and two Si-O bonds more than the Zr_3 model, while the Zr_3 model contains two Si-Si and two Zr-O bonds more than the Zr_1 model. The Zr-Si bonds of the Zr_1 model (2.61-2.62 $\mathring{A}$) are

measured to be 11-14% longer than the corresponding Si-Si bonds of the Zr_3 model (2.31-2.35 $\mathring{A}$). The Zr-O bonds of the Zr_3 model (1.93-1.95 $\mathring{A}$) are 17-22% longer than the corresponding Si-O bonds of the Zr_1 model (1.60-1.64 $\mathring{A}$). To the extent that longer bonds imply weaker bonds, there is an energy cost associated with forming Zr-Si and Zr-O bonds. Similarly, the Hf-Si bonds of the Hf_1 model (2.55-2.56 $\mathring{A}$) are 9-11% longer than the corresponding Si-Si bonds of the Hf_3 model (2.31-2.35 $\mathring{A}$), while the Hf-O bonds of the Hf_3 model (1.88-1.90 $\mathring{A}$) are 15-19% longer than the corresponding Si-O bonds of the Hf_1 model (1.60-1.64 $\mathring{A}$). Evidently the cost of forming Zr-Si and Hf-Si bonds in the Zr_1 and Hf_1 models more than offsets the cost of forming Zr-O and Hf-O bonds in the Zr_3 and Hf_3 models.

The observed energy cost of forming silicide-like bonds may be explained in part by the observation that the Zr-Si and Hf-Si bonds form at the interface, where bonding is constrained by the rigidity of the underlying Si substrate which cannot accommodate the local distortion needed to incorporate the much larger Zr and Hf atoms. In contrast, the Zr-O and Hf-O bonds form in the bulk of the oxide, where greater relaxation is possible. Oxygen is known to form flexible bonds between neighboring tetrahedral units, so that local distortions can be accommodated with little energy cost [100]. The added cost of forming Zr-Si or Hf-Si bonds suggests that Zr or Hf incorporation within the structural transition region is energetically unfavorable.

4.3.4 Electronic structure analysis

The electronic structure of the model interfaces was also investigated through band structure calculations. Figure 4.6 illustrates the reciprocal lattice of the reference Si/SiO_2 interface model. Since periodicity, and hence dispersion, is only expected in the plane parallel to the interface, the reciprocal lattice was sampled along the path shown. The band structure of the model interface corresponds to the merged band structures of Si and SiO_2. Since the band alignment places the Si bandgap within the SiO_2 bandgap, it is expected that bands near the bandgap of the interface structure mainly correspond to Si states.

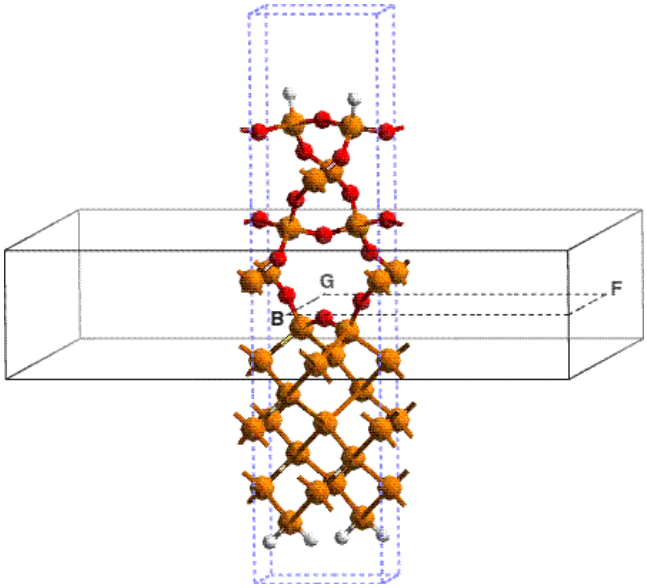

Figure 4.6 Brillouin zone of the reference Si/SiO_2 interface model. The dashed lines indicate the reciprocal space path along which the band structure is sampled.

The band structure for the reference Si/SiO_2 interface is shown in Figure 4.7. The bandgap value of 0.71eV closely resembles that of bulk Si. The band structure of the Zr_1 silicate interface model shown in Figure 4.8 indicates a lowering of the lowest unoccupied conduction band. Recalling that the Zr_1 model consists of silicide-like Zr-Si bonds at the interface, it is expected that the lowered band corresponds to an interface state associated with the Zr atom. The band is approximately 0.18eV below the conduction band of the reference model, indicating that a relatively deep energy level is introduced. The band structure near the bandgap of the Zr_1 model is also qualitatively different from that of the Si/SiO_2 model, showing that Zr states are likely hybridizing with Si states. In contrast, the band structure near the bandgap of the Zr_3 silicate interface model shown in Figure 4.9 appears nearly identical to that of the Si/SiO_2 model. It should not be surprising that the Zr state is swept out of the Si bandgap, since the interface bonding in the Zr_3 model is Si/SiO_2-like. Instead, the Zr_3 model is expected to introduce states into the band structure of SiO_2, which are not visible in the range of energies shown in Figure 4.9. The resulting

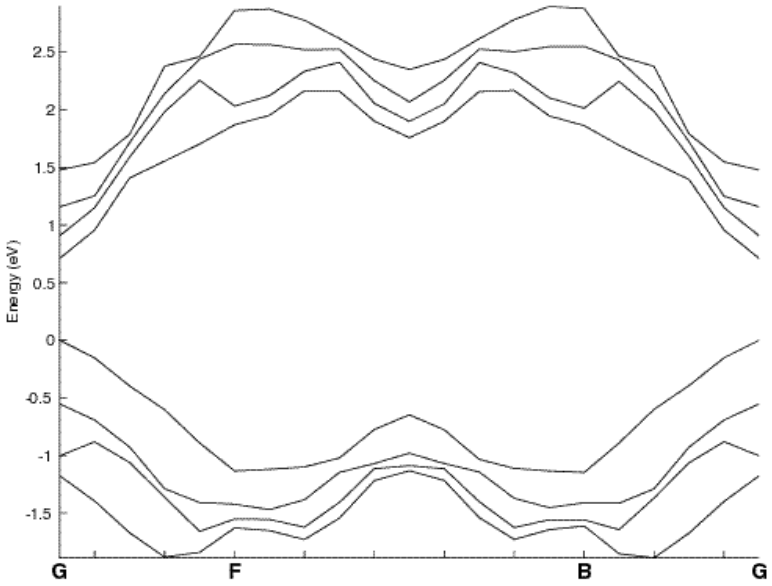

Figure 4.7 Band structure of the reference Si/SiO_2 interface. Four highest valence bands and four lowest conduction bands are shown. The top of the valence band has been normalized to 0eV.

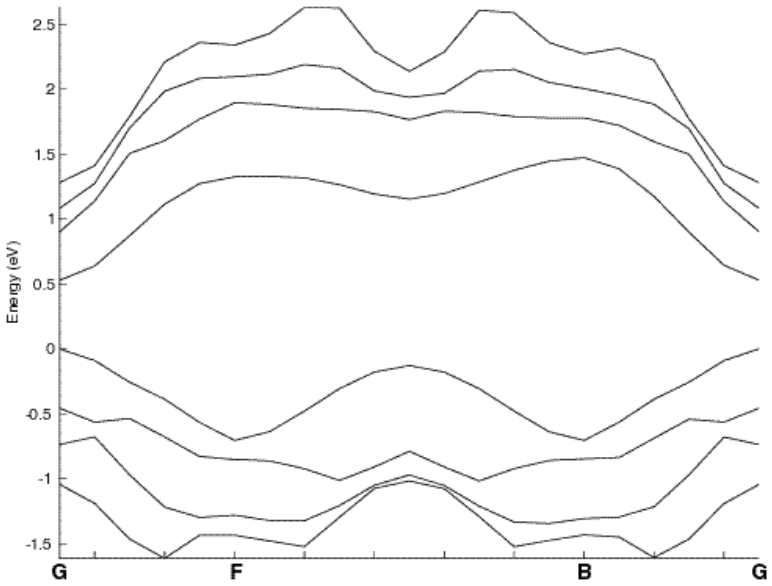

Figure 4.8 Band structure of the Zr_1 Si/silicate interface model.

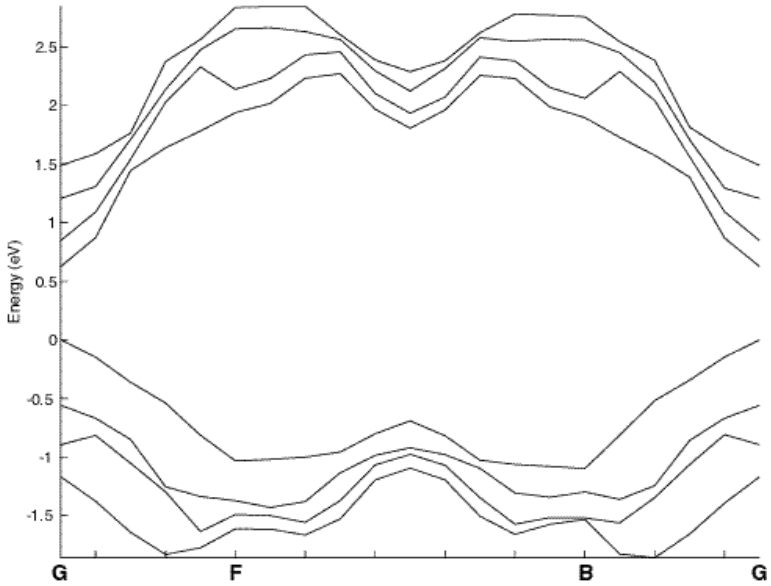

Figure 4.9 Band structure of the Zr_3 Si/silicate interface model.

decrease in the SiO_2 bandgap effectively lowers the band offset at the Si/silicate interface. Band offsets are investigated in greater detail in Chapter 5.

To further characterize the electronic structure at the interface, the electron charge density corresponding to the lowest unoccupied conduction band of each model is plotted in Figure 4.10. In both Figures 4.10(a) and 4.10(c), corresponding to the Si/SiO_2 and Zr_3 interface models, respectively, the charge density appears diffused throughout the Si region, indicating the delocalized character of the band. This is the expected result from basic considerations of conduction mechanisms in bulk Si. In contrast, Figure 4.10(b) shows the charge density for the Zr_1 model which contains Zr-Si bonding at the interface. The charge corresponding to the lowest conduction band of the Zr_1 model appears much more localized and qualitatively resembles a d-state surrounding the Zr atom. Such a localized state can serve as a trap for conduction electrons in the channel region and is expected to degrade transistor performance. The electronic structure analysis essentially confirms the silicide-like character of Zr-Si bonding at the Si interface.

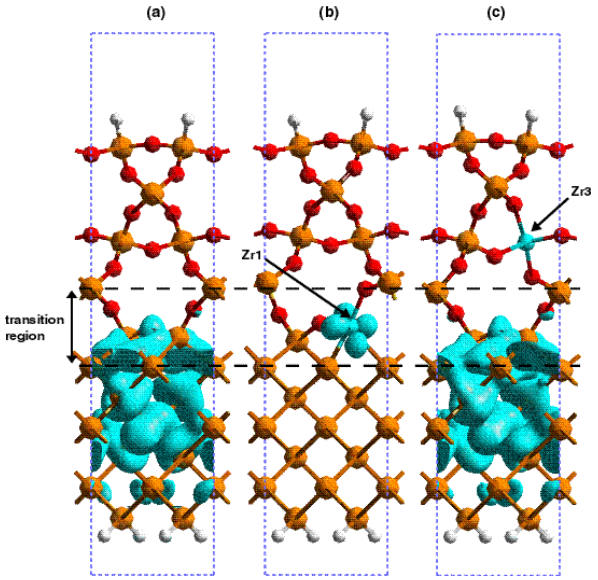

Figure 4.10 Isosurfaces of electron charge density corresponding to the lowest unoccupied conduction band state in the (a) Si/SiO_2 (b) Zr_1 Si/silicate and (c) Zr_3 Si/silicate interface models.

4.3.5 Local volume strain

Because Zr and Hf atoms are much larger than the Si atoms they replace, it was also suspected that incorporating them into the silicate film would lead to localized volume strains. To characterize these strains, the volumes of tetrahedra associated with local SiO_4, ZrO_4, and HfO_4 bonding units were measured. Figure 4.11(a) shows the local tetrahedra associated with bulk Si, bulk SiO_2, and the interfacial transition region for the reference Si/SiO_2 model. As shown in Figure 4.11(b), it was observed that the volume of the tetrahedron associated with Zr incorporation near the Si interface (Zr_1 model) was 45% larger than that of the corresponding Si atom in the reference Si/SiO_2 model. For the Hf_1 model, the difference was 37%. Similarly, as shown in Figure 4.11(c), the volume of the tetrahedron associated with Zr incorporation in the bulk silicate (Zr_3 model) was 69% larger than that of the corresponding Si atom in the reference model. For the Hf_3 model, the difference was 58%.

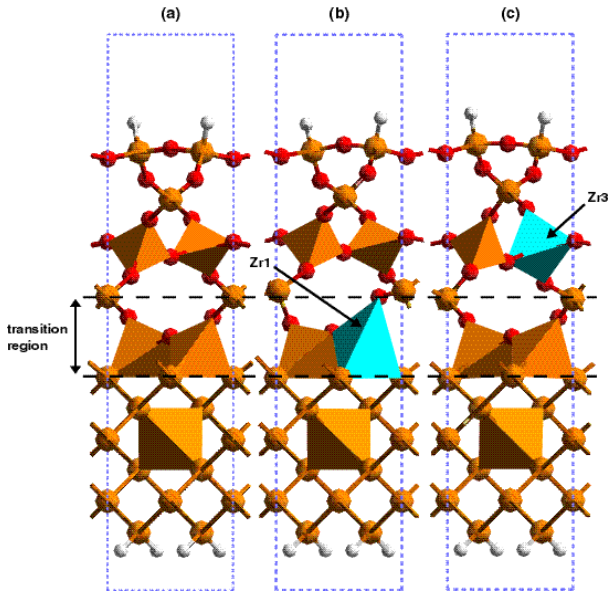

Figure 4.11 Local tetrahedral volumes associated with Si and Zr atoms. (a) Reference Si/SiO_2 interface model formed by attaching β-quartz SiO_2 to Si(001). (b) and (c) Relaxed structures for model Si/silicate interface with Zr incorporation one layer (Zr_1 model) and three layers (Zr_3 model) above the interface.

It is well known that the transition region at the Si/SiO_2 interface contains substantial strain from having to accommodate lattice and bond density mismatches between bulk Si and bulk SiO_2. Pasquarello *et al* have quantified these strains using model Si/SiO_2 interface calculations and concluded that these strains are largely localized within the transition region [104]. Recent experiments on ultrathin oxide reliability by Yang *et al* have correlated the oxidation-induced strain state of the transition region with oxide breakdown during electrical stressing [107,108]. The additional volume strains introduced by Zr or Hf incorporation within the transition region may further degrade the reliability of the dielectric material.

4.3.6 Interface structure with suboxide bonding

The previous sections have considered the properties of model Si/silicate interfaces based on an abrupt Si/SiO_2 interface containing the minimum transition region required to

accommodate the structural change from bulk Si to bulk SiO_2. To be fully consistent with core-level photoelectron spectroscopy measurements of experimental Si/SiO_2 interfaces, however, all three partial oxidation states of Si (e.g. Si^{1+},Si^{2+},Si^{3+}) should be present in the transition region in comparable amounts [106]. Suboxide bonding has been observed at nearly all Si/SiO_2 interfaces, and to the extent that the silicate system is a modification of SiO_2, it is expected that suboxides should also be present at Si/silicate interfaces. It is therefore important to understand the effects of suboxide bonding on the resulting Si/ silicate interface properties.

By removing a single O atom from the transition region of the abrupt interface model, a Si/SiO_2 interface containing the Si^{1+}, Si^{2+}, and Si^{3+} partial oxidation states was formed, as shown in Figure 4.12(a). Since all bonds remain fully saturated, the interface stays electrically ideal, as required. The most important effect of introducing the additional suboxide states is that the structural transition region between bulk Si and bulk SiO_2 has

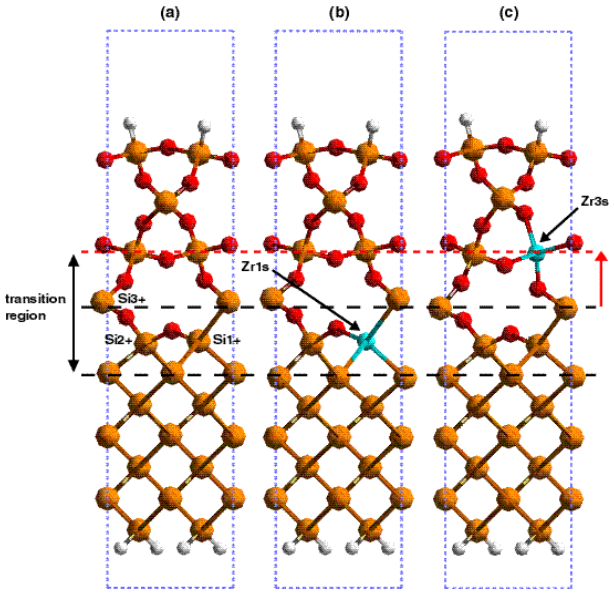

Figure 4.12 (a) Reference Si/SiO_2 interface model with suboxide bonding formed by removing an O atom from the transition region of the model of Figure 4.4(a). (b) and (c) Relaxed structures for suboxide Si/silicate interface with Zr incorporation one layer (Zr_{1s} model) and three layers (Zr_{3s} model) above the interface.

been extended, as illustrated in Figure 4.12(a). While it is difficult to define the boundaries of the transition region precisely, a reasonable approach is to identify the last layer of bulk Si atoms and the first layer of bulk SiO_2 atoms as the boundaries. For the abrupt interface model, the top boundary corresponds to the middle dashed line of Figure 4.12(a). In contrast, for the suboxide interface model, the presence of the Si^{3+} state places the top boundary of the transition region higher by a monolayer, thus extending the transition region.

The process of removing O atoms from the transition region is expected to be a fairly general prescription for generating suboxide states near the Si interface. Since the suboxide region can be further extended by removing additional O atoms, the model of Figure 4.12(a) contains the minimum suboxide region consistent with experimental observations of the interface. Starting with this new reference Si/SiO_2 interface, Zr atoms were once again substituted for Si atoms. The corresponding structures for Zr incorporation one and three layers above the interface are shown in Figures 4.12(b) and 4.12(c) and are referred to as the Zr_{1s} and Zr_{3s} models, respectively. Similar models using Hf were also studied. Each model was relaxed in the same manner as the previous interface structures.

Comparing the total energies of the Zr_{1s} and Zr_{3s} models again provides insight into the relative stability of silicide-like and oxide-like interfaces. The Zr_{3s} model is 1.6eV lower in energy than the Zr_{1s} model. This should be compared to an energy difference of 0.7eV for the Zr_3 and Zr_1 models. Similarly, the Hf_{3s} model is 2.2eV lower in energy than the Zr_{1s} model, compared to an energy difference of 1.3eV for the Hf_3 and Hf_1 models. These larger energy differences indicate that oxide-like bonding at the interface is even more favorable when additional suboxide states are present.

This result is consistent with the previous analysis of the abrupt interface model which attributed the energy difference to the added energy cost of forming Zr-Si or Hf-Si bonds close to the rigid Si substrate. The Zr_1 and Hf_1 models contain two Zr-Si or Hf-Si bonds at the abrupt interface, while the Zr_{1s} and Hf_{1s} models contain three Zr-Si or Hf-Si bonds at

the suboxide interface. Since by definition suboxidation increases the density of Si-Si bonds which may form energetically costly Zr-Si or Hf-Si bonds when substituted for by Zr or Hf atoms, these results suggest that Zr or Hf incorporation within the structural transition region becomes even less favorable in the presence of additional suboxide states.

4.4 EOT limit due to interfacial transition region

The model interface calculations presented in this chapter suggest that Zr or Hf incorporation within the structural transition region is energetically unfavorable. This leads to the formation of a relatively low-*k* interfacial layer between the bulk Si and bulk silicate regions. This stacked structure is illustrated in Figure 4.1(b) and is analogous to the stacked structure resulting from deposition of a pure metal oxide such as ZrO_2 directly on Si. As described in Section 2.3.3, the presence of such an interfacial layer implies that the gate stack appears electrically as a series capacitance. Recall that the following relation for the EOT of the dielectric stack can be written assuming that the interfacial layer has the dielectric properties of SiO_2,

$$t_{eq} = t_{SiO_2} + \left(\frac{k_{SiO_2}}{k_{high-k}}\right) t_{high-k}. \tag{4.1}$$

From Equation 4.1, it is clear that the minimum EOT, and hence the maximum achievable gate capacitance of the stack, is limited by the extent of the interfacial transition region. The minimum transition regions expected at realistic interfaces can be estimated from the abrupt and suboxide interfaces considered earlier. As shown in Figure 4.13(a), the transition region of the abrupt interface model is approximately $3.5\,\mathring{A}$ thick. The presence of additional suboxide states extends the transition region to approximately $5\,\mathring{A}$ thick, as illustrated in Figure 4.13(b). These values compare very well with experimental estimates of the minimum transition region, which generally range from $3\,\mathring{A}$ to $5\,\mathring{A}$, consisting of approximately $3\,\mathring{A}$ for an abrupt structural transition from bulk Si to

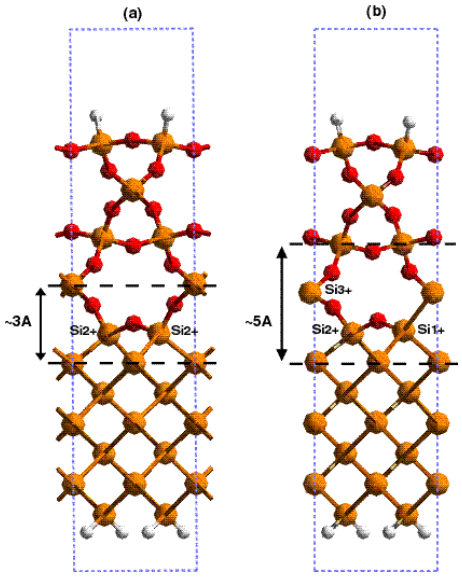

Figure 4.13 Transition region boundaries for model Si/SiO_2 interface with (a) abrupt transition and (b) additional suboxide bonding within the transition region.

bulk SiO_2 and an additional $2\,\mathring{A}$ to accommodate the minimum amount of suboxide observed experimentally [12,17,106].

Based on these transition region thicknesses, it is possible to estimate the scaling limits of the silicate system from the point of view of EOT. For reference, the expected EOT targets for upcoming technology nodes discussed in Chapter 2 are repeated in Figure 4.14. Figure 4.15 shows the expected minimum achievable EOT as a function of silicate layer thickness assuming a *k*-value of 15, the expected maximum dielectric constant of Zr silicate, and the presence of a $5\,\mathring{A}$ thick interfacial transition region with a *k*-value of 4, corresponding to the dielectric constant of SiO_2. Also shown are the $10\,\mathring{A}$ and $6\,\mathring{A}$ EOT targets for the 100nm and 70nm technologies, respectively. It can be observed that the silicate layer can be $20\,\mathring{A}$ thick to meet the requirements of the 100nm technology, whereas the silicate layer can only be about $4\,\mathring{A}$ thick to satisfy the requirements of the 70nm technology. The tunneling current through such a thin dielectric layer will almost certainly be unacceptably high. Clearly, the minimum EOT is limited by the thickness of

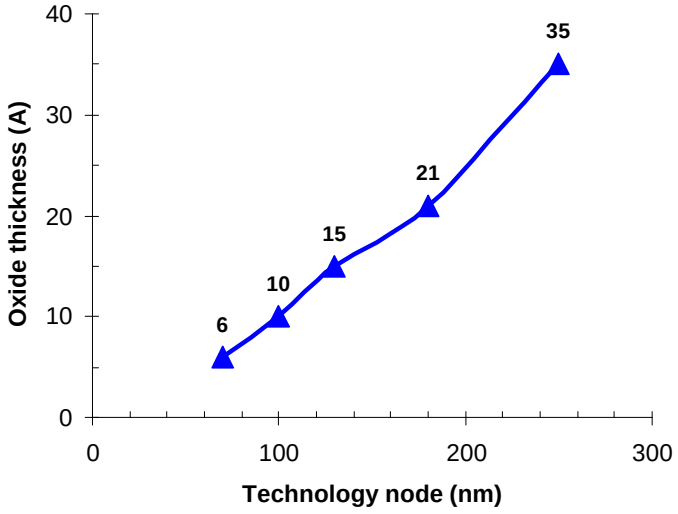

Figure 4.14 Extrapolated gate oxide scaling trends. The vertical axis refers to physical oxide thickness.

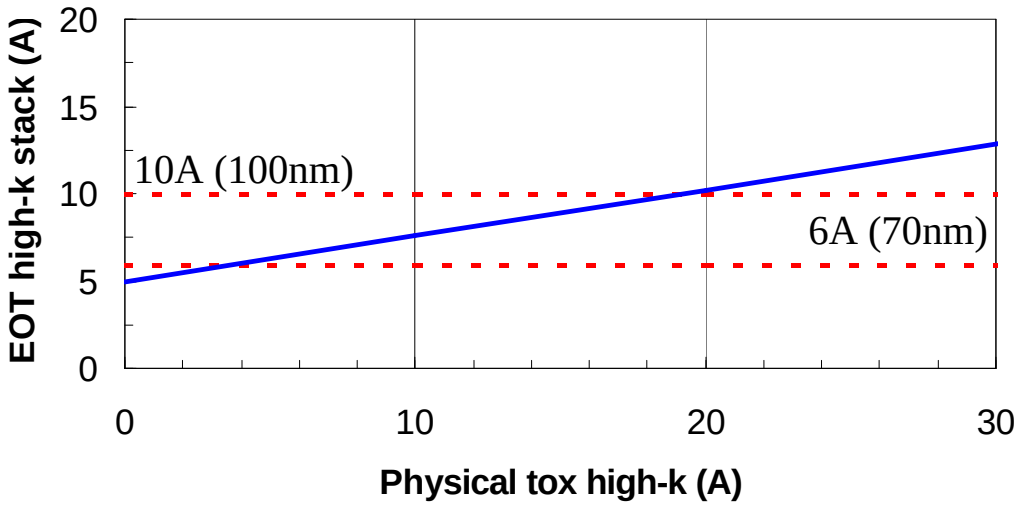

Figure 4.15 Plot of minimum equivalent oxide thickness (EOT) achievable with Zr silicate. The Zr silicate is assumed to have $k = 15$. The presence of a 5A interfacial layer with $k = 4$ is assumed.

the interfacial transition region, which the present calculations suggest are primarily determined by the amount of suboxide formation near the interface.

Since the limitations to scaling EOT for the silicate system arise from the suboxide properties of a nominally Si/SiO_2-like interface, an important conclusion from these studies is that solutions to overcoming such limitations can be based on existing knowledge of the Si/SiO_2 system. It is particularly important to take measures to reduce the formation of excess suboxide. For example, Lucovsky *et al* have reported a 25% reduction in the areal density of Si atoms in suboxide bonding arrangements for oxides grown by remote plasma-assisted oxidation at $300°C$ and then subjected to inert ambients at temperatures to $900°C$ [109].

It may also be necessary to further investigate specific properties of the Si/SiO_2 interface. For example, the detailed properties of the interfacial transition region are not yet fully understood. Extensive x-ray photoelectron spectroscopy (XPS) and electrical measurements have provided a relatively clear picture of the local bonding structure within the transition region. However, since the suboxide region has bonding characteristics intermediate to those in bulk Si and bulk SiO_2, it is expected that the electronic properties of the region will differ from those in the bulk. The STEM experiments by Muller *et al* as well as the theoretical studies by Tang *et al* and Kaneta *et al* described in Section 2.2.2 have shown that the local energy gap within the transition region are much less than that of bulk SiO_2 [12,14,15]. The approximately inverse relation between bandgap and dielectric constant discussed in Section 2.3.2 would then suggest that the dielectric constant of the transition region may be higher than that of bulk SiO_2.

In fact, preliminary experimental results by McIntyre suggest that for a $Si/SiO_2/ZrO_2$ stack grown by ALCVD, the resulting C-V curves are consistent with a dielectric constant in the range of 7 to 8 for the $10\ \mathring{A}$ SiO_2 region [110]. Chemical analysis using a variety of approaches shows no detectable amount of Zr in the SiO_2 region, so that the dielectric enhancement appears to originate from a chemically pure SiO_2 layer. A substantial portion of the $10\ \mathring{A}$ film is expected to consist of suboxide regions associated with the Si/SiO_2 and

SiO_2/ZrO_2 interfaces. Considering that the static dielectric constants of bulk Si and bulk SiO_2 are approximately 12 and 4, respectively, a *k*-value near 8 for the suboxide region, which has a bonding arrangement intermediate to that of Si and SiO_2, is not unreasonable.

The possible dielectric enhancement of the transition region suboxide implies that the contribution of that region to the overall EOT of the dielectric stack can be made less than its physical thickness. Assuming a factor of two increase in the dielectric constant, this brings the intercept of the EOT curve of Figure 4.15 down to 2.5 $\mathring{A}$, thus significantly extending the scalability of the silicate system. Further theoretical investigation of the dielectric behavior of the transition region suboxide would be very valuable in clarifying this possibility.

4.5 Comparison of Zr and Hf silicate structures

Because they are isoelectronic elements, Zr and Hf are expected to have similar structural and electronic properties in the silicate phase. Experimental results seem to favor Hf silicates, since higher dielectric constants and increased stability against phase separation relative to Zr silicates have been reported [30].

The calculations presented in this chapter indicate that Zr atoms consistently form longer bonds with their neighbors than do Hf atoms. The Hf silicate models also exhibit a larger energy cost for silicide formation at the interface relative to the Zr silicate models. Since there is a slight difference between the pseudopotentials used for Zr and Hf, it is important to investigate whether the observed structural properties result from these differences. Conventionally, pseudopotentials only include the outermost shell of electrons in the valence configuration, thus removing the effect of other core electrons. However, it has been reported that for some materials, it is necessary to include the effects of additional core electrons in the valence configuration to accurately reproduce structural properties. In particular, Kralik *et al* observed that the ground state of cubic ZrO_2 could not be reproduced without including additional semi-core states in the Zr pseudopotential

[74]. The Zr pseudopotentials used throughout this work include six semi-core p-electrons in addition to the outermost d- and s-electrons in the valence configuration. In contrast, the Hf pseudopotentials only include the outermost shell of d- and s-electrons in the valence configuration.

To investigate the effects of the pseudopotentials, the ground state structural properties of several Zr and Hf silicate and oxide crystals were determined through full geometry relaxations. The results are reported in Table 4.4 along with experimental values. While the lattice parameters for Zr silicates and oxides are in good agreement with experiment, the Hf oxide values are in error by a few percent and consistently underestimate experimental values. Thus, the results for Hf silicate structures are expected to be in error by a few percent as well. Though not a trivial task, generating an ultrasoft Hf pseudopotential which includes additional semi-core states in the valence configuration will be useful for further study of Hf-based structures.

Table 4.4 Structural properties of known Zr and Hf silicate and oxide crystals. Experimental values for $ZrSiO_4$, ZrO_2, and HfO_2 are noted in parentheses where available [35,103].

Model	**a**	**b**	**c**
$ZrSiO_4$	6.61 (6.61)	6.61 (6.61)	5.95 (6.00)
monoclinic ZrO_2	5.07 (5.15)	5.23 (5.21)	5.30 (5.31)
cubic ZrO_2	5.08 (5.07)		
monoclinic HfO_2	5.03 (5.12)	5.11 (5.17)	5.13 (5.29)
cubic HfO_2	5.04 (5.12)		

4.6 Summary

First principles calculations have been performed to quantify the atomic scale effects of Zr and Hf incorporation at a model Si/silicate interface. The calculated energy cost of forming Zr-Si or Hf-Si bonds suggests that Zr or Hf incorporation within the interfacial transition region is energetically unfavorable, especially when excess suboxide states are present. This leads to the formation to a low-*k* interfacial layer between the bulk Si and bulk silicate regions which limits the maximum achievable gate capacitance of the dielectric stack. Because the transition region is not likely to incorporate Zr or Hf atoms, possible solutions to overcoming these limitations can be based on understanding of a nominally Si/SiO_2-like interface.

Chapter 5

Scaling Limits Imposed by Interface Electronic Properties

This chapter presents first principles calculations aimed at investigating the scaling trends of band offsets at model Si/Zr silicate interfaces. Owing to the d-character of Zr silicate conduction bands, the bandgap and band offset are shown to decrease as the Zr concentration is increased. Since the valence band character of silicates remains unchanged relative to SiO_2, the conduction band offset alone decreases, leading to increasingly asymmetric band offsets at higher Zr concentrations. The use of charge transfer dipoles at the interface is investigated as a possible remedy to restore the band offset symmetry by shifting the silicate bands relative to the silicon bands. The discussion closely follows the material we presented in Reference 111.

Section 5.1 describes the limitations to scaling which arise from the apparent tradeoff between bandgap and dielectric constant of the silicate material.

Section 5.2 describes the computational approach to computing band offsets from first principles, following a method proposed by Van de Walle and Martin [112].

Section 5.3 describes the bulk structural and electronic properties of several high-*k* dielectrics with varying concentrations of Zr, from silicates to pure ZrO_2.

Section 5.4 describes the expected scaling trends of Zr silicate band offsets using model interface calculations. The use of charge transfer dipoles at the interface is proposed as a possible solution to the inherent asymmetry of silicate band offsets.

5.1 Tradeoff between bandgap and dielectric constant

Leakage through an ultrathin oxide arises from direct tunneling of carriers through the potential barrier presented by the insulator. Since the transmission through such a potential depends exponentially on the barrier thickness, much effort has focused on the development of high-*k* gate dielectrics. The higher dielectric constants allow for physically thicker films, thus potentially reducing tunneling transmission while maintaining the gate capacitance needed for scaled device operation. This is illustrated by the band diagram of the MOS system shown in Figure 5.1.

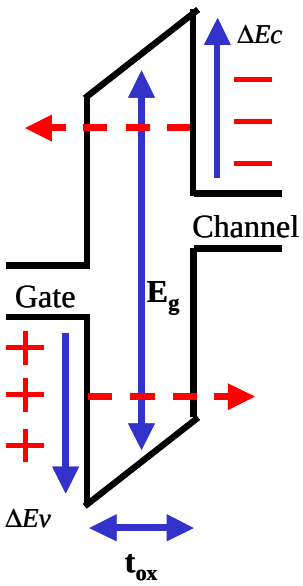

Figure 5.1 Band diagram of the MOS system.

Recall that Zr silicate can be modeled as a mixture of ZrO_2 and SiO_2, $(ZrO_2)_x(SiO_2)_{1-x}$. The conventional wisdom is that the concentration of the transition metal in the silicate can be steadily increased to meet the capacitance requirements of each technology generation, while maintaining a sufficiently thick film to prevent excessive gate leakage. However, increases in the transition metal concentration also tend to reduce the bandgap of the material, since the silicate then becomes increasingly ZrO_2-like, which has a smaller bandgap than SiO_2. The reduction of the insulator bandgap consequently degrades the height of the potential barrier presented to tunneling carriers, indicated on Figure 5.1 as ΔE_c and ΔE_v, the conduction and valence band offsets, respectively. Assuming that gate leakage can be modeled to first-order as direct tunneling through a rectangular potential barrier, the tunneling transmission can be shown to depend on both the barrier thickness and the barrier height, according to the following relationship,

$$T \propto \exp\left(-t_{ox}\sqrt{\Delta E_{c,v}}\right). \tag{5.1}$$

Thus, it is clear that an important design tradeoff arises between the film thickness, which depends on the dielectric constant, and the band offset as the transition metal concentration is increased in future technology generations.

5.2 Computational approach

To determine the band offsets, the bulk energy levels of Si and Zr silicate must be aligned at the interface. However, the lack of a well-defined absolute energy reference in an infinite periodic solid prevents a direct comparison of energy levels from two different bulk materials. A variety of theoretical approaches have been proposed to overcome this difficulty. The band offset calculations presented in this chapter follow a particularly effective approach first proposed by Van de Walle and Martin and employed in a variety of studies of Si/SiO_2 and III-V interfaces [14,102,112-115]. Figure 5.2 shows the procedure graphically.

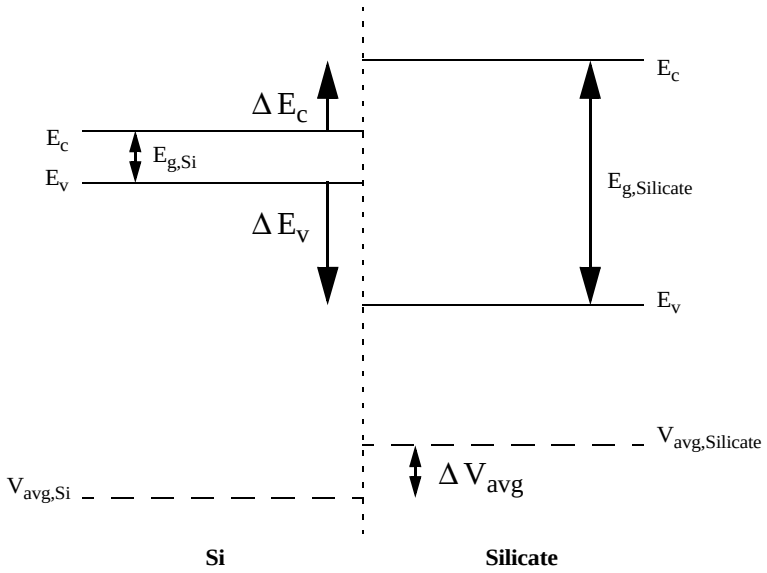

Figure 5.2 Diagram showing Van de Walle's band offset calculation procedure. The band structures and average potential energies ($V_{avg,Si}$ and $V_{avg,Silicate}$) are obtained from bulk calculations. The potential shift ΔV_{avg} between the average levels in Si and Zr silicate is obtained from a superlattice calculation.

Van de Walle's theory first requires separate calculations of the bulk electronic structure to obtain the conduction (E_c) and valence (E_v) band energies, bandgap (E_g), and average potential energy (V_{avg}) for each material. V_{avg} is derived from a three-dimensional grid of potential energy values by first averaging over a plane parallel to the expected interface and then averaging those plane-averaged values through the direction perpendicular to the expected interface. Once V_{avg} is determined, E_c, E_v, and E_g are referenced relative to V_{avg}.

The bulk calculations are followed by a superlattice calculation which requires the formation of an interface between the bulk materials. Since in general lattice mismatch and other strains exist throughout the superlattice structure, it is necessary to allow for atomic relaxation to obtain the ground state configuration. The plane-averaged potential energy is calculated through the superlattice in the direction perpendicular to the interface. V_{avg} terms are then calculated for each side of the interface to extract a potential shift

ΔV_{avg} between the average bulk potential levels. The ΔV_{avg} term includes the effects of structural relaxation and charge transfer dipoles at the interface on the resulting band offsets.

5.3 Bulk calculations

Calculations of several bulk oxides and silicates were carried out within DFT-LDA to study the effect of increasing Zr concentration on the underlying electronic structure. Three known crystals served as references for comparison: β-cristobalite SiO_2 with zero atomic percent Zr; the silicate zircon, $ZrSiO_4$, with 16.7 atomic percent Zr; and monoclinic ZrO_2 with 33 atomic percent Zr [35,99,103]. Since only the SiO_2 model can be used to form a well-defined, lattice-matched interface with crystalline Si, the $ZrSiO_4$ and ZrO_2 crystals alone cannot be used to study the expected behavior of band offsets at the Si interface. Thus two additional model silicates were formed as described below.

5.3.1 Bulk structure

Cubic β-cristobalite was chosen as the reference SiO_2 crystal [99]. The equilibrium lattice constant was found to be 7.34 $\mathring{A}$, in good agreement with 7.39-7.41 $\mathring{A}$ as predicted by previous first principles studies [14,96]. At this lattice constant, the Si-O bond length was 1.59 $\mathring{A}$ and the Si-O-Si bond angle was 180 degrees. In order to form an SiO_2 model compatible with the Si lattice, a prescription first proposed by Herman *et al* was followed [116]. The Herman construction has been used in a number of previous theoretical studies of the Si/SiO_2 interface [14,101,102,117]. A tetragonal lattice which is nearly lattice-matched with Si(001) was first formed by rotating the β-cristobalite 45 degrees along its c-axis. This tetragonal cell has a lattice constant of 5.19 $\mathring{A}$ along the a-axis, representing a 4.4% lattice mismatch with Si. In practice, all proposed crystalline models of the Si/SiO_2 interface introduce such mismatch, and it is standard practice to simply expand or contract the SiO_2 model to match the Si lattice constant [15,104]. By a Poisson's ratio argument, it is expected that expansion along the a-axis would cause contraction along the c-axis. By

searching for the total energy minimum, the optimized c-axis lattice constant was found to be 6.90 $\mathring{A}$. The resulting lattice-matched crystal structure is shown in Fig. 5.3(a), and the relevant structural parameters of both models are summarized in Table 5.1.

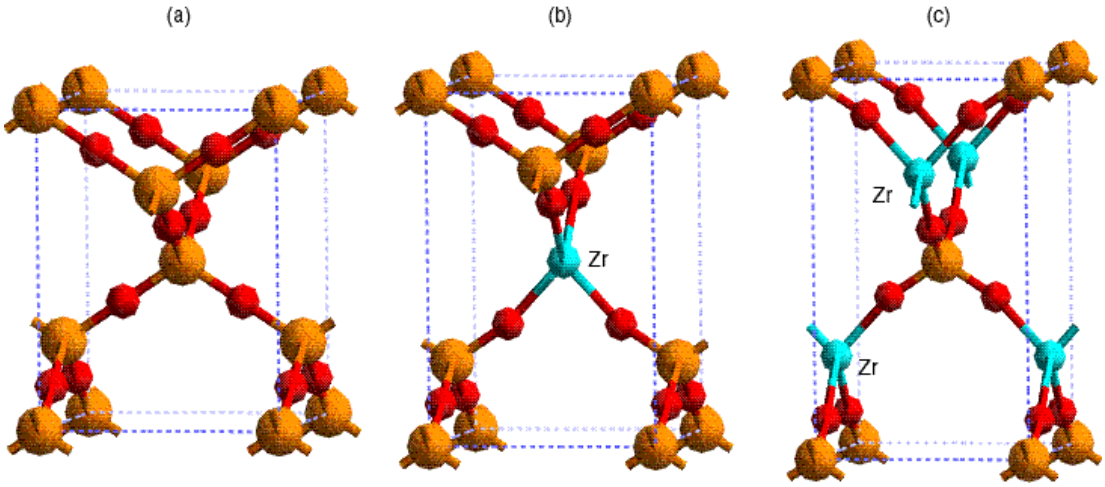

Figure 5.3 (a) Crystal structure of β-cristobalite SiO_2. (b) Structure of model silicate, $Zr_1Si_3O_8$, with 8.3 atomic % Zr concentration. (c) Structure of $Zr_2Si_2O_8$ with 16.7 atomic % Zr concentration. Each model is lattice matched to the Si lattice constant. Large atoms are Si, small atoms are O. Zr atoms are indicated.

The high degree of symmetry of the lattice-matched β-cristobalite structure allows it to be completely specified by a single Si-O bond length of 1.61 $\mathring{A}$ and Si-O-Si bond angle of 180 degrees. This facilitates an important goal of the model silicate study, which is to isolate as much as possible the effect of varying the Zr concentration by keeping constant all other factors, such as the Si-O bonding and lattice parameters. Based on the lattice-matched β-cristobalite structure, a model silicate ($Zr_1Si_3O_8$) with 8.3 atomic percent Zr was formed by replacing a single Si atom in the SiO_2 model with Zr. By varying only the Zr-O bond length to accommodate the larger Zr atom, the lowest energy structure was found at a Zr-O bond length of 1.97 $\mathring{A}$. This compares reasonably to a Zr-O bond length of 1.94 $\mathring{A}$ obtained in a previous study in which a β-quartz SiO_2 model with Zr substitution for Si at 11 atomic percent Zr was allowed to fully relax towards its total energy minimum

Table 5.1 Structural properties and bandgap values of model silicates based on the β-cristobalite SiO_2 crystal. Both the raw LDA and corrected LDA bandgap (E_g) values are given. An empirical correction factor of 1.66 has been used to obtain the latter values. Note that all Si-O-Si bond angles are 180 degrees and all Zr-O-Si bond angles are 166 degrees. (*) indicates models lattice-matched to the Si lattice constant.

Model	**Atomic % Zr**	**Lattice const. (A)**	**O-coord. around Zr**	**Si-O bond length (A)**	**Zr-O bond length (A)**	**LDA E_g (eV)**	**Corr. LDA E_g (eV)**
β-crist. SiO_2	0	5.19, 5.19, 7.34	4	1.59	--	5.37	8.9
β-crist. SiO_2 (*)	0	5.43, 5.43, 6.90	4	1.61	--	5.06	8.39
$Zr_1Si_3O_8$ (*)	8.3	5.43, 5.43, 8.03	4	1.61	1.97	3.98	6.59
$Zr_2Si_2O_8$ (*)	16.7	5.43, 5.43, 9.16	4	1.61	1.97	3.84	6.36

[94]. A second model silicate ($Zr_2Si_2O_8$) with 16.7 atomic percent Zr was formed by replacing a second Si atom with Zr and maintaining the Zr-O bond length at 1.97 $\mathring{A}$. Figures 5.3(b) and 5.3(c) show the resulting model silicate structures, and structural parameters of both models are summarized in Table 5.1.

The assumption that Zr is four-fold coordinated by oxygen (O) at the concentrations considered is an important limitation of the study. While Zr does indeed appear to be tetrahedrally bonded to O at low Zr concentration, recent experiments have shown that the Zr coordination increases at higher concentrations. Based on extended x-ray absorption fine structure spectroscopy (EXAFS) measurements of Zr silicate films, Lucovsky has found that the average Zr coordination indeed increased from 4.5 ± 1 for samples with ~3.3 atomic percent Zr to 7.2 ± 1 for samples with ~8.3 atomic percent Zr [36]. However,

the difficulty in defining a silicate structure with eight-fold coordinated Zr that can form a lattice-matched interface with Si prevents direct study of the interface properties of such silicates.

While their interface properties are not explicitly addressed, the bulk structural and electronic properties of two known crystals with higher than four-fold Zr coordination are studied and compared to those of model silicates based on the β-cristobalite structure. Zircon, $ZrSiO_4$, is a known crystalline silicate with 16.7 atomic percent Zr [35]. The tetragonal unit cell consists of parallel chains of edge-sharing four-fold coordinated SiO_4 units and eight-fold coordinated ZrO_8 units. Monoclinic ZrO_2 with 33 atomic percent Zr is the known ground state of Zr oxide and consists of seven-fold coordinated Zr atoms [103]. Structural parameters of both crystals obtained from full relaxation within DFT-LDA are listed in Table 5.2 along with experimental values. DFT typically predicts ground state

Table 5.2 Structural properties and bandgap values of known Zr silicate and oxide crystals. Both the raw LDA and corrected LDA bandgap (E_g) values are given. Experimental values for $ZrSiO_4$ and ZrO_2 are noted in parentheses [35,103].

Model	**Atomic % Zr**	**Lattice const. (A)**	**O-coord. around Zr**	**Si-O bond length (A)**	**Zr-O bond length (A)**	**LDA E_g (eV)**	**Corr. LDA E_g (eV)**
$ZrSiO_4$	16.7	6.61, 6.61, 5.95 (6.61, 6.61, 6.00)	8	1.61 (1.62)	2.14, 2.26 (2.13, 2.27)	4.58	7.59
monocl. ZrO_2	33	5.07, 5.23, 5.30 (5.15, 5.21, 5.31)	7	--	2.05-2.24 (2.04-2.26)	3.41	5.64

structural properties very accurately, and the agreement with experiment in this case is quite good. An interesting observation is that the mass density of the tetrahedral model silicate $Zr_2Si_2O_8$ (1.4 amu/ $\mathring{A}^3$) is approximately half that of $ZrSiO_4$ (2.8 amu/ $\mathring{A}^3$). The large density difference implies that local stress-strain conditions may influence the stability of various oxygen coordinations within the silicate film. Since the $Zr_2Si_2O_8$ and $ZrSiO_4$ structures contain the same Zr concentration, it is also possible to directly compare their total energies. The $Zr_2Si_2O_8$ model contains two $ZrSiO_4$ bonding units and has an energy of -54.79eV per Zr bonding unit while zircon contains four $ZrSiO_4$ bonding units and has an energy of -57.32eV per Zr bonding unit, so that the higher coordinated zircon model is 2.52eV per Zr bonding unit more stable. This large energy difference helps to explain the higher average Zr coordinations observed in experimental silicate films with higher than a few atomic percent Zr [36].

5.3.2 Bulk electronic structure

The electronic structure of each silicate was analyzed by calculating the partial density of states (PDOS) and the band structure. The PDOS is obtained by projecting the total DOS onto individual atomic orbitals and is particularly useful for identifying the nature of bonding in a material. It is well known that in SiO_2, the lowest conduction band states are formed from the Si s-states, while the highest valence band states are formed from the O p-states [118]. In contrast, the PDOS of the model silicate $Zr_1Si_3O_8$ shown in Figure 5.4 indicates that the lowest conduction band states are formed from the Zr d-states, while the highest valence band states are still formed from the O p-states. The $Zr_2Si_2O_8$ model has a very similar PDOS and is not shown. The PDOS of the known silicate $ZrSiO_4$ was also computed as shown in Figure 5.5. Comparing the two PDOS near the bandgap, the bonding character in four-fold coordinated and eight-fold coordinated Zr silicates is qualitatively similar. The lowest conduction band states consist of Zr d-states, while the highest valence band states consist of O p-states. Since d-electron levels are lower in energy than s-electron levels, the conduction band energies in Zr silicates are expected to

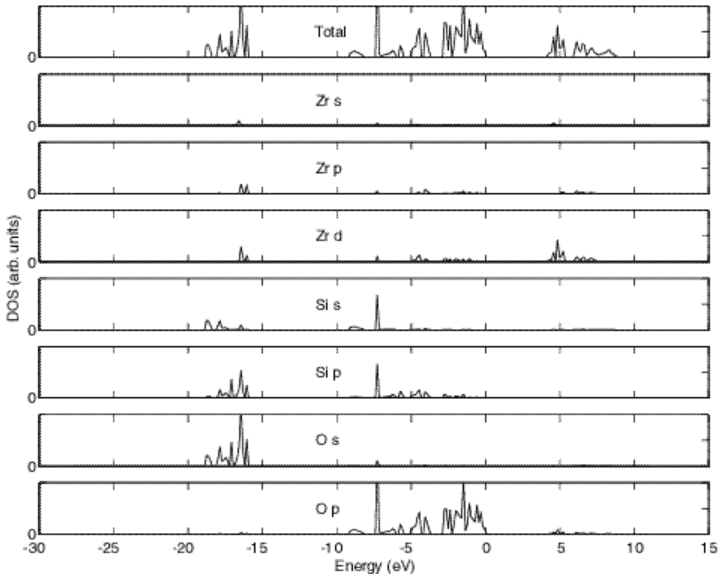

Figure 5.4 Partial density of states (PDOS) of the model silicate $Zr_1Si_3O_8$. The zero of energy represents the Fermi level.

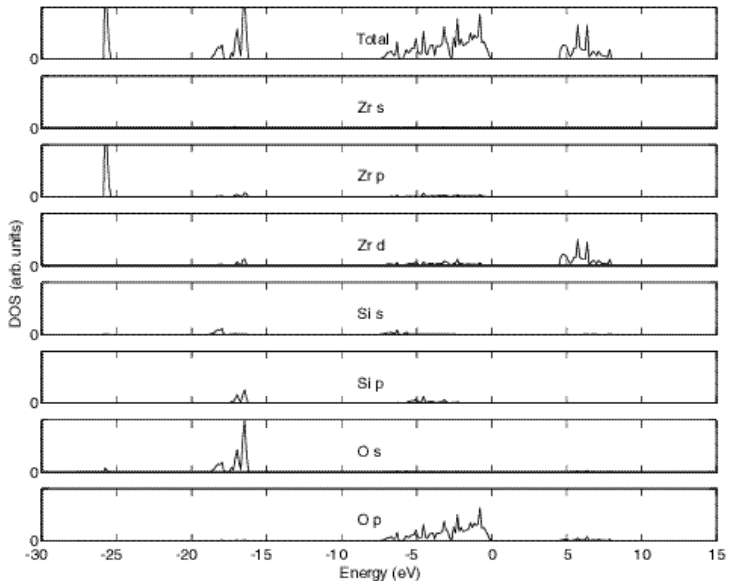

Figure 5.5 PDOS of the crystal zircon, $ZrSiO_4$. The zero of energy represents the Fermi level.

decrease with increasing Zr character (i.e. concentration). In contrast, the similarity of the valence band character between Zr silicate and SiO_2 suggests that the valence band energies will remain constant even with increasing Zr concentration. The net effect of a decreasing conduction band and a constant valence band is an expected reduction in the bandgap of Zr silicates with increasing Zr concentration. This has been identified as an important shortcoming of transition metal silicates and oxides in general [118,119].

5.3.3 LDA limitations on bandgap calculation

The minimum bandgap values were determined by analyzing the calculated band structures and are reported in Tables 5.1 and 5.2. An important limitation of the local density approximation (LDA) employed in most first principles calculations is that excited state energies, including the bandgap, are typically underestimated. Compared to experimental bandgaps of 8.9eV for SiO_2 and 5.83eV for monoclinic ZrO_2, the present calculations yield 5.37eV and 3.41eV, respectively [120]. A common first-order correction is to empirically fit the LDA bandgap to a known experimental value by employing the scissors operator described in Section 3.3.1.1. The difficulty with this approach for this calculation is that experimental bandgap measurements for Zr silicates are not available, and it is not clear whether a single, uniform shift can describe the bandgap enhancement across a range of Zr concentrations. It can be observed, however, that an empirical, multiplicative factor of 1.66 which fits the SiO_2 bandgap, also brings the ZrO_2 bandgap within 3% of experiment. The remainder of this study assumes that the same empirical factor which fits the end members SiO_2 and ZrO_2 can also be applied to silicates across a range of Zr concentrations. While the correction factor is empirical, it is expected that the important trends of silicate band offsets observed are still meaningful. It is worth noting that the quasiparticle GW method, which represents a higher level of theory beyond DFT-LDA, has been shown to accurately predict excited state energies for a wide range of materials, including transition metal oxides such as ZrO_2 [71,74]. While

the GW approach is more computationally intensive than DFT-LDA, such a study of silicate band structures may be of significant interest to the high-*k* community.

The bandgaps of the lattice-matched model silicates were also calculated and are shown in Table 5.1. It should be noted that the Zr-O bond length of 1.97 $\mathring{A}$ chosen for these models is shorter than the Zr-O nearest neighbor distances of 2.1 $\mathring{A}$ and 2.3 $\mathring{A}$ reported for experimental silicate films by Lucovsky [36]. To explore the effect of the bond length, additional silicate models were studied with different Zr-O distances. The bandgap was found to decrease more than 30% as the Zr-O bond length was increased from 1.9 $\mathring{A}$ to 2.1 $\mathring{A}$. By comparing the fully-relaxed and lattice-matched SiO_2 structures, it was also observed that accommodating the 4.4% lattice mismatch between SiO_2 and Si led to a 6% decrease in the bandgap. Again the decrease in bandgap was accompanied by an increase in the Si-O bond length, from 1.59 $\mathring{A}$ to 1.61 $\mathring{A}$. Figure 5.6 summarizes the corrected LDA bandgaps of all structures studied as a function of atomic percent Zr. The

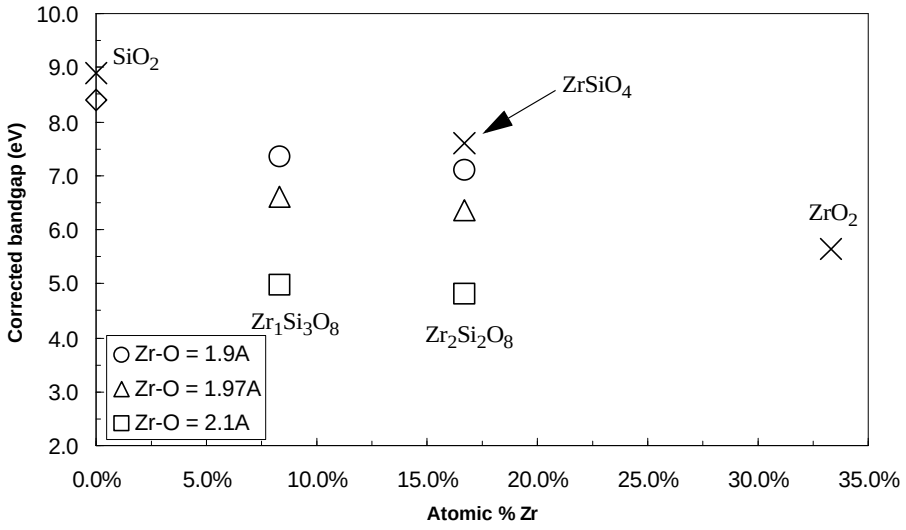

Figure 5.6 Corrected LDA bandgaps as a function of atomic % Zr. An empirical correction factor of 1.66 has been used. Models that were fully allowed to relax are indicated by 'x'. All other models were lattice-matched along the a-axis to the Si lattice constant.

sensitivity of the bandgap to Zr-O bond length and lattice mismatch suggest that local stress-strain conditions in the bulk and at the interface will impact band offsets.

5.4 Interface calculations

When two different semiconductors are brought together, there is generally some transfer of charge to equalize the chemical potential across the interface. The resulting interface dipole, along with the electron affinity of the two semiconductors, determines the band lineups [119,121,122]. In the case of Zr silicates, the band offsets are expected to depend on the role of Zr in altering the electronic structure of the reference Si/SiO_2 interface. An interesting observation to this end can be made based on the bonding character of silicates as revealed by the PDOS analysis in the previous section. Recall that the Zr d-states form the conduction bands in silicates while Si s-states form the conduction bands in SiO_2. O p-states form the valence bands in both materials. In the absence of differences in interface dipoles, the valence band offset in silicates is expected to remain similar to that in SiO_2. On the other hand, it is expected that the conduction band offset in silicates will be lower than in SiO_2, since d-electron levels are lower in energy than s-electron levels. It can then be projected that the conduction band offset alone would decrease with increasing Zr concentration, while the valence band offset will remain unaltered, leading to increasingly asymmetric offsets. Similar conclusions have been drawn based on a Harrison tight-binding model of Zr silicates [64,65,123]. Robertson has also predicted asymmetric offsets for a wide range of high-*k* materials consisting of d-electron transition metals [119]. The inherent asymmetry of barrier heights in silicates would imply increased susceptibility to electron tunneling relative to hole tunneling.

Several authors have studied the effect of interface dipoles on band lineups at the Si/SiO_2 interface through theoretical methods [101,102,124,125]. Kageshima *et al* correlated the strength of dipoles arising from different surface terminations at model Si/SiO_2 interfaces to changes in the valence band offset using first principles supercell calculations

[101,102]. Massoud and Lucovsky *et al* estimated the change in conduction band offset due to dipoles at pure, nitrided, and suboxide Si/SiO_2 interfaces based on empirical and first principles cluster calculations [124,125]. These results suggest that it may be possible to explicitly introduce dipoles at Si/silicate interfaces to restore the symmetry of barrier heights implied by the PDOS analysis. Robertson has suggested such a solution for the case of the Ta_2O_5/Si interface, which has a very asymmetric alignment due to a small conduction band offset [119]. These ideas are explored for the Zr silicate system to gain insight into the design of optimal interface properties.

5.4.1 Interface models

Following the method of Van de Walle and Martin outlined earlier, Si/silicate interface band offset calculations were carried out using the lattice-matched models developed in Section 5.3 [112]. Previous studies have followed a similar approach to study band offsets at the Si/SiO_2 interface [14,102]. It is customary to fully relax the atomic positions in order to obtain the lowest energy interface structure. However, in this study, atomic relaxations were limited to the first Si and O layers at the Si/SiO_2 and $Si/Si_1Zr_3O_8$ interfaces. The relaxation led to structural changes at the interface, as the Si-O bond length was observed to change from 1.61 $\mathring{A}$ to 1.61-1.64 $\mathring{A}$ and the Si-O-Si bond angle was observed to change from 180 to 165-168 degrees. No relaxation was allowed at the $Si/Si_2Zr_2O_8$ interface, so that the Si-O bond length remained 1.61 $\mathring{A}$ and the Zr-O-Si bond angle remained 166 degrees. These limitations were imposed in order to maintain a constant ZrO_4 bonding unit to facilitate comparison of band offsets at different Zr concentrations.

5.4.2 Effect of interface dipoles

The Herman construction of the Si/SiO_2 interface is known to leave a single Si dangling bond at the interface [116,117]. In the first set of calculations, the dangling bond in each interface model was hydrogen terminated. The resulting H-terminated models for the $Si/Si_1Zr_3O_8$ and $Si/Si_2Zr_2O_8$ interfaces are shown in Figures 5.7(a) and 5.8(a),

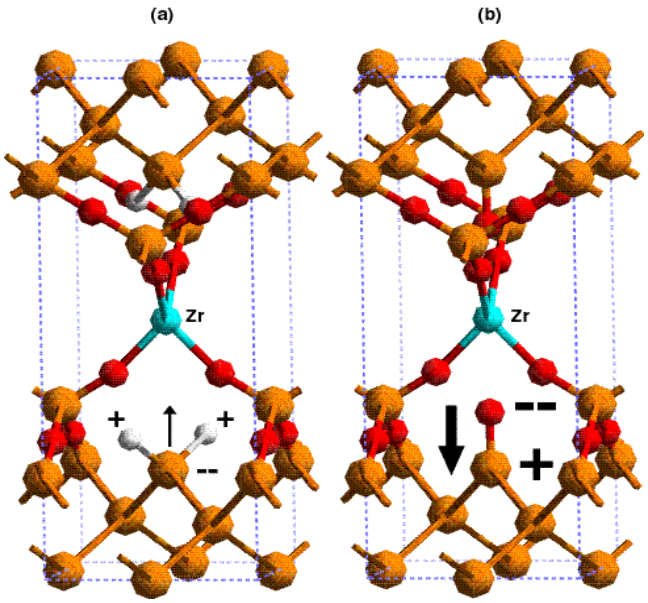

Figure 5.7 Interface structure between Si and model silicate, $Zr_1Si_3O_8$. In (a), the Si dangling bond at the interface is H-terminated. In (b), the Si dangling bond at the interface is O-terminated. The charge transfer dipole at the interface is indicated.

respectively. It should be noted that a superlattice structure is required by the Van de Walle method, so that there are two identical interfaces in each supercell. The Si/SiO_2 interface model is not shown. The potential shift ΔV_{avg} across the interface was calculated for each model to extract the band offsets listed in Table 5.3. As shown in Figure 5.9, the valence band offsets remain nearly constant around 4.5eV, while the conduction band offsets degrade substantially from 2.8eV with increasing Zr concentration. This behavior is consistent with a decreasing bandgap, which occurs primarily through a reduction of the conduction band energies, as expected based on the previous PDOS analysis. The increasingly asymmetric ratio of conduction to valence band offset is shown in Table 5.3.

Changing the surface termination of the Si dangling bond is a direct and controlled way of altering the interface dipole. A number of such terminations for the Si/SiO_2 interface have been considered by Kageshima *et al*, and the formation of a Si=O double

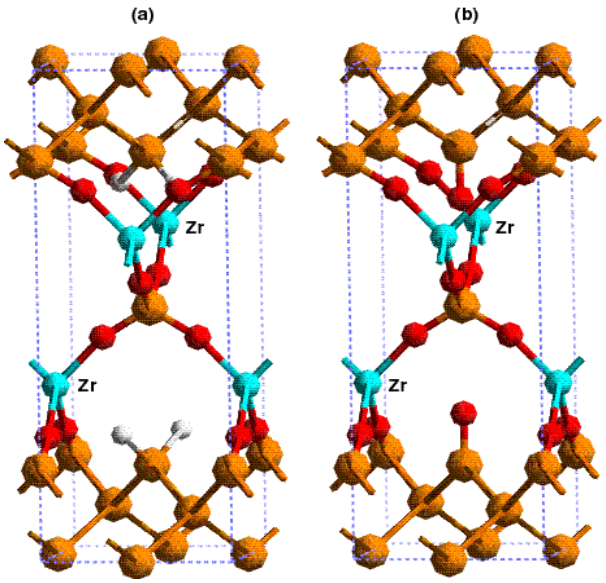

Figure 5.8 Interface structure between Si and model silicate, $Zr_2Si_2O_8$. In (a), the Si dangling bond at the interface is H-terminated. In (b), the Si dangling bond at the interface is O-terminated.

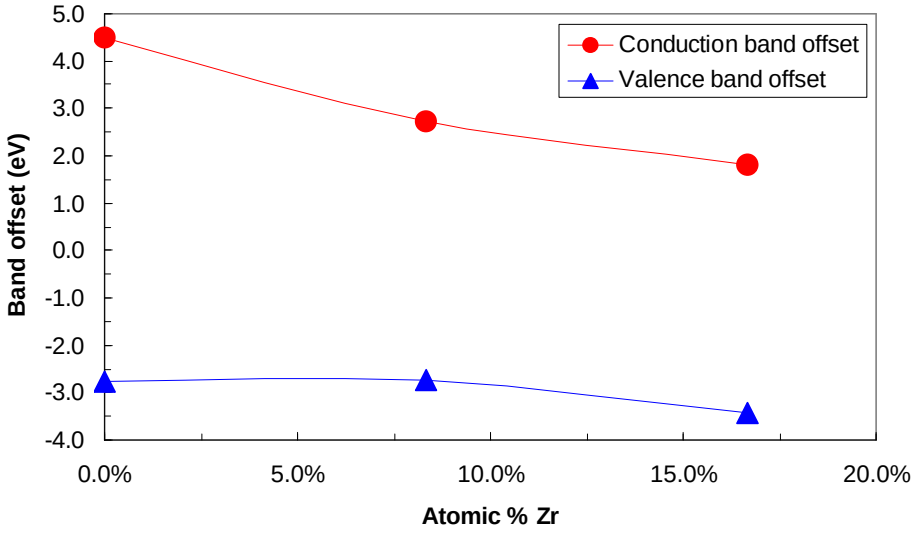

Figure 5.9 Conduction and valence band offsets of Si/silicate interface vs atomic % Zr. The interface Si dangling bond is H-terminated.

bond has been shown to saturate the Si dangling bond [101,102]. Since the Si=O bond is much more polar than the Si-H bond, a large change in the interface charge transfer is expected. The resulting O-terminated models for the $Si/Si_1Zr_3O_8$ and $Si/Si_2Zr_2O_8$ interfaces are shown in Figures 5.7(b) and 5.8(b), respectively. Figure 5.7 compares the expected interface dipole effect for H- and O-termination of the $Si/Si_1Zr_3O_8$ interface.

Table 5.3 Conduction and valence band offsets of model Si/silicate interfaces with H- and O-termination of the Si dangling bond at the interface. The ratio of conduction to valence band offset is also indicated.

Interface model	**Termination of Si dangling bond**	**Conduction band offset ΔE_c (eV)**	**Valence band offset ΔE_v (eV)**	**Ratio of conduction to valence band offset**
Si/SiO_2	H	2.77	4.49	0.62
	O	4.48	2.78	1.61
$Si/Zr_1Si_3O_8$	H	1.05	4.43	0.24
	O	2.74	2.74	1.00
$Si/Zr_2Si_2O_8$	H	0.61	4.63	0.13
	O	1.80	3.44	0.52

The calculated band offsets are listed in Table 5.3. As expected, substantial shifts in the band offset energies are observed for H- versus O-termination. Defining an explicit interface boundary for the plane-averaged potentials is an important technical consideration when employing Van de Walle's method. In order to compute the average potentials for each bulk material, the potential energy of some of the structural transition region between the bulk regions must be assigned to the Si side of the interface, while the remainder must be assigned to the SiO_2 side. This demarcation must be made consistently for each superlattice model so that accurate comparisons can be made. A reasonable approach is to define the interface boundary at the midpoint between the first bulk-bonded atomic layers on either side of the interface. This approach is nearly equivalent to the

method chosen by Kageshima *et al*, in which the interface boundary is defined as being the midpoint between the two types of Si surface atoms at the interface [101,102].

As shown in Figure 5.10, the general trend that valence band offsets remain nearly constant while the conduction band offsets degrade considerably with increasing Zr concentration holds as in the H-terminated case. However, the conduction band offsets are shifted up while the valence band offsets are shifted down relative to the H-terminated model by 1.2-1.7eV. This is consistent with an upward shift of the silicate bands relative to the Si bands, as depicted in Figure 5.11. The potential shift ΔV_{dipole} arises from the electric field due to the charge transfer dipole, as can be shown by successive integrations of Poisson's equation across the interface. The key insight is that the dipole must point from the silicate into the Si substrate. As a consequence of the shift in potential, a more symmetric band alignment has been restored, as shown in Table 5.3. Restoring the symmetry is considered important since degraded barrier heights on the order of 1eV can lead to additional conduction mechanisms, such as Schottky emission, as illustrated in Figure 5.12 [119]. Since the predicted valence band offsets are substantially in excess of 1eV, it may be desirable to deliberately tradeoff valence for conduction band offset through the introduction of interface dipoles.

In addition to the explicit dipole introduced by Si dangling bond termination, a more subtle dipole effect exists at the model silicate interface. It can be observed that the valence band offsets for H-termination change by less than 4% with increasing Zr concentration relative to the Si/SiO_2 interface. For O-termination, the valence band offset is seen to decrease by 2% at the $Si/Si_1Zr_3O_8$ interface and to increase by 24% at the $Si/Si_2Zr_2O_8$ interface relative to the Si/SiO_2 interface. The large increase at the O-terminated $Si/Si_2Zr_2O_8$ interface implies that the effect of the charge transfer dipole due to O-termination has been reduced. To confirm this, the charge transfer at the Si interface in each O-terminated model was estimated by summing one-half of the total charge density in the bulk Si region and comparing to the H-terminated Si/SiO_2 case. The estimated charge transfer is observed to scale nearly linearly with the valence band offset, as shown

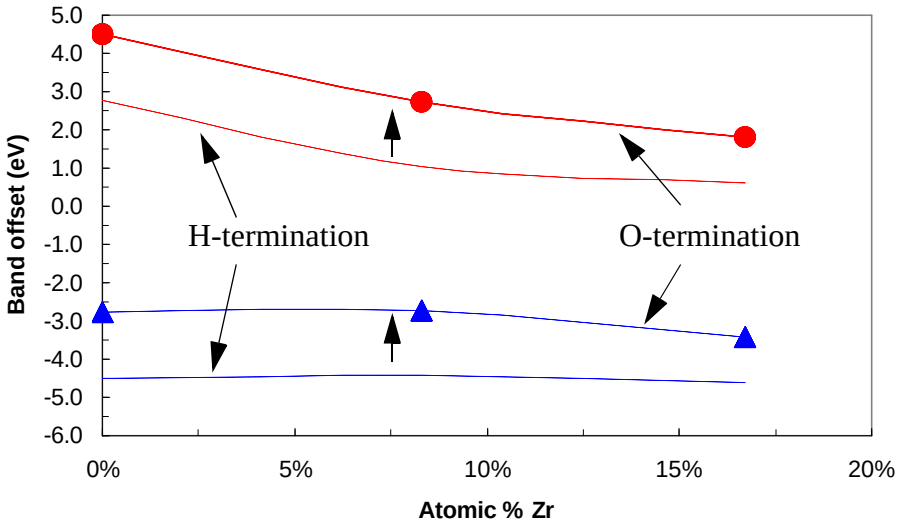

Figure 5.10 Conduction and valence band offsets of model Si/silicate interfaces vs atomic % Zr showing the effects of altering the termination of the Si dangling bond.

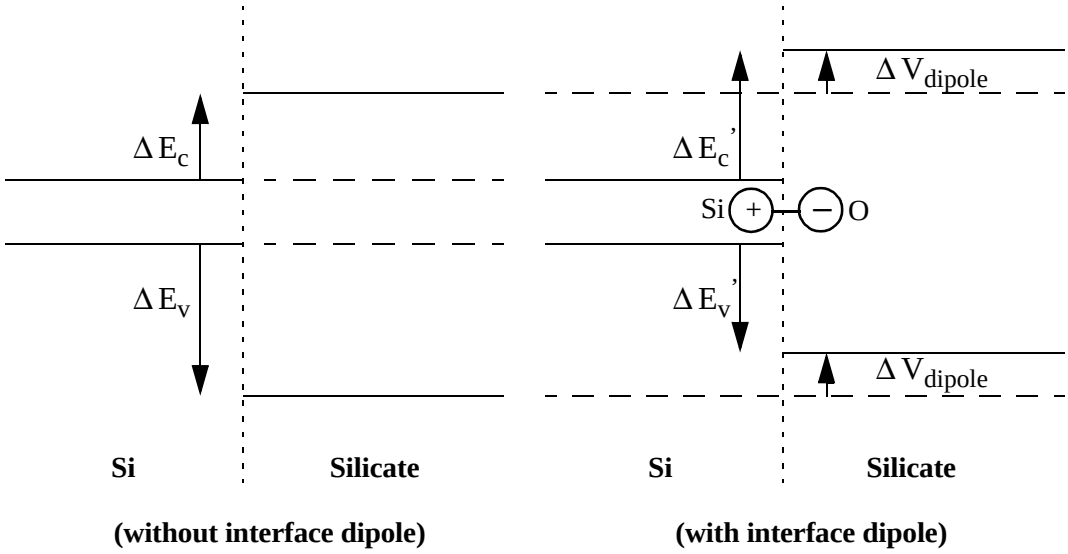

Figure 5.11 Band diagram showing role of interface dipoles in altering the conduction and valence band offsets.

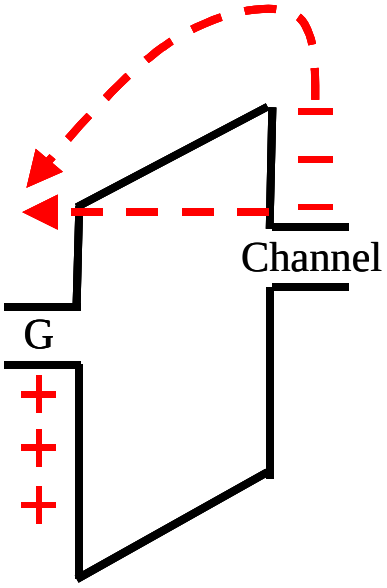

Figure 5.12 Diagram illustrating Schottky emission over the shallow conduction band barrier, in addition to direct tunneling.

in Figure 5.13. As suspected, substantially less charge transfer occurs at the O-terminated $Si/Si_2Zr_2O_8$ interface, consistent with the observed shift in the valence band offset.

To account for the difference in charge transfer, it can be observed that an obvious feature of the $Si/Si_2Zr_2O_8$ interface model is the presence of Si-O-Zr bonding at the interface, whereas the other models consist of Si-O-Si bonding at the interface. It might be expected that the enhanced polarizability of the Zr-O bond would somehow affect the Si-O interface dipole by transferring additional charge to the O atom. However, any such effect at the model interface is expected to cancel since the Zr atom is tetrahedrally bonded to O atoms in a symmetric manner. The absence of a large change in the band offset at the H-terminated $Si/Si_2Zr_2O_8$ interface also supports this view. However, it is worth noting that an experimental interface is likely to break the perfect symmetry of the tetrahedral bonding units assumed in this study, in which case the presence of Zr-O-Si bonding at the interface may well affect the band lineup. As an alternative explanation for the decreased charge transfer, it is suggested that the observed change may be due to the

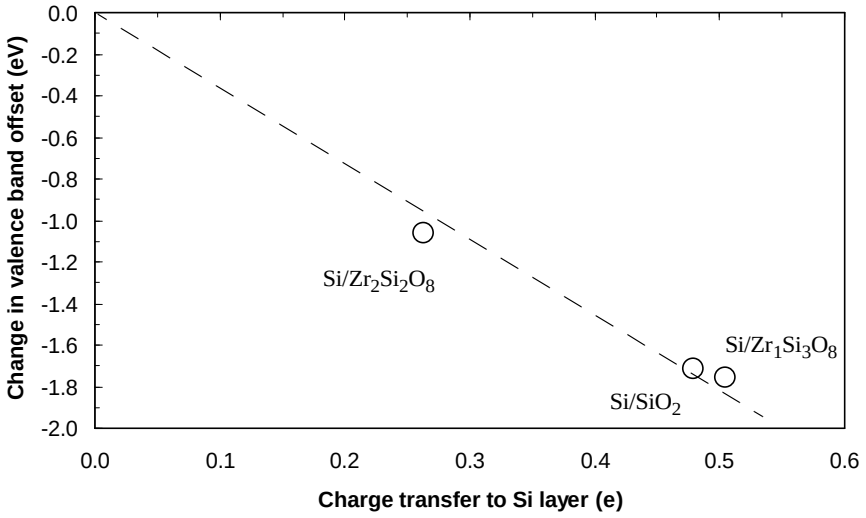

Figure 5.13 Change in valence band offset as a function of charge transfer to Si layer for O-terminated interface models.

electrostatic attraction between the surface O atom, which has a net negative charge, and the Zr atom, which has a net positive charge. Since the $Si/Si_2Zr_2O_8$ interface model places the Zr atom closer to the surface O atom, the effect is expected to be stronger. The Si=O bond has indeed been measured to be 5% longer at the $Si/Si_2Zr_2O_8$ interface, and in general less charge transfer is expected at longer bond lengths. The observed difference in charge transfer may also be due in part to substrate-induced charge redistribution caused by changes in the surface bonding arrangement. Direct calculation of the effective charge of interface atoms by means of response functions may help to clarify the mechanism further [78].

5.4.3 Discussion and comparisons with other work

It is necessary to mention that the controlled assumptions made throughout this study introduce some uncertainty into the quantitative predictions presented. For example, the present calculations predict conduction and valence band offsets for the H-terminated Si/SiO_2 model of 2.8eV and 4.5eV, compared to experimental values of 3.5eV and 4.4eV,

respectively [126]. It is difficult to know whether the conduction band error arises from the empirical correction factor introduced to fit the LDA bandgap to experiment, the assumed interface bonding structure, or the observed decrease in bandgap due to lattice mismatch strain. For the Si/silicate interface, the present results predict conduction and valence band offsets of 0.61eV and 4.63eV, respectively, for H-termination and 1.80eV and 3.44eV, respectively, for O-termination. Robertson's study based on tight-binding calculations predicts conduction and valence band offsets of 1.5eV and 3.4eV, respectively [119]. The agreement of the O-terminated model with Robertson's results is most likely accidental, however. The present study assumes a tetrahedrally bonded silicate structure whose corrected bandgap is 6.36eV. Robertson used the higher coordinated silicate $ZrSiO_4$, whose bandgap he estimated to be 6eV, whereas the present calculations predict 7.59eV for the same structure. Experimental studies of Zr silicate electronic structure will be needed to further clarify the discrepancies. However, the observed qualitative scaling trends of silicate band offsets are expected to be valid, and the controlled manner in which the present calculations were performed provides insight into the dependence of band offsets on such properties as the Zr-O bond length, the lattice mismatch strain, and the charge transfer dipole at the interface.

The expected effects of higher than four-fold Zr coordination largely depend on the resulting changes in the interface structure. If the interface bonding remains similar to the case of tetrahedral bonding, then any change in the bandgap is expected to directly affect the conduction band offset alone, since the interface dipole properties remain unchanged. This is analogous to the observed 1.8eV decrease in bandgap and conduction band offset which occurs in going from the Si/SiO_2 to $Si/Zr_1Si_3O_8$ interface models, since the interface bonding there remains nearly identical. If the interface bonding were to change significantly due to higher Zr coordination, it is expected that the effects of interface dipoles would be greater, since a higher density of O atoms would accompany the Zr atoms. However, whether the additional dipole effects would improve or degrade the band offset asymmetry would depend on the detailed interface structure.

5.4.4 Interface design issues

The high concentration of Si=O surface termination dipoles used in this study is likely unachievable in practice. In addition, the calculations presented here have not considered the relative stability of H- and O-termination. While H-termination of Si dangling bonds is widely believed to occur, much less experimental evidence is available for O-termination, though some correlations suggest that such termination may exist [102,127-129]. Nonetheless, the present calculations have shown that the O-termination is stable and fully saturates the Si dangling bonds.

The O termination has demonstrated that dipoles pointing into the Si substrate can help to restore symmetry in silicate band offsets. This insight can be applied to evaluate the potential impact of various interface processing steps on the Si/silicate band offsets. For example, Hess *et al* have shown that dramatic improvements in reliability at the Si/SiO_2 interface can be obtained by annealing with deuterium instead of hydrogen [130]. Since this isotope effect arises from differences in the Si-H and Si-D vibrational modes, not from chemical changes in interface bonding, the use of deuterium is not expected to improve the degraded conduction band offset.

In contrast, recent experimental results provide further evidence of the existence of dipole effects at the Si/SiO_2 interface. For example, the use of monolayer interface nitridation, which has been found to greatly suppress gate leakage at the Si/SiO_2 interface, may also be beneficial at the Si/silicate interface. While the physical mechanism underlying the leakage suppression is still being debated, Yang *et al* observed that the leakage reduction due to interface nitridation can be modeled with an increase in the conduction band offset relative to suboxide interfaces [131]. Since nitrogen (N) atoms are believed to substitute for Si atoms at the interface, a possible explanation for this effect is that Si-N bonds replace suboxide Si-Si bonds [132]. It is known that Si-N bonds are more polarizable than Si-Si bonds, so that greater charge transfer across the interface is expected. In order for this effect to increase the conduction band offset, the Si-N dipole would need to point towards the Si substrate. Theoretical calculations by Lucovsky *et al*

employing first principles molecular cluster methods support Yang's interpretation of the nitridation data [125]. Along similar lines, it is expected that an interface which minimizes suboxide bonding at the surface is preferred, since a fully oxidized Si atom with two Si-O bonds should lead to increased charge transfer compared to a suboxidized Si atom with one or more Si-Si bonds instead.

In summary, steadily increasing the Zr concentration is expected to lead to a number of observable changes in the material properties of silicates. The dielectric constant should increase, leading to a physically thicker film and a thicker barrier to tunneling. At the same time, the bandgap should decrease, so that carriers see a lower potential barrier to tunneling. In addition to this tradeoff caused by increasing Zr concentration, the actual position of Zr incorporation relative to the Si interface will also play an important role, since any effect on the interface dipole will lead to changes in the band offset. These effects need to be well understood, since an existing design goal requires Zr incorporation close to the Si interface. It is desirable to form a uniform Si/silicate interface rather than an intermediate SiO_2-like transition layer, since this maximizes the effective capacitance of the high-k dielectric stack. It is expected that the closer the Zr lies to the interface, the stronger will be any resulting dipole effect, though it may raise or lower the band offsets depending on the resulting structure. These considerations may or may not be achievable in practice, however, since the calculations presented in Chapter 4 suggest that volume strains generated by the larger size and longer equilibrium bond lengths of Zr atoms relative to Si atoms make Zr incorporation close to the interface energetically unfavorable [94].

5.5 Summary

First principles calculations were performed to study the scaling trends of band offsets at model Si/Zr silicate interfaces. Based on bulk calculations, the silicate bandgap was shown to decrease with increasing Zr concentration. Interface calculations showed that in

the absence of changes in interface dipoles, the decrease in the bandgap causes a lowering of the conduction band offsets relative to Si/SiO_2, while the valence band offsets remain unchanged. This was projected to lead to increasingly asymmetric barrier heights for electrons and holes. Thus, as the Zr concentration is increased, a tradeoff develops between barrier thickness, which depends on the dielectric constant, and the barrier height, which depends on the band offsets. Interface dipoles were then explicitly introduced by varying the surface termination at the interface. Dipoles pointing toward the Si substrate were shown to raise the silicate bands relative to the Si bands, thus increasing the conduction band offset and decreasing the valence band offset, leading to more symmetric band offsets.

While the study explicitly focused on Zr silicates, the insight provided by the study is expected to be generally applicable to a wide range of alternative dielectrics, since silicates are representative of a broader class of high-*k* materials composed of d-electron transition metals. The net effect of the tradeoff between barrier thickness and barrier height on the resulting tunneling transmission needs further investigation in order to evaluate the feasibility of transition metal oxides and silicates as a possible replacement gate dielectric material for SiO_2. The extent to which the inherent asymmetry of barrier heights may affect scaled CMOS device performance also needs to be studied. Though it remains to be seen how strong an effect can be practically realized, the introduction of interface dipoles appears to be one promising way to overcome the limitations of barrier asymmetry exhibited by transition metal oxides and silicates.

Chapter 6

Contributions and Recommendations

6.1 Contributions

This thesis presents one of the first applications of atomic scale modeling methods to the challenging problem of high-*k* gate dielectric engineering. After studying several different theoretical approaches, the use of first principles density functional theory was selected. Specifically, the research investigated the Zr and Hf silicate material system. Motivated by the belief that properties at the Si interface will ultimately determine the feasibility of any alternative dielectric, the research has focused primarily on the interface properties of the silicate system, with emphasis on those properties which may eventually limit the scaling of silicates to end-of-the-roadmap technologies. Specific contributions of this work are described below.

1) This research has provided insight into the structural properties of the Si/silicate interface at the atomic scale. Using first principles density functional theory, model interface calculations have been performed to show that SiO_2-like bonding is energetically favored at the Si interface relative to silicide-like bonding, in agreement with experimental studies of the interface. Possible volume strain effects associated with the incorporation of

Zr and Hf atoms close to the Si interface have also been quantified. Extended suboxide states within the interfacial transition region have been identified as significantly limiting the scalability of the silicate system from the point of view of equivalent oxide thickness. Because these limitations arise at a nominally Si/SiO_2-like interface, these calculations suggest that solutions can be built on knowledge of the Si/SiO_2 system.

2) This research has also provided insight into the electronic structure of the Si/silicate interface. First principles calculations have been performed to quantify the expected lowering of the conduction band offset with increasing Zr concentration. The use of charge transfer dipoles at the interface has been proposed as a means of overcoming the inherent asymmetry of silicate band offsets. Again, because these limitations arise at a nominally Si/SiO_2-like interface, it is believed that solutions can be built on knowledge of the Si/SiO_2 system.

6.2 Recommendations for future work

1) Application of the density functional perturbation theory (DFPT) approach to the study of dielectric constant scaling in pseudo-binary alloys would be very useful. In particular, the dielectric behavior of the transition region suboxide at Si/SiO_2 interfaces needs to be better understood, since this has important implications on the scalability of nearly all high-*k* dielectrics.

2) The effects of transition metal incorporation close to the Si interface still requires further study. It will be especially important to understand the effects on channel mobility, which is expected to depend on the scattering potential introduced by the transition metal. Similar considerations apply to the possible use of charge transfer dipoles at the interface, since this is also expected to alter the scattering potential near the interface. Segregation of

the transition metal at the Si interface will also need to be studied, since incorporation within the bulk Si region is expected to degrade transistor performance substantially.

3) The first principles approach should be extended to the study of a wider range of alternative high-*k* dielectrics, including pure binary metal oxides (e.g. ZrO_2, HfO_2) as well as Al_2O_3-based pseudo-binary alloys (e.g. aluminates). It will be especially useful to study the properties of the interfaces of those materials with silicon.

References

Chapter 1

[1] See http://public.itrs.net/ for most recent updates to the International Technology Roadmap for Semiconductors.

[2] P. Packan, “Pushing the limits,” *Science*, vol. 285, p. 2079, 1999.

Chapter 2

[3] R. Dennard, F. Gaensslen, H.-N. Yu, V. Rideout, E. Bassous, and A. LeBlanc, "Design of ion-implanted MOSFET's with very small physical dimensions," *IEEE Journal of Solid-State Circuits*, vol. SC-9, p. 256, 1974.

[4] T. Ghani, K. Mistry, P. Packan, S. Thompson, M. Stettler, S. Tyagi, and M. Bohr, "Scaling challenges and device design requirements for higher performance sub-50nm gate length planar CMOS transistors," Symposium on VLSI Technology Digest, 2000.

[5] T. Ghani, S. Ahmed, P. Aminzadeh, J. Bielefeld, P. Charvat, C. Chu, M. Harper, P. Jacob, C. Jan, J. Kavalieros, C. Kenyon, R. Nagisetty, P. Packan, J. Sebastian, M. Taylor, J. Tsai, S. Tyagi, S. Yang, and M. Bohr, "100nm gate length high performance / low power CMOS transistor structure," IEDM Technical Digest, p. 415, 1999.

[6] M. Hargrove, S. Crowder, E. Nowak, R. Logan, L. Han, H. Ng, A. Ray, D. Sinitsky, P. Smeys, F. Guarin, J. Oberschmidt, E. Crabbe, D. Yee, and L. Su, "High-performance sub-0.08um CMOS with dual gate oxide and 9.7ps inverter delay," IEDM Technical Digest, p. 627, 1998.

[7] M. Rodder, S. Hattangady, N. Yu, W. Shiau, P. Nicollian, T. Laaksonen, C. Chao, M. Mehrotra, C. Lee, S. Murtaza, and S. Aur, "A 1.2V, 0.1um gate length CMOS technology: design and process issues," IEDM Technical Digest, p. 623, 1998.

[8] S.-H. Lo, D. Buchanan, and Y. Taur, "Modeling and characterization of quantization, polysilicon depletion, and direct tunelling effects in MOSFETs with ultrathin oxides," *IBM Journal of Research and Development*, vol. 43, p. 327, 1999.

[9] C. Choi, Ph.D. thesis, Electrical Engineering, Stanford University, 2001.

[10] F. Pollak, "New microarchitecture challenges in the coming generations of CMOS process technologies," 32nd Annual International Symposium on Microarchitecture, Haifa, Israel, November 16-18, 1999.

[11] S. Lo, D. Buchanan, Y. Taur, and W. Wang, "Quantum-mechanical modeling of electron tunneling current from the inversion layer of ultra-thin-oxide nMOSFET's," *IEEE Electron Device Letters*, vol. 18, p. 209, 1997.

[12] D. Muller, T. Sorsch, S. Moccio, F. Baumann, K. Evans-Lutterodt, and G. Timp, "The electronic structure at the atomic scale of ultrathin gate oxides," *Nature*, vol. 399, p. 758, 1999.

[13] M. Schulz, "The end of the road for silicon?," *Nature*, vol. 399, p. 729, 1999.

[14] S. Tang, R. Wallace, A. Seabaugh, and D. King-Smith, "Evaluating the minimum thickness of gate oxide on silicon using first-principles method," *Applied Surface Science*, vol. 135, p. 137, 1998.

[15] C. Kaneta, T. Yamasaki, T. Uchiyama, T. Uda, and K. Terakura, "Structure and electronic property of Si(100)/SiO_2 interface," *Microelectronic Eng*ineering, vol. 48, p. 117, 1999.

[16] A. Kingon, J.-P. Maria, and S. Streiffer, "Alternative dielectrics to silicon dioxide for memory and logic devices," *Nature*, vol. 406, p. 1032, 2000.

[17] G. Wilk, R. Wallace, and J. Anthony, "High-*k* gate dielectrics: Current status and materials properties considerations," *Journal of Applied Physics*, vol. 89, p. 5243, 2001.

[18] D. Buchanan, "Scaling the gate dielectric: Materials, integration, and reliability," *IBM Journal of Research and Development*, vol. 43, p. 245, 1999.

[19] B. Cheng, M. Cao, P. Vande Voorde, W. Greene, H. Stork, Z. Yu, and J. Woo, "Design considerations of high-*k* gate dielectrics for sub-0.1-um MOSFET's," *IEEE Transactions on Electron Devices*, vol. 46, p. 261, 1999.

[20] G. Lucovsky, "Local bonding, phase stability and interface properties of replacement gate dielectrics, including silicon oxynitride alloys and nitrides, and film 'amphoteric' elemental oxides and silicates," to be published.

[21] C. Kittel, *Introduction to Solid State Physics*, 7th Edition, John Wiley & Sons, Inc., New York, 1996.

[22] K. Cho, "First principles modeling of high-*k* gate dielectric materials," *Computational Materials Science*, in press.

[23] C. Chaneliere, J. Autran, R. Devine, and B. Balland, "Tantalum pentoxide (Ta_2O_5) thin films for advanced dielectric applications," *Materials Science & Engineering*, vol. R22, p. 269, 1998.

[24] G. Alers, D. Werder, Y. Chabal, H. Lu, E. Gusev, E. Garfunkel, T. Gustafsson, and R. Urdahl, "Intermixing at the tantalum oxide/silicon interface in gate dielectric structures," *Applied Physics Letters*, vol. 73, p. 1517, 1998.

[25] S. Campbell, D. Gilmer, X. Wang, M. Hsich, H. Kim, W. Gladfelter, and J. Yan, "MOSFET transistors fabricated with high permittivity TiO_2 dielectrics," *IEEE Transactions on Electron Devices*, vol. 44, p. 104, 1997.

[26] S. Campbell, R. Smith, N. Hoilien, B. He, and W. Gladfelter, "Group IVB metal oxides: TiO_2, ZrO_2, and HfO_2 as high permittivity gate insulators," Proceedings of MRS Workshop on High-*k* Gate Dielectrics, p. 9, New Orleans, June 2000.

[27] Y. Nishioka, H. Shinriki, and K. Mukai, "Influence of SiO_2 at the Ta_2O_5/Si interface on dielectric characteristics of Ta_2O_5 capacitors," *Journal of Applied Physics*, vol. 61, p. 2335, 1987.

[28] G. Wilk and R. Wallace, "Electrical properties of hafnium silicate gate dielectrics deposited directly on silicon," *Applied Physics Letters*, vol. 74, p. 2854, 1999.

[29] G. Wilk and R. Wallace, "Stable zirconium silicate gate dielectrics deposited directly on silicon," *Applied Physics Letters*, vol. 76, p. 112, 2000.

[30] G. Wilk, R. Wallace, and J. Anthony, "Hafnium and zirconium silicates for advanced gate dielectrics," *Journal of Applied Physics*, vol. 87, p. 484, 2000.

[31] J. Lee, W. Qi, R. Nieh, B. Lee, L. Kang, K. Onishi, Y. Jeon, and E. Dharmarjan, "HfO_2, ZrO_2 and their silicates for gate dielectric applications," Proceedings of MRS Workshop on High-*k* Gate Dielectrics, p. 23, New Orleans, June 2000.

[32] M. Copel, M. Gribelyuk, and E. Gusev, "Structure and stability of ultrathin zirconium oxide layers on Si(001)," *Applied Physics Letters*, vol. 76, p. 436, 2000.

[33] C. Perkins, B. Triplett, P. McIntyre, K. Saraswat, S. Haukka, and M. Tuominen, unpublished.

[34] G. Jun and K. Cho, private communication.

[35] Z. Mursic, T. Vogt, H. Boysen, and F. Frey, "Single-crystal neutron diffraction study of metamict zircon up to 2000K," *Journal of Applied Crystallography*, vol. 25, p. 519, 1992.

[36] G. Lucovsky and G. Rayner, "Microscopic model for enhanced dielectric constants in low concentration SiO_2-rich noncrystalline Zr and Hf silicate alloys," *Applied Physics Letters*, vol. 77, p. 2912, 2000.

[37] D. Buchanan, private communication.

Chapter 3

[38] A. Kawamoto, J. Jameson, K. Cho, and R. Dutton, “Challenges for atomic scale modeling in alternative gate stack engineering,” *IEEE Transactions on Electron Devices*, vol. 47, p. 1787, 2000.

[39] A. Nakano, M. Bachlechner, P. Branicio, T. Campbell, I. Ebbsjo, R. Kalia, A. Madhukar, S. Ogata, A. Omeltchenko, J. Rino, F. Shimojo, P. Walsh, and P. Vashishta, “Large-scale atomistic modeling of nanoelectronic structures,” *IEEE Transactions on Electron Devices*, vol. 47, p. 1804, 2000.

[40] D. Yong and P. Kollman, “Pathways to a protein folding intermediate observed in a 1-microsecond simulation in aqueous solution,” *Science*, vol. 282, p. 740, 1998.

[41] B. Brooks, R. Bruccoleri, B. Olafson, D. States, S. Swaminathan, and M. Karplus, “CHARMM: a program for macromolecular energy, minimisation, and dynamics calculations,” *Journal of Computational Chemistry*, vol. 4, p. 187, 1983.

[42] G. Gilmer, T. de la Rubia, D. Stock, and M. Jaraiz, “Diffusion and interactions of point defects in silicon: molecular dynamics simulations,” *Nuclear Instruments and Methods in Physics Research B*, vol. B102, p. 247, 1995.

[43] D. Stock, G. Gilmer, M. Jaraiz, and T. de la Rubia, “Point defect accumulation in silicon irradiated by energetic particles: a molecular dynamics simulation,” *Nuclear Instruments and Methods in Physics Research B*, vol. B102, p. 207, 1995.

[44] F. Stillinger and T. Weber, “Computer simulation of local order in condensed phases of silicon,” *Physical Review B*, vol. 31, p. 5262, 1985.

[45] J. Tersoff, “Empirical interatomic potential for silicon with improved elastic properties,” *Physical Review B*, vol. 38, p. 9902, 1988.

[46] J. Justo, M. Bazant, E. Kaxiras, V. Bulatov, and S. Yip, “Interatomic potential for silicon defects and disordered phases,” *Physical Review B*, vol. 58, p. 2539, 1998.

[47] S. Tsuneyuki, Y. Matsui, H. Aoki, and M. Tsukada, “New pressure-induced structural transformations in silica obtained by computer simulation,” *Nature*, vol. 339, p. 209, 1989.

[48] P. Vashishta, K. Rajiv, J. Rino, and I. Ebbsjo, “Interaction potential for SiO_2: a molecular-dynamics study of structural correlations,” *Physical Review B*, vol. 41, p. 12197, 1990.

[49] P. Ewald, *Ann. Physics*, vol. 64, p. 253, 1921.

[50] T. Wantanabe, H. Fujiwara, H. Noguchi, T. Hoshino, and I. Ohdomari, "Novel interatomic potential energy function for Si, O mixed systems," *Japanese Journal of Applied Physics*, vol. 38, pt. 2, p. 366, 1998.

[51] T. Watanabe and I. Ohdomari, "Modeling of SiO_2/Si(100) interface structure by extended Stillinger-Weber potential," *Thin Solid Films*, vol. 343, p. 370, 1999.

[52] T. Watanabe and I. Ohdomari, "Modeling of a SiO_2/Si(100) structure including step and terrace configurations," *Applied Surface Science*, vol. 162, p. 116, 2000.

[53] J. Jameson and A. Kawamoto, GONZO simulation package, Stanford University, 1998.

[54] P. Hohenberg and W. Kohn, "Inhomogeneous electron gas," *Physical Review*, vol. 136, p. B864, 1964.

[55] W. Kohn and L. Sham, "Self-consistent equations including exchange and correlation effects," *Physical Review*, vol. 140, p. A1133, 1965.

[56] D. Ceperley and B. Alder, "Ground state of the electron gas by a stochastic method," *Physical Review Letters*, vol. 45, p. 566, 1980.

[57] J. Perdew and A. Zunger, "Self-interaction correction to density-functional approximations for many-electron systems," *Physical Review B*, vol. 23, p. 5048, 1981.

[58] D. Hamann, M. Schluter, and C. Chiang, "Norm-conserving pseudopotentials," *Physical Review Letters*, vol. 43, p. 1494, 1979.

[59] L. Kleinman and D. Bylander, "Efficacious form for model pseudopotentials," *Physical Review Letters*, vol. 48, p. 1425, 1982.

[60] A. Rappe, K. Rabe, E. Kaxiras, and J. Joannopoulos, "Optimized pseudopotentials," *Physical Review B*, vol. 41, p. 1227, 1990.

[61] M. Payne, M. Teter, D. Allan, T. Arias, and J. Joannopoulos, "Iterative minimization techniques for *ab initio* total-energy calculations: molecular dynamics and conjugate gradients," *Reviews of Modern Physics*, vol. 64, p. 1045, 1992.

[62] M. Yin and M. Cohen, "Theory of static structural properties, crystal stability and phase transformations: application to Si and Ge," *Physical Review B*, vol. 26, p. 5668, 1992.

[63] C. Van de Walle, Ph.D. thesis, Electrical Engineering, Stanford University, 1986.

[64] W. Harrison, Electronic Structure and the Properties of Solids, Freeman, San Francisco, 1980.

[65] W. Harrison, Elementary Electronic Structure, World Scientific, Singapore, 1999.

[66] M. Menon and K. Subbaswamy, "Universal parameter tight-binding molecular dynamics: application to C_{60}," *Physical Review Letters*, vol. 67, p. 3487, 1991.

[67] I. Kwon, R. Biswas, C. Wang, K. Ho, and C. Soukoulis, "Transferable tight-binding models for silicon," *Physical Review B*, vol. 49, p. 7242, 1994.

[68] M. Tang, L. Colombo, J. Zhu, and T. de la Rubia, "Intrinsic point defects in crystalline silicon: Tight-binding molecular dynamics studies of self-diffusion, interstitial-vacancy recombination, and formation volumes," *Physical Review B*, vol. 55, p. 14279, 1997.

[69] S. Sze, invited talk at Center for Integrated Systems, Stanford University, 1999.

[70] R. Godby, M. Schluter, and L. Sham, "Self-energy operators and exchange-correlation potentials in semiconductors," *Physical Review B*, vol. 37, p. 10159, 1988.

[71] M. Hybertsen and S. Louie, "Electron correlation in semiconductors and insulators: Band gaps and quasiparticle energies," *Physical Review B*, vol. 34, p. 5390, 1986.

[72] O. Zakharov, A. Rubio, X. Blase, M. Cohen, and S. Louie, "Quasiparticle band structures of six II-VI compounds: ZnS, ZnSe, ZnTe, CdS, CdSe, and CdTe," *Physical Review B*, vol. 50, p. 10780, 1994.

[73] S. Zhang, M. Cohen, S. Louie, D. Tomanek, and M. Hybertsen, "Quasiparticle band offset at the (001) interface and band gaps in ultrathin superlattices of GaAs-AlAs heterojunctions," *Physical Review B*, vol. 41, p. 10058, 1990.

[74] B. Kralik, E. Chang, and S. Louie, "Structural properties and quasiparticle band structure of zirconia," *Physical Review B*, vol. 57, p. 7027, 1998.

[75] O. Pulci, G. Onida, A. Shkrebtii, R. Del Sole, and B. Adolph, "Plane-wave pseudopotential calculation of the optical properties of GaAs," *Physical Review B*, vol. 55, p. 6685, 1997.

[76] Y. Xu and W. Ching, “Electronic and optical properties of all polymorphic forms of silicon dioxide,” *Physical Review B*, vol. 44, p. 11048, 1991.

[77] Y. Xu and W. Ching, “Electronic structure and optical properties of α and β phases of silicon nitride, silicon oxynitride, and with comparison to silicon dioxide,” *Physical Review B*, vol. 51, p. 17379, 1995.

[78] X. Gonze and C. Lee, “Dynamical matrices, Born effective charges, dielectric permittivity tensors, and interatomic force constants from density-functional perturbation theory,” *Physical Review B*, vol. 55, p. 10355, 1997.

[79] X. Gonze, D. Allan, and M. Teter, “Dielectric tensor, effective charges, and phonons in α-quartz by variational density-functional perturbation theory,” *Physical Review Letters*, vol. 68, p. 3603, 1992.

[80] F. Bernardini, V. Fiorentini, and D. Vanderbilt, “Polarization-based calculation of the dielectric tensor of polar crystals,” *Physical Review Letters*, vol. 79, p. 3958, 1997.

[81] F. Bernardini and V. Fiorentini, “Electronic dielectric constants of insulators calculated by the polarization method,” *Physical Review B*, vol. 58, p. 15292, 1998.

[82] G. Jun, G.-M. Rignanese, X. Gonze, and K. Cho, private communication.

[83] G. Jun, K. Cho, and R. Dutton, private communication.

[84] Cambridge Serial Total Energy Package (CASTEP) is commercially licensed through Accelrys Inc. at http://www.accelrys.com.

[85] FHI98MD package is licensed through the Fritz-Haber-Institut der Max-Planck-Gesellschaft at http://www.fhi-berlin.mpg.de/th/fhimd/.

[86] DFT++ package is licensed through MIT at http://dft.mit.edu/dft++/.

[87] G. Kresse and J. Hafner, “Ab initio molecular dynamics for liquid metals,” *Physical Review B*, vol. 47, p. 558, 1993.

[88] G. Kresse and J. Furthmuller, “Efficiency of ab-initio total energy calculations for metals and semiconductors using a plane-wave basis set,” *Computational Materials Science*, vol. 6, p. 15, 1996.

[89] G. Kresse and J. Furthmuller, “Efficient iterative schemes for ab initio total-energy calculations using a plane-wave basis set,” *Physical Review B*, vol. 54, p. 11169, 1996.

[90] D. Vanderbilt, “Soft self-consistent pseudopotentials in a generalized eigenvalue formalism,” *Physical Review B*, vol. 41, p. 7892, 1990.

[91] G. Kresse and J. Hafner, “Norm-conserving and ultrasoft pseudopotentials for first-row and transition elements,” *Journal of Physics: Condensed Matter*, vol. 6. p. 8245, 1994.

[92] Gaussian98 is licensed through Gaussian Inc. at http://www.gaussian.com.

[93] G. Jomard, T. Petit, A. Pasturel, L. Magaud, G. Kresse, and J. Hafner, “First-principles calculations to describe zirconia psudopolymorphs,” *Physical Review B*, vol. 59, p. 4044, 1999.

Chapter 4

[94] A. Kawamoto, J. Jameson, P. Griffin, K. Cho, and R. Dutton, "Atomic scale effects of zirconium and hafnium incorporation at a model silicon/silicate interface by first principles calculations," *IEEE Electron Device Letters*, vol. 22, p. 14, 2001.

[95] D. Allan and M. Teter, "Nonlocal pseudopotentials in molecular-dynamical density-functional theory: application to SiO_2," *Physical Review Letters*, vol. 59, p. 1136, 1987.

[96] F. Liu, H. Garofalini, D. King-Smith, and D. Vanderbilt, "First-principles study of crystalline silica," *Physical Review B*, vol. 49, p. 12528, 1994.

[97] T. Demuth, Y. Jeanvoine, J. Hafner, and J. Angyan, "Polymorphism in silica studied in the local density and generalized-gradient approximations," *Journal of Physics*: *Condensed Matter*, vol. 11, p. 3833, 1999.

[98] R. Wyckoff, Crystal Structures 2d. ed., Vol. 1, p. 312, Interscience Publishers, New York, 1965.

[99] R. Wyckoff, Crystal Structures, 2d. ed., Vol. 1, p. 318, Interscience Publishers, New York, 1965.

[100] R. Buczko, S. Pennycook, and S. Pantelides, "Bonding arrangements at the Si-SiO_2 and SiC-SiO_2 interfaces and a possible origin of their contrasting properties," *Physical Review Letters*, vol. 84, p. 943, 2000.

[101] H. Kageshima and K. Shiraishi, "Theoretical study of the band offset at silicon-oxide/silicon interfaces with interfacial defects," *Surface Science*, vol. 407, p. 133, 1998.

[102] H. Kageshima and K. Shiraishi, "Microscopic mechanism for SiO_2/Si interface passivation: Si=O double bond formation," *Surface Science*, vol. 380, p. 61, 1997.

[103] R. Wyckoff, Crystal Structures, 2d. ed., Vol. 1, p. 244, Interscience Publishers, New York, 1965.

[104] A. Pasquarello, M. Hybertsen, and R. Car, "Structurally relaxed models of the Si(001)-SiO_2 interface," *Applied Physics Letters*, vol. 68, p. 625, 1996.

[105] A. Pasquarello, M. Hybertsen, and R. Car, "Theory of Si 2p core-level shifts at the Si(001)-SiO_2 interface," *Physical Review B*, vol. 53, p. 10942, 1996.

[106] F. Himpsel, F. McFeely, A. Taleb-Ibrahimi, and J. Yarmoff, "Microscopic structure of the SiO_2/Si interface," *Physical Review B*, vol. 38, p. 6084, 1988.

[107] T. Yang and K. Saraswat, "Effect of physical stress on the degradation of thin SiO_2 films under electrical stress," *IEEE Transactions on Electron Devices*, vol. 47, p. 746, 2000.

[108] T. Yang, Ph.D. thesis, Electrical Engineering, Stanford University, 1999.

[109] G. Lucovsky, H. Yang, N. Niimi, J. W. Keister, J. E. Rowe, M. F. Thorpe, and J. C. Phillips, "Intrinsic limitations on device performance and reliability from bond-constraint induced transition regions at interfaces of stacked dielectrics," *Journal of Vacuum Science and Technology B*, vol. 18, p. 1742, 2000.

[110] P. McIntyre, private communication.

Chapter 5

[111] A. Kawamoto, K. Cho, P. Griffin, and R. Dutton, "First principles investigation of scaling trends of zirconium silicate interface band offsets," *Journal of Applied Physics*, vol. 90, p. 1333, 2001.

[112] C. Van de Walle and R. Martin, "Theoretical study of band offsets at semiconductor interfaces," *Physical Review B*, vol. 35, p. 8154, 1987.

[113] X. Zhang, S. Chua, S. Xu, and W. Fan, "Band offsets at the InAlGaAs/InAlAs (001) heterostructures lattice matched to an InP substrate," *Journal of Applied Physics*, vol. 83, p. 5852, 1998.

[114] A. Continenza, S. Massidda, and A. Freeman, "Stability and electronic properties of InAs/InP strained superlattices," *Physical Review B*, vol. 41, p. 12013, 1990.

[115] M. Murayama and T. Nakayama, "Chemical trend of band offsets at wurtzite/zinc-blende heterocrystalline semiconductor interfaces," *Physical Review B*, vol. 49, p. 4710, 1994.

[116] F. Herman and R. Kasowski, "Electronic structure of defects at Si/SiO_2 interfaces," *Journal of Vacuum Science and Technology*, vol. 19, p. 395, 1981.

[117] M. Hane, Y. Miyamoto, and A. Oshiyama, "Atomic and electronic structures of an interface between silicon and *B*-cristobalite," *Physical Review B*, vol. 41, p. 12637, 1990.

[118] G. Lucovsky and J. Phillips, "The effects of bonding and band offset constraints at Si-dielectric interfaces on the integration of alternative high-k dielectrics into aggressively-scaled CMOS Si devices," *Microelectronic Engineering*, vol. 48, p. 291, 1999.

[119] J. Robertson, "Band offsets of wide-band-gap oxides and implications for future electronic devices," *Journal of Vacuum Science and Technology B*, vol. 18, p. 1785, 2000.

[120] R. French, S. Glass, F. Ohuchi, Y. Xu, and W. Ching, "Experimental and theoretical determination of the electronic structure and optical properties of three phases of ZrO_2," *Physical Review B*, vol. 49, p. 5133, 1994.

[121] J. Tersoff, "Theory of semiconductor heterojunctions: the role of quantum dipoles," *Physical Review B*, vol. 30, p. 4874, 1984.

[122] J. Tersoff, "Schottky barrier and semiconductor band structures," *Physical Review B*, vol. 32, p. 6968, 1985.

[123] J. Jameson, private communication.

[124] H. Massoud, "Charge-transfer dipole moments at the Si-SiO_2 interface," *Journal of Applied Physics*, vol. 63, p. 2000, 1988.

[125] G. Lucovsky, H. Yang, and H. Massoud, "Heterointerface dipoles: applications to (a) Si-SiO_2, (b) nitrided Si-N-SiO_2, and (c) SiC-SiO_2 interfaces," *Journal of Vacuum Science and Technology B*, vol. 16, p. 2191, 1998.

[126] J. Keister, J. Rowe, J. Kolodziej, H. Niiki, T. Madey, and G. Lucovsky, "Band offsets for ultrathin SiO2 and Si3N4 films on Si(111) and Si(100) from photoemission spectroscopy," *Journal of Vacuum Science and Technology B*, vol. 17, p. 1831, 1999.

[127] Y. Kanemitsu, T. Ogawa, K. Shiraishi, and K. Takeda, "Visible photoluminescence from oxidized Si nanometer-sized spheres: exciton confinement on a spherical shell," *Physical Review B*, vol. 48, p. 4883, 1993.

[128] Y. Kanemitsu, "Light emission from porous silicon and related materials," *Physics Reports*, vol. 263, p. 1, 1995.

[129] Y. Takahashi, T. Furuta, Y. Ono, T. Ishiyama, and M. Tabe, "Photoluminescence from a silicon quantum well formed on separation by implanted oxygen substrate," *Japanese Journal of Applied Physics*, vol. 34, p. 950, 1995.

[130] K. Hess, L. Register, B. Tuttle, J. Lyding, and I. Kizilyalli, "Impact of nanostructure research on conventional solid-state electronics: the giant isotope effect in hydrogen desorption and CMOS lifetime," *Physica E*, vol. 3, p. 1, 1998.

[131] H. Yang, H. Niimi, Y. Wu, G. Lucovsky, J. Keister, and J. Rowe, "The effects of interfacial suboxide transition regions on direct tunneling in oxide and stacked oxide-nitride gate dielectrics," *Microelectronic Engineering*, vol. 48, p. 307, 1999.

[132] G.-M. Rignanese, A. Pasquarello, J.-C. Charlier, X. Gonze, and R. Car, "Nitrogen incorporation at Si(001)-SiO_2 interfaces: relation between N 1s core-level shifts and microscopic structure," *Physical Review Letters*, vol. 79, p. 5174, 1997.